Summer 1999

Seismic Characterization of the Northern Puget Lowland, Washington

Lori K. (Lori Kelly) Roberts
Western Washington University

SEISMIC CHARACTERIZATION OF THE NORTHERN PUGET LOWLAND, WASHINGTON

BY

Lori K. Roberts

Accepted in Partial Completion

of the Requirements for the Degree

Master of Science

Moheb A. Ghali, Dean of the Graduate School

ADVISORY COMMITTEE

Chair, Dr. David C. Engebretson

Dr. Russell Burmester

Dr. Don J. Easterbrook

Dr. John Field

MASTER'S THESIS

In presenting this thesis in partial fulfillment of the requirements for a master's degree at Western Washington University, I agree that the Library shall make its copies freely available for inspection. I further agree that copying this thesis in whole or in part is allowable only for scholarly purposes. It is understood, however, that any copying or publication of this thesis for commercial purposes, or for financial gain, shall not be allowed without my written permission.

Signature _____

Date 7-26-99

MASTER'S THESIS

In presenting this thesis in partial fulfillment of the requirements for a master's degree at Western Washington University, I grant to Western Washington University the non-exclusive royalty-free right to archive, reproduce, distribute, and display the thesis in any and all forms, including electronic format, via any digital library mechanisms maintained by WWU.

I represent and warrant this is my original work and does not infringe or violate any rights of others. I warrant that I have obtained written permissions from the owner of any third party copyrighted material included in these files.

I acknowledge that I retain ownership rights to the copyright of this work, including but not limited to the right to use all or part of this work in future works, such as articles or books.

Library users are granted permission for individual, research and non-commercial reproduction of this work for educational purposes only. Any further digital posting of this document requires specific permission from the author.

Any copying or publication of this thesis for commercial purposes, or for financial gain, is not allowed without my written permission.

Name: Lori Roberts

Signature: _____

Date: 5/24/18

SEISMIC CHARACTERIZATION OF THE NORTHERN PUGET LOWLAND, WASHINGTON

A Thesis

Presented to the Faculty of

Western Washington University

In Partial Fulfillment

of the Requirements for the Degree

Master of Science

---

by

Lori K. Roberts

July, 1999

Abstract

Records show that thousands of earthquakes have occurred in the northern Puget Lowland since 1969. At least fifteen of these events have been greater than magnitude 4, and one (Deming mag. 5.2, 1990) was the second largest recorded shallow crustal event in Washington for the last hundred years. Despite the evidence that suggests that the potential for great earthquakes capable of severe damage in the northern Puget Lowland is very real, the seismicity in the area is poorly understood. This is in part due to the wide scattering and apparently random assortment of recorded events. This thesis attempts to create a better understanding of the structures along which these earthquakes occur. A better understanding the active structures can help to better evaluate the full potential for destructive earthquakes.

Conclusions in this thesis are based primarily on historical seismic records from the Washington Regional Seismic Network, and include earthquake activity from 1969 to 1995. Focal mechanisms from the Washington Regional Seismic Network and Western Canadian Telemetered Network databases are for seismic events that were recorded at enough stations to meet quality standards. The records used were limited to events with foci within the upper 30 km of the North American crust and lie within the boundaries of the northern Puget Lowland.

Depth distributions of earthquake foci were used to determine the extent and location of seismic deformation. Results show that events are concentrated within two

general depth intervals in the crust. This bimodal distribution includes a shallow concentration between the surface and 5 km depth and another concentration at approximately 17+/- 3 km. Depth distribution across the region suggests that a wedge-shaped body is being deformed seismically. This wedge-shaped body roughly conforms to low temperature regions defined by geothermal modeling for the region, suggesting a direct correlation between low heat flow and seismic deformation.

This thesis introduces a modified technique of fault classification that can be used to analyze focal mechanisms for a region as a group, rather than just an event-by-event basis. The plunges of the pressure and tension axes from focal mechanisms were used to classify earthquakes by fault type. The results were consistent with the study region being in a transpressive regime, with 74% of the events being clearly reverse and strike-slip. However, deformation is not uniform. A depth distribution plot shows a change from predominantly reverse faulting above 20 km to predominantly strike-slip faulting below 20 km. This could be the result of a swapping of σ_2 and σ_3 due to an increased lithostatic load, the result of faulting along preexisting zones of weakness, or the result of spatial distribution of both.

Maps of focal mechanisms of a single fault type helped to define possible trends in an otherwise seemingly random assortment of focal mechanisms. Right lateral strike-slip faulting between 20 and 30 km along the trend of the southern Whidbey Island fault was most apparent. Shallower than 20 km, the stresses appear diffused into the northern part of the study region that forms the wedge.

A statistical Chi-square analysis for planar distributions of earthquake foci was developed and used over the entire region to investigate possible correlations with maps of focal mechanisms. Planar distributions that met statistical criteria that indicated they are significant show some interesting patterns. The eastern portion of the Devil's Mountain fault had planar distributions that aligned with focal mechanisms showing shallow strike slip and reverse faulting. Clear reverse faulting around 15 km depth along the trace of the Vedder Mountain lineament was also observed.

Acknowledgements

I cannot thank Dr. David C Engebretson enough for all his help, support, assistance, inspiration, enthusiasm, encouragement, patience, guidance, and most of all friendship. He has helped to make this a truly wonderful experience. Thank you to Dr. Russ Burmester for his insightful comments and conversation. I also wish to thank Dr. John Field and Dr. Don Easterbrook for their thorough editorial reviews. I would like to thank Steve Malone and Tammi Lynn Mulder for providing me with the data from which this material was compiled.

Friends who have helped me along the way I would also like to thank; Alice Shilhanek, Clark Blake, Susan Boundy-Sanders, Neil Duffin, Talia Henze, Dori Kovanen., Chris Sutton, and Vicki Critchlow.

I would also like to thank my coworkers who have been supportive in allowing me to take the time needed to finish this, especially Don Roberts and Dave Smith.

Thanks to my family for support and inspiration. A special thanks to my husband John for his support and patience while I immersed myself in this project.

TABLE OF CONTENTS

LIST OF FIGURES

CHAPTER 1. INTRODUCTION

Geographic Setting

The northern Puget Lowland is located in the northwest corner of Washington (Figure 1 and 2). The Puget Lowland is an elongate topographic and structural depression that stretches from the Strait of Georgia, in Canada, to just south of Olympia (Easterbrook and Rahm, 1970). The study area is bounded to the east by the Cascade volcanic arc, to the west by Vancouver Island, to the north by the Canadian mainland, and to the south by western Washington and the Puget Lowland. Because most of this region lies outside of the confines of major population centers of Vancouver, BC and Seattle, WA, too little attention has been given to it's seismicity.

Statement of Purpose

The study region is seismically active, but little is known about specific structures on which earthquakes occur. This is due in part to a wide distribution of historical earthquakes, which hinder the precise delineation of active faults. However, historical records leave little doubt for the possibility of damaging earthquakes in the future. Therefore, the study of seismicity and crustal structure is important for a better understanding of the full potential for destructive earthquakes in the northern Puget Lowland.

The primary intent of this study is to characterize the structural setting of earthquakes by linking recorded seismic events to mapped and unmapped faults. This is

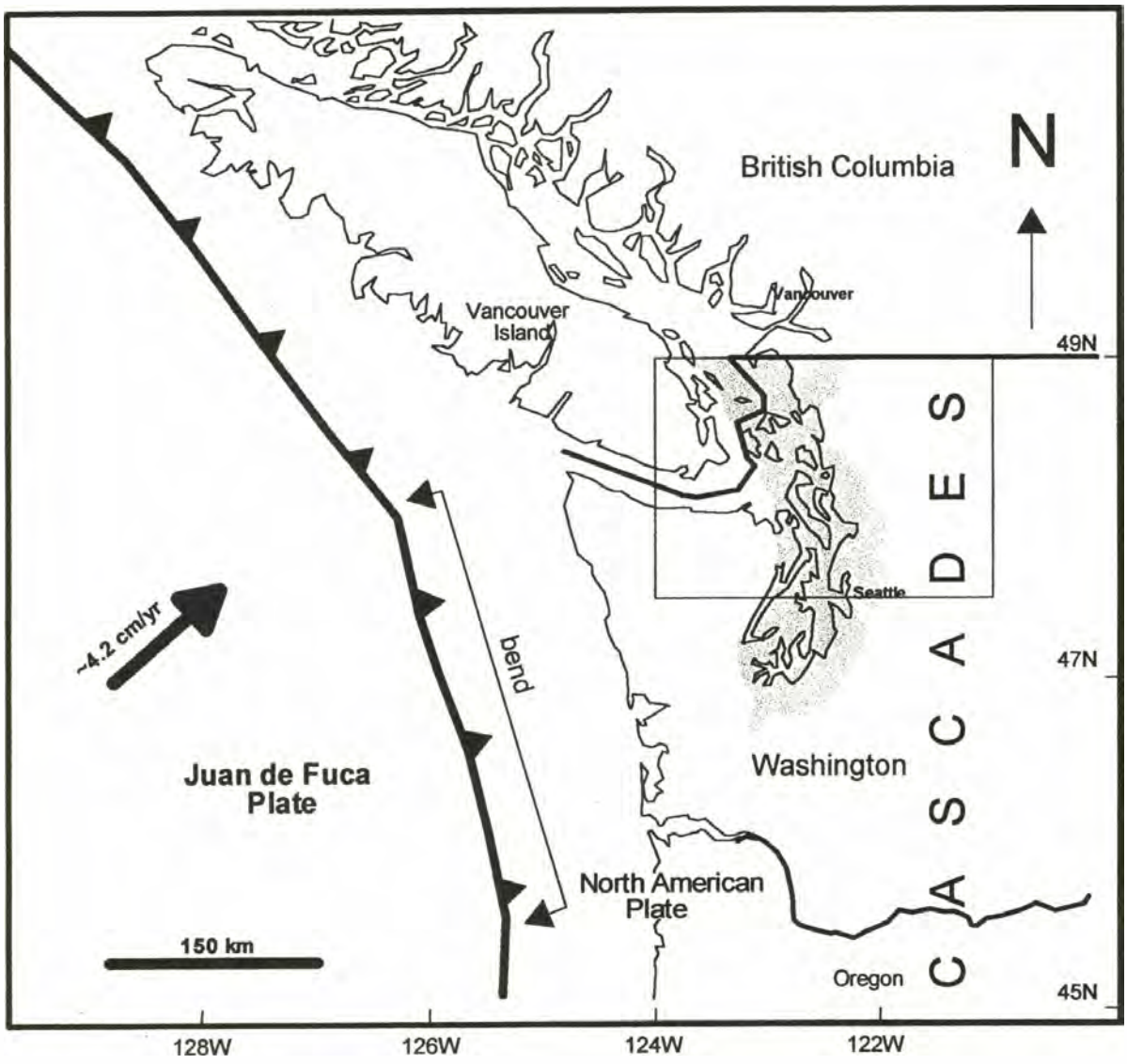

Figure 1. Geographical setting of the study region. The study region is in the boxed area. Arrow indicates motion of the Juan de Fuca plate relati region is the boundary of the Puget Lowland.

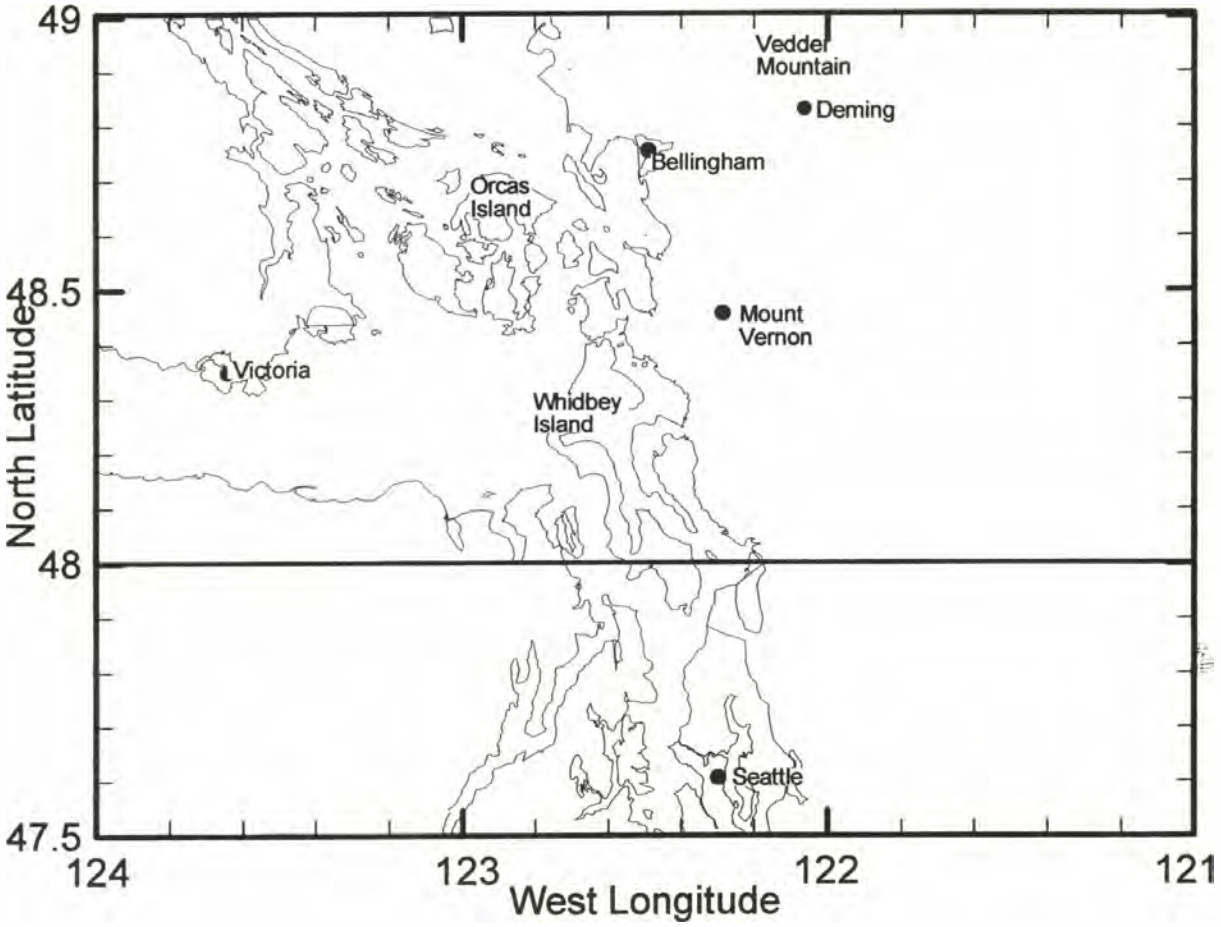

Figure 2. Inset of boxed region in Figure 1. Includes details of shorelines and geographic names shown in figures that follow. The study area is primarly north of 48° latitude. Focal mechanism maps do, however, extend as far south as 47.5° latitude.

accomplished by analyzing available seismic records. Earthquake epicenters and available focal mechanisms are used to create a better understanding of the active structures on which these events have occurred.

Generalized Geologic History

Mesozoic Geology

Western North America is composed of numerous terranes, some of which are exotic (Jones and others, 1983; Figure 3). Most geologists agree that many terranes were accreted to western North America by the late Cretaceous (Cowan, 1994). These terranes were then transported northward by coast-parallel slip to their present-day positions between 80 and 60 Ma (Cowan, 1994). Since then, they have made up the framework of the western Washington continental margin. This framework includes structural weaknesses that may have accommodated subsequent deformation within and between terranes. Present day tectonic stresses may reactivate these inherited weaknesses and result in active faulting.

Cenozoic Geology

At the beginning of the Eocene, around 57 Ma, this region was covered by a vast alluvial floodplain within a lowland semitropical rain forest (McLellan, 1927; Mustoe and Gannaway, 1997). A thick sequence of sedimentary rocks, the Chuckanut Formation, was deposited within a faulted, down-dropped basin (Johnson, 1983). Sediment compositions and paleocurrent directions indicate the source was far to the east (Johnson, 1983; Mustoe

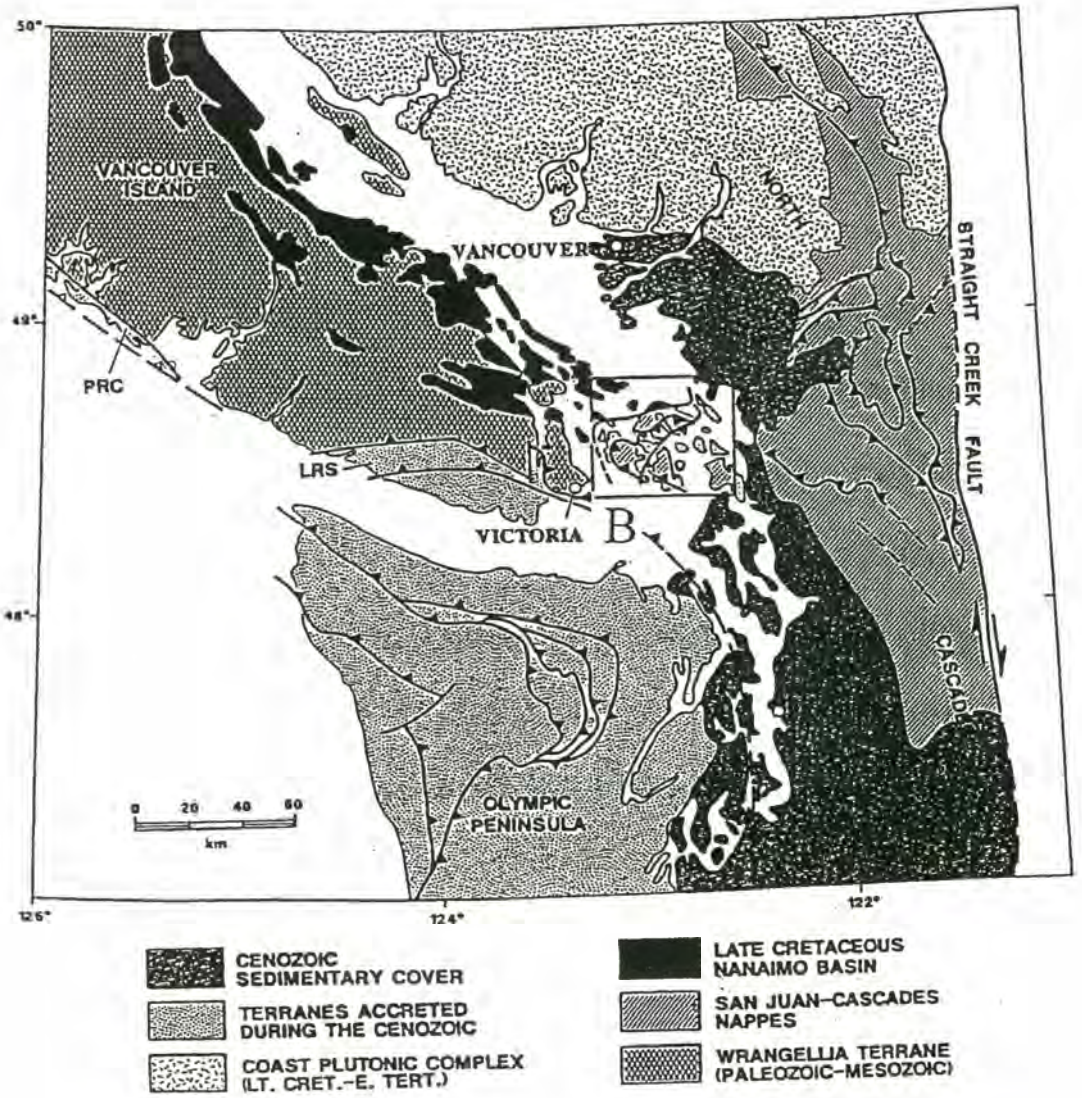

Figure 3. Regional tectonic setting of the Puget Lowland showing generalized geology and accreted terranes. Geology east of the Straight Creek fault is not shown. Rocks on the Olympic Peninsula are buttressed against the adjacent mainland along an approximately located boundary labeled B (Taken from Brandon and others, 1987).

and Gannaway, 1997). This depositional environment ended when dextral displacement on the Straight Creek fault altered the drainage, and uplift of the lowland basins effectively cut off the sediment source (Engels and others, 1976; Johnson, 1983; Mustoe and Gannaway, 1997).

Around 42 Ma, the Cascade arc began forming. Subduction of younger, more buoyant plate caused the convergence rates to slow from an average 150 km/Ma to near present day rates of 45 km/Ma (Engebretson and others, 1984). This resulted in a shift of the volcanic axis westward to its present day position (Wells and others, 1984). Also at this time regional tectonics changed from a transtensional regime to a transpressional regime, initiating the folding and thrusting of the Chuckanut Formation (England and others, 1997). It is likely that previously existing structures in the basement of the Chuckanut were reactivated during this time.

Quaternary / Recent Geology

Western Washington had at least six episodes of Cordillerian Ice Sheet advance during the Pleistocene (Easterbrook, 1992, 1994). During the last major advance, the northern Puget Lowland was under 1,800 meters of ice at its maximum (Easterbrook, 1963, 1992). The last of the ice sheets retreated from the northern Puget Lowland by 10,000 years ago (Easterbrook, 1963, 1992). Glacial rebound has taken place at a rate approximately equal to eustatic sea level rise throughout most of the Holocene (Easterbrook, 1992).

Strata, the youngest being the Everson glaciomarine drift, ~12,000 Ma, record tectonic displacements near Deming (Figure 4). This strata consists of the Kulshan glaciomarine drift, the Deming sand and the Bellingham glaciomarine drift (Figure 4). Change in relief across this sequence of sediments indicates this region underwent about 200 m of vertical offset more than once, in addition to isostatic rebounding (Easterbrook, 1963, 1992; Figure 4). Dating of these sediments indicates that this area emerged, resubmerged, and reemerged sometime between 10,000 and 12,000 years ago (Easterbrook, 1963, 1992; Figure 4). The retreat and advance of ice during glaciation does not account for this magnitude of vertical offset during that time period. The most likely explanation for these offsets is crustal deformation caused by tectonism.

Tectonic Setting

The study area is located above the Cascadia subduction zone where young oceanic lithosphere of the Juan de Fuca plate is descending beneath North America (Figure 5). The Juan de Fuca plate is a remnant of the Farallon plate, which has been actively subducting along the North American continental margin since the mid-Mesozoic (Engebretson and others, 1985). Present-day relative motions indicate that the Juan de Fuca plate is moving northeasterly toward the North American plate at a rate of approximately 4.3 cm/yr. (Riddihough, 1977, 1984; Figure 1).

The oblique approach of the Juan de Fuca plate relative to North America causes transpressive deformation within the crust of the North American plate (Stanley and others, 1996; Wells and others, 1998). Transpressive deformation is occurring in the

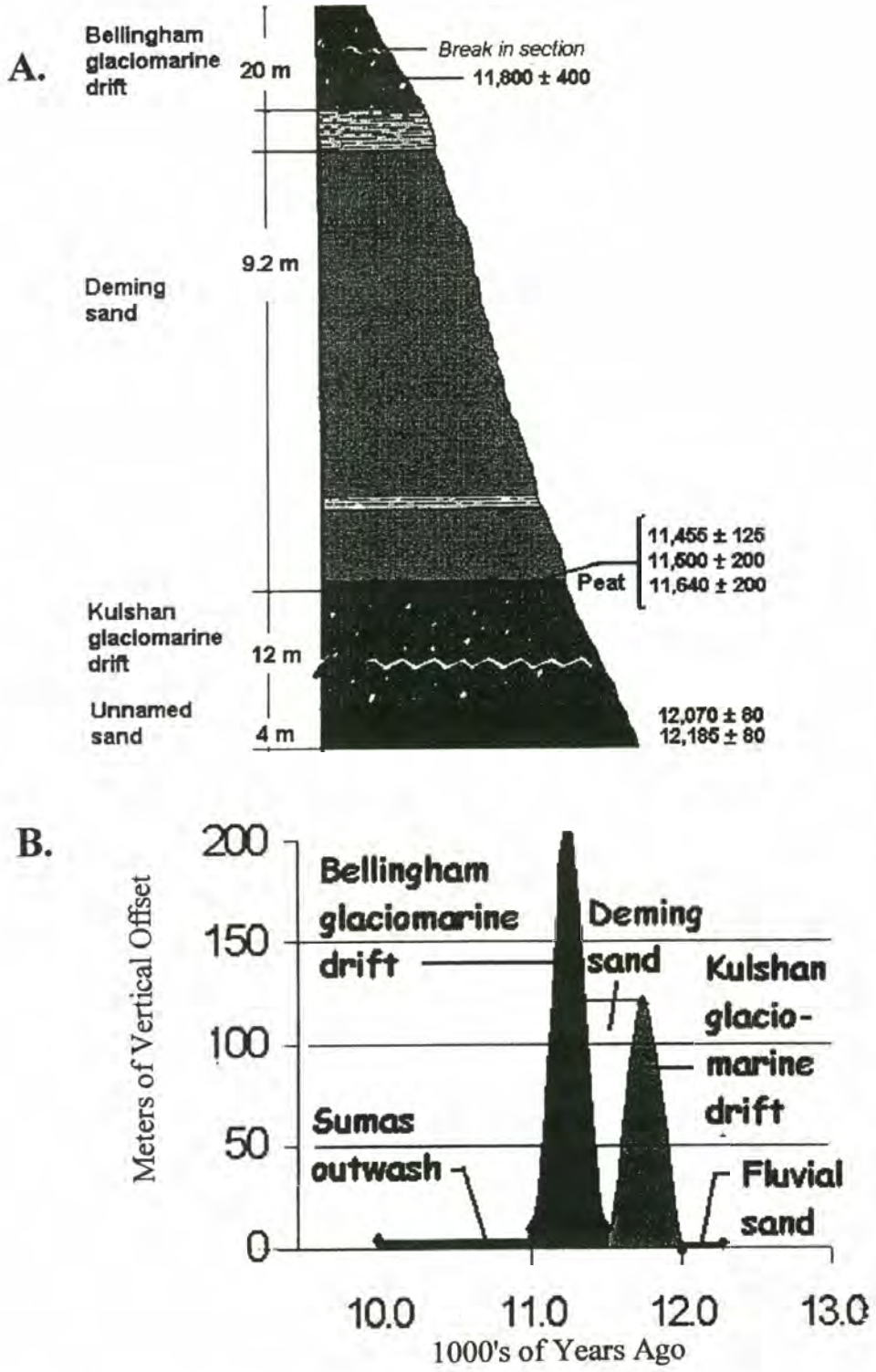

Figure 4. A.) Diagrammatic section of the Everson glaciomarine drift at its type locality near Deming. B.) Vertical offset relative to present day elevation each section underwent from ten to twelve thousand years ago. Isostatic rebounding cannot account for this magnitude of vertical offset. Tectonics is the most likely explanation. (From Easterbrook, personal communication).

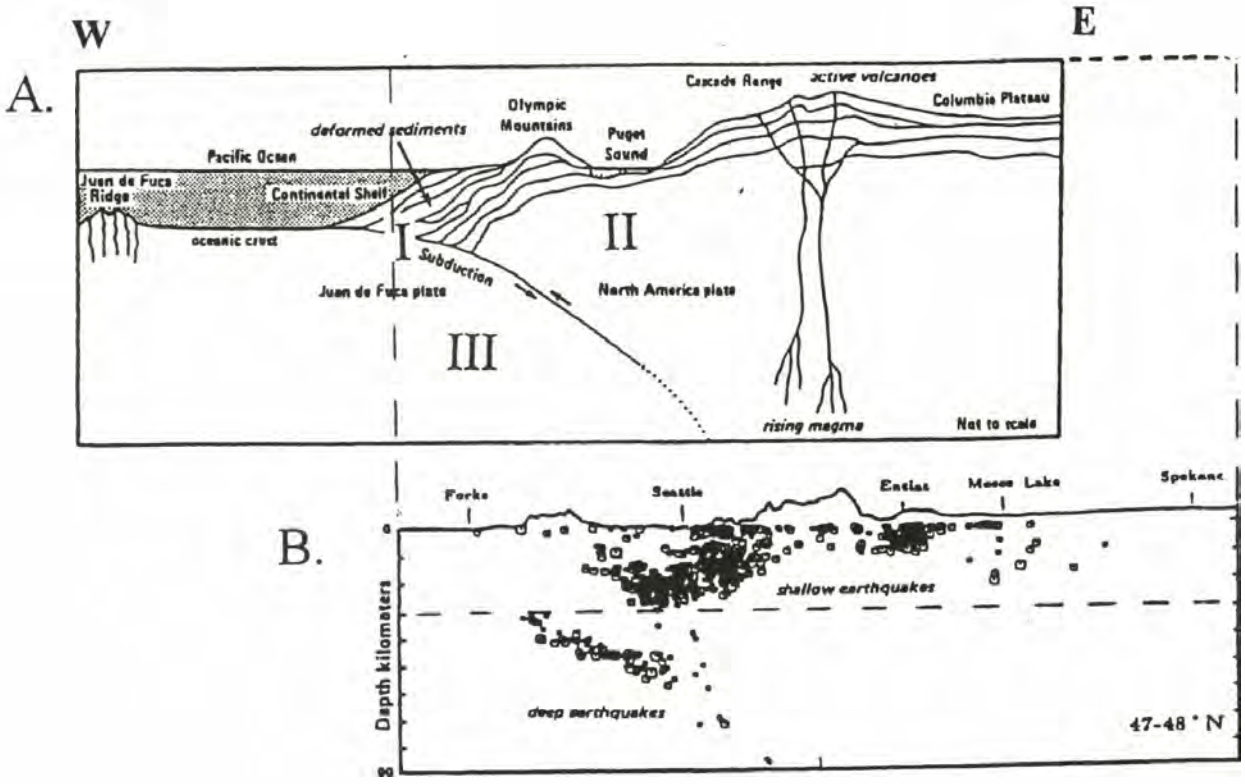

Figure 5. Cross section of Washington and the Cascadia Subduction Zone. The boundaries of the Juan de Fuca and North American plates are defined in part using earthquake hypocentral locations. (A.) Shows major topographic features and generalized underlying geologic structures of Washington. Regions labeled I, II, and III are the three source regions for earthquakes experienced in the Pacific Northwest. Region I is the intersection of the subducting Juan de Fuca and the overriding North American plates. Region II is the overriding North American plate. Region III is the subducting Juan de Fuca plate. (B.) Selected hypocenters of earthquakes that occurred from 1982 to 1986, from 47° to 48° N. Below sea level the vertical exaggeration is 2 to 1. The deeper earthquakes are events that occurred in the subducting plate. The shallower earthquakes are events that occurred in the overriding crust (Taken from Noson and others, 1988).

Cascadia forearc, between the Juan de Fuca plate and the North American plate. Arc-parallel transport of the Cascadia forearc is estimated to be as much as .9 cm/year (Wells and others, 1998).

Change in the trend of the subduction front, shown in Figure 1, from roughly north - south off Oregon to northwest - southeast off Vancouver Island causes further structural complexities in the study area. The general direction of motion of the Juan de Fuca plate and the curved subduction front results in change of relative motions between the two plates along the subduction front. A result of these changes in relative motions along the subduction front is a buttress that has formed within the North American plate (Beck and others, 1993; Figure 3). There basement rocks of the Crescent Formation, part of the Cascadia forearc, move northward and encounter the relatively stationary basement rocks of Vancouver Island and the North Cascades (Figure 3; Stanley and others, 1995; Wells and others, 1998). The northern Puget Lowland lies within the buttress zone just inland from the bend on the subduction front. The change in relative plate motion in relation to the subduction front and a buttress likely causes deformation unique to the forearc region just south of it (Beck and others, 1993; Stanley and others, 1996; Wells and others, 1998).

Regional Seismicity

Earthquake Source Regions

Three source regions for earthquakes in the Pacific Northwest are recognized (Rogers and others, 1996; Noson and others,1988; Figure 5). They lie within the boundary zone between the two converging plates, and within the converging plates

themselves (Rogers and others, 1996; Noson and others,1988; Figure 5).

The largest and most threatening earthquakes occur in the boundary between the converging plates. They result from the subducting slab sticking to the overriding crust (Figure 5a, region I; Rogers and others, 1996). Elastic strain rates measured along the front of the North American plate margin demonstrate that the subduction zone off the Puget Lowland is locked (Figure 6; Dragert and Hyndman, 1995). Locking of the subducting slab to the overriding crust is causing the outer plate margin to uplift and shorten. This subduction zone extends from Canada to Oregon and has the potential for the largest earthquakes. While literally thousands of events have been recorded, not one of the recorded events is known to have been the result of deformation at the boundary between the two plates (Figure 5a, region I). All recorded seismic events in the Pacific Northwest are considered to have occurred within one of the two plates (Figure 5a, regions II and III).

Within the overriding crust of the North American plate, crustal deformation is shallow and extends into the forearc. This is the result of the trench-parallel component of the approaching subducting plate causing transpressive deformation in the forearc (Figure 5a, region II; Stanley and others, 1996).

Many of the largest earthquakes felt in historical times have taken place within the subducted slab of the Juan de Fuca plate. These events are believed to be the result of stresses caused by downward gravitational pull of the oceanic crust into the Earth's mantle (Figure 5a, region III; Rogers and others, 1996).

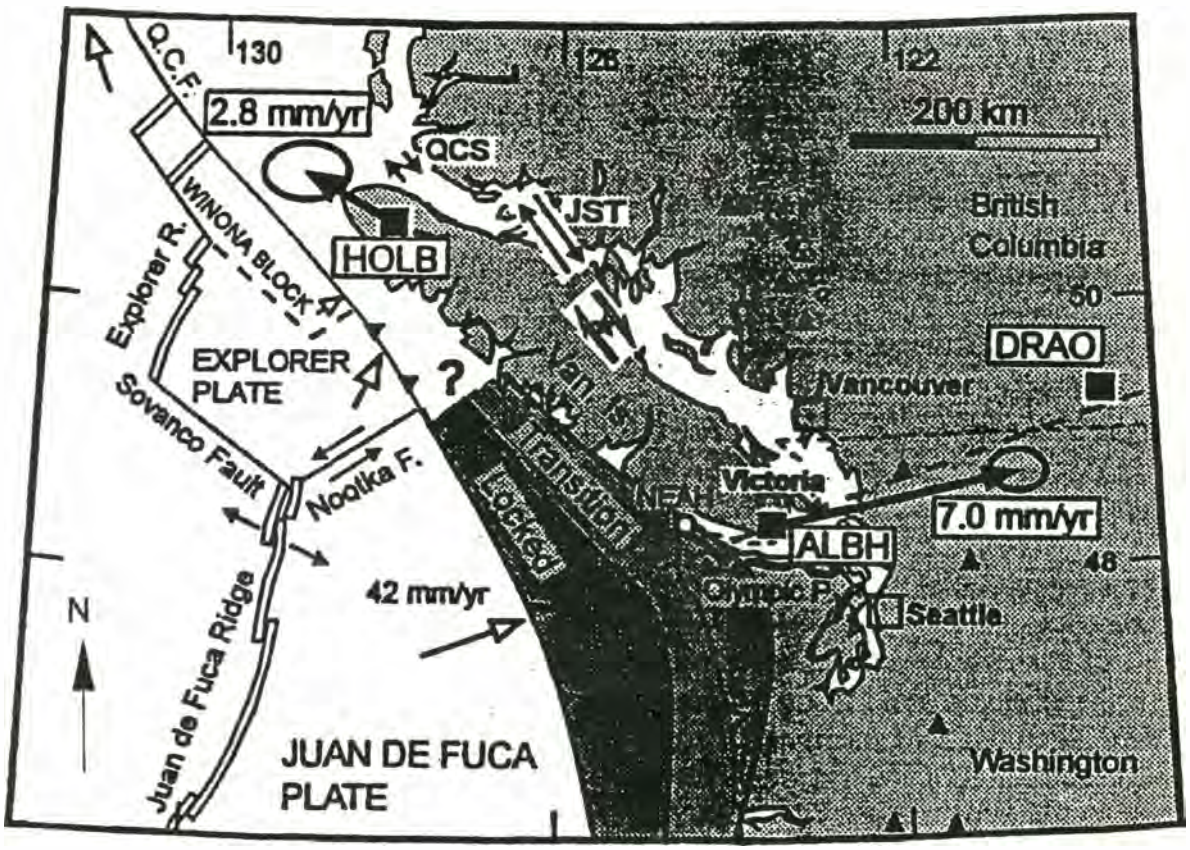

Figure 6. Map of the northern Cascadia margin showing the plate tectonic setting and the position of the locked and transition zones for the subduction thrust (from Dragert and others, 1994a; Hyndman and Wang, 1995). Solid squares indicate GPS tracking sites. The arrows and their 95% confidence ellipses at HOLB and ALBH indicate horizontal motion relative to DRAO. Notice that the present motion of HOLB is consistent with translation of the forearc northwestward, whereas ALBH suggests much larger easterly convergence across the Puget Lowland (Taken from Dragert and others, 1995).

Large Holocene Earthquakes

Geologic records indicate that several large earthquakes (magnitude 8 or greater) have occurred along the Cascadia subduction zone within the past 3000 years (Figure 5, region I; Atwater, 1987). The most recent event, about 300 years ago, may have involved rupture along most of the Juan de Fuca - North American margin (Figure 6; Adams, 1992). Evidence for this event and its timing comes mainly from tree ring dating of submerged and damaged trees in coastal marshes, radiocarbon dating of tsunami deposits, and Japanese tsunami records from January 1700 (Yamaguchi and others, 1997). Dating of other deposits resulting from earlier large subduction events suggests a recurrence interval of 300 to 1200 years (Atwater, 1996).

A large earthquake (estimated to be magnitude 7.5) occurred in the shallow crust immediately beneath Seattle less than 1,100 years ago (Figure 5, region II; Adams, 1992). During this event, a marine terrace along southern Bainbridge Island was uplifted 21 feet (Buckman and others, 1992). Other evidence of this event consists of tsunami deposits (Atwater and Moore, 1992), tree ring cross dating data linked to the abrupt deaths of trees (Jacoby and others, 1992), landslides and turbidite deposits within lake sediments (Karlin and Abella, 1992), and rock avalanche deposits (Schuster and others, 1992). The entire Puget Sound region apparently has faults and the potential for earthquakes similar to this shallow crustal one, but most of these faults are poorly understood (Rogers and others, 1996).

Some of the first direct evidence of moderate to large prehistoric earthquakes in the northern Puget Lowland may be liquefaction features found at six sites just south of

Vancouver BC within 20 km of the study region (Figure 1; Clague and Naesgaard, 1992). Upper limiting ages of 3,500 years and 2,400 years were found for these events, but because sand dikes intrude older peat layers, liquefaction features are believed to be much younger. Liquefaction features have also been found just south of Deming along the South Fork of the Nooksack River (Figure 6; Kovanen, 1996). A seismic cause is likely considered, based on the size of the feature (Kovanen, 1997, personal communication).

Recorded Historical Seismicity

Earthquakes as large as magnitude 7.4 have occurred in the Pacific Northwest during the region's recorded history. Records of earthquakes date back to 1846 in Canada and 1872 in Washington (Mulder, 1995; Madole and others, 1995). These records show that large earthquakes occurred within the crust and subducting-slab (Figure 5, regions II and III), but not along the Cascadia subduction zone (Figure 5, region I; Heaton and Kanamori, 1984; Rogers and others, 1996). Recorded seismicity within the study area reveals active shallow crustal deformation (Figure 7). Fifteen events larger than magnitude 4 have occurred in the study region since 1969 and Canadian records show at least 20 events of magnitude 4.5 or greater occurred in this portion of the North American plate between 1846 and 1975 (Mulder, 1995). The largest and oldest event recorded in the Pacific Northwest was a magnitude 7.4 event in 1872 (Figure 7; Madole and others, 1995). It is the only large (> 6.0 magnitude) shallow crustal earthquake in historical records and is estimated to have occurred in the easternmost part of the study region (Figure 7; Madole and others, 1995). The magnitude 5.2 1990 Deming earthquake

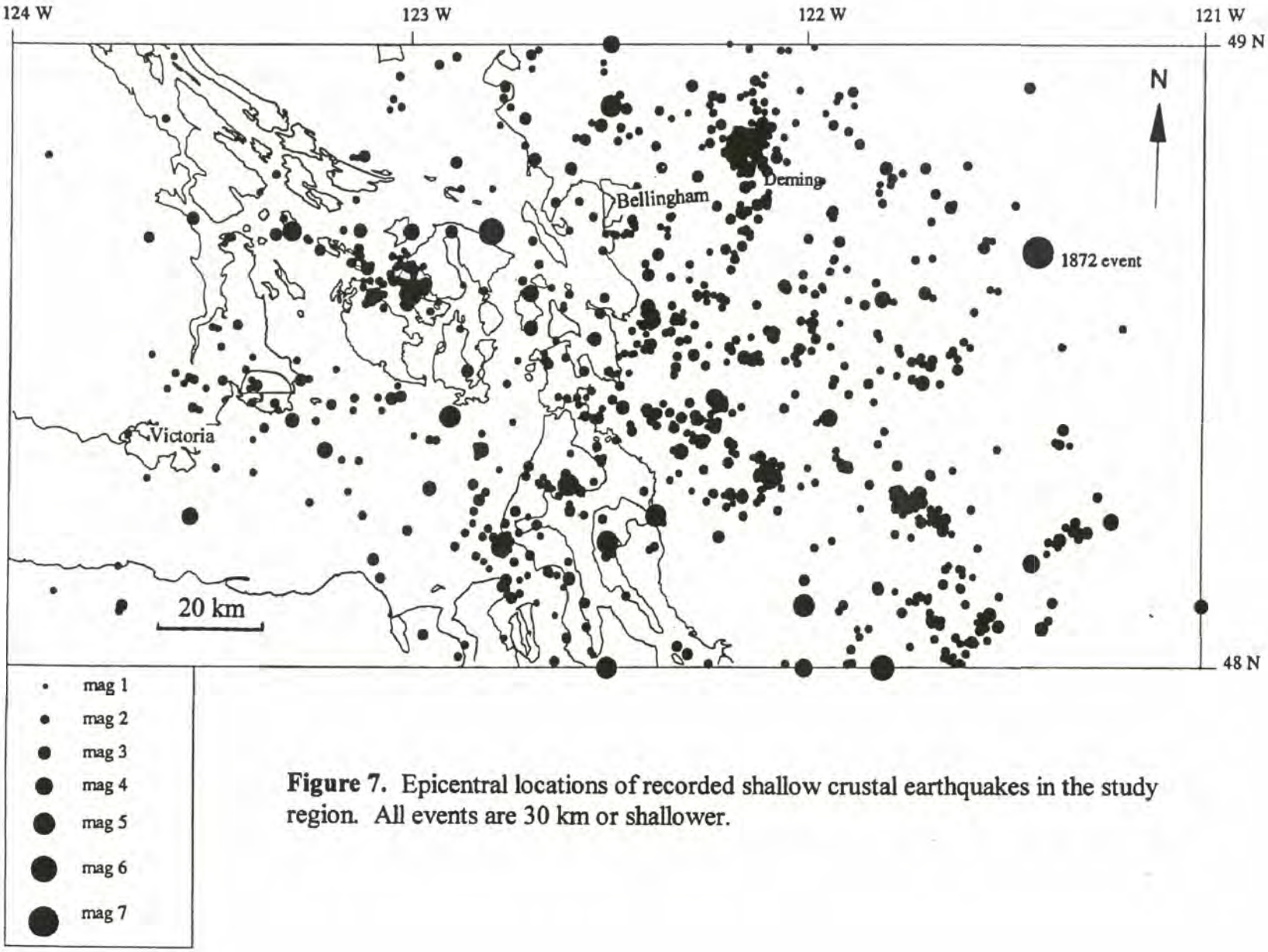

Figure 7. Epicentral locations of recorded shallow crustal earthquakes in the study region. All events are 30 km or shallower.

was the second largest crustal earthquake in WA since 1920, the largest being the 1996 magnitude 5.3 Duvall earthquake that occurred just north of Seattle.

Crustal Faults and Lineaments

Active deformation in the northern Puget Lowland has received little attention. One reason for this is that active faults are difficult to delineate because this area is highly vegetated, undergoes rapid erosion, and much of it is heavily glaciated and covered with thick Quaternary deposits. However, several faults to the south and east have been documented (Figure 8; Gower and others, 1985, Cheney, 1987, Johnson and others, 1996; Pratt and others, 1997). Evidence has been found for Quaternary movement on the southern Whidbey Island fault (Figure 8; Johnson and others, 1996). In the study region, the Devils Mountain fault and an extension of the Mount Vernon fault into Bellingham Bay and were found to have Eocene displacement. Evidence for this is based on surveys and cross cutting relationships, but whether recent displacement has occurred is less certain (Figure 8; Cheney, 1987). The 5.2 Deming earthquake occurred along the Macaulay Creek Thrust, although no surface rupture was found (Figure 9; Dragovich and others, 1997). Several potentially active faults and lineaments have been documented in the northern portion of the region based on earthquake and potential field studies (Figure 9; Mulder, 1995).

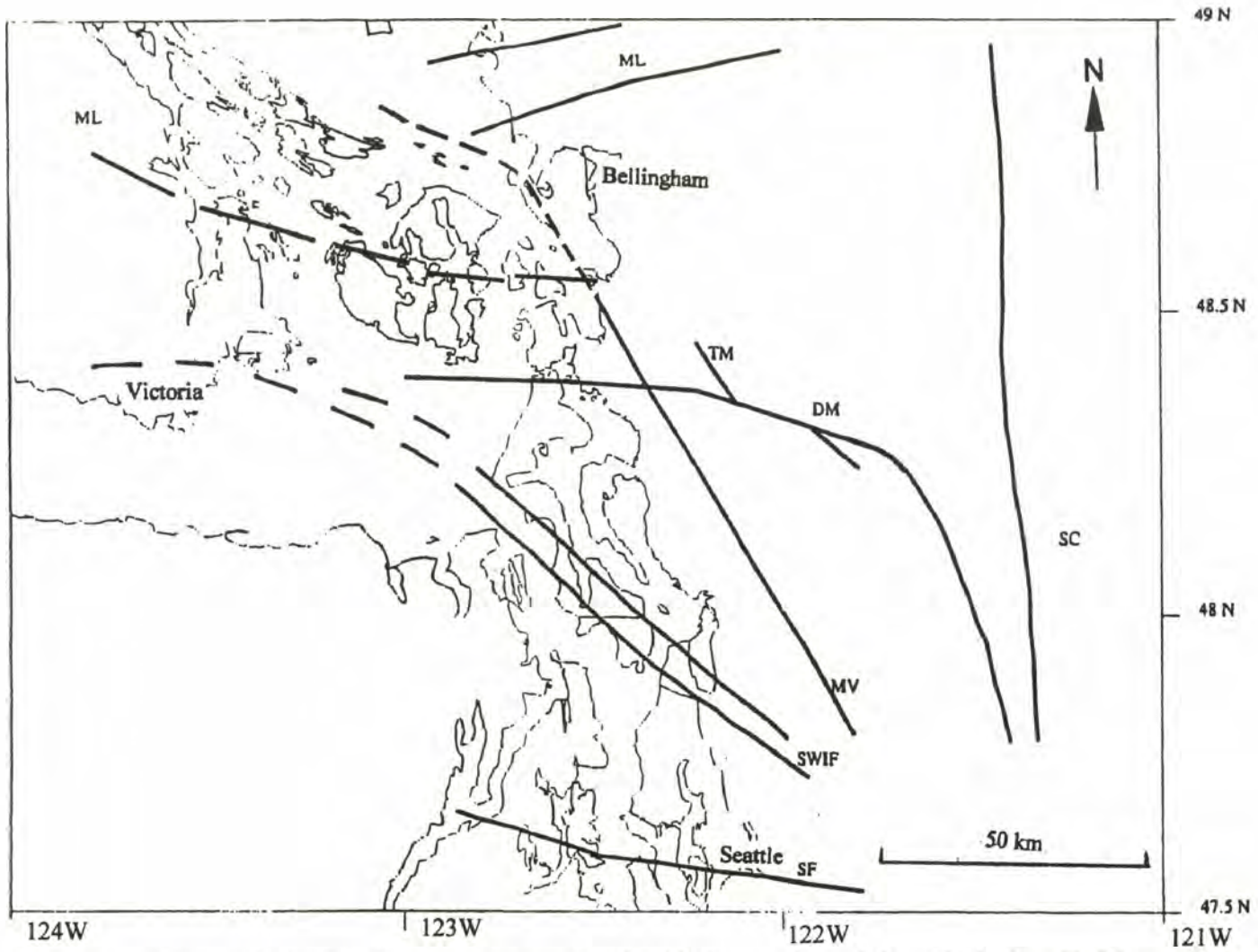

Figure 8. Documented major faults and lineaments associated with Cenozoic activity. DM - Devil's Mountain fault (Cheney, 1987); ML - lineaments (Mulder, 1995); MV - Mount Vernon fault (Cheney, 1987); TM - Table Mountain fault (Cheney, 1987); SC - Straight Creek fault (Cheney, 1987); SF - Seattle fault (Johnson, 1994); SWIF - Southern Whidbey Island fault (Johnson and others, 1996).

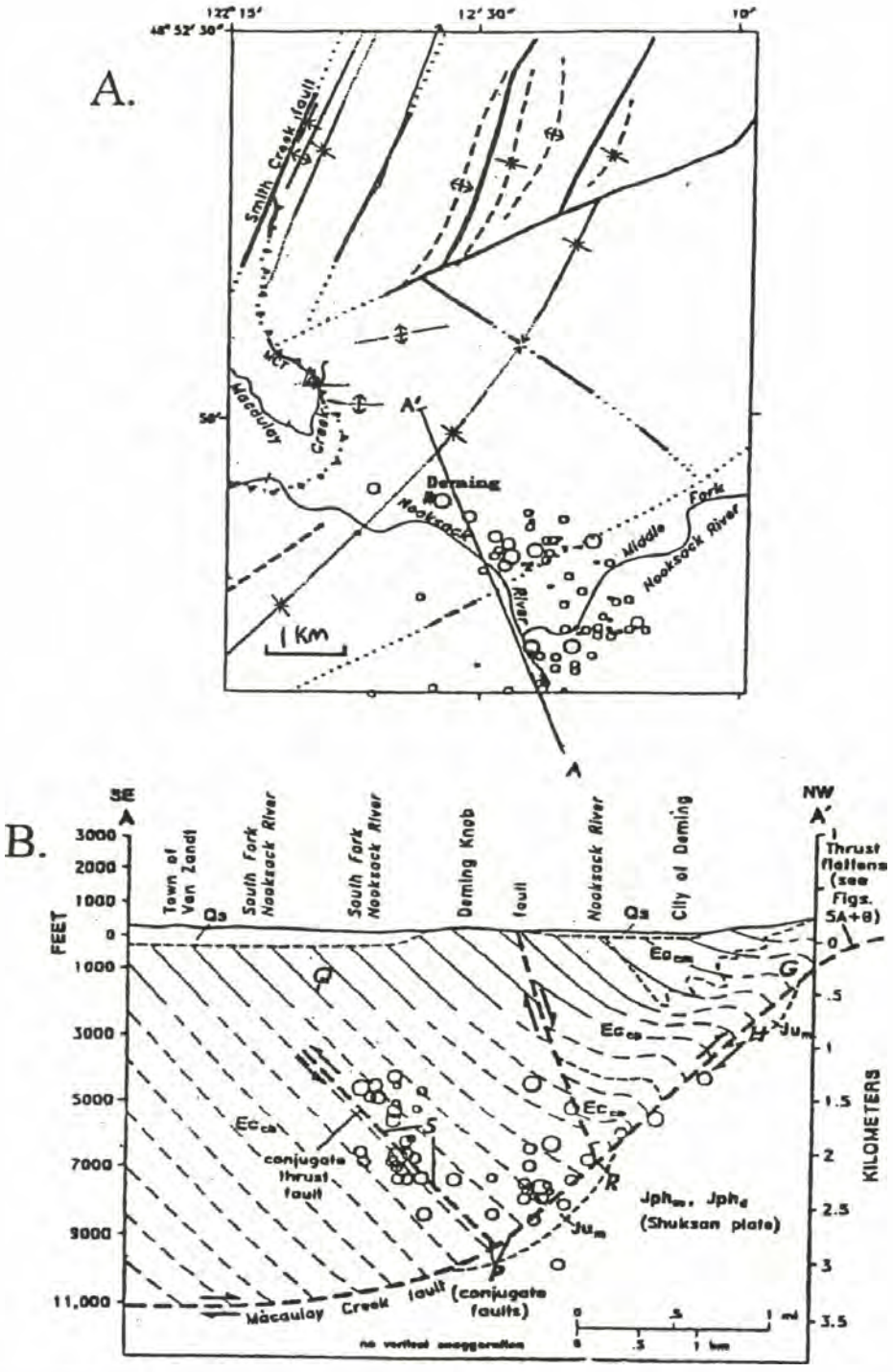

Figure 9. A.) Location map of cross section A - A' through Deming. Deming is located on Figure 2. B.) Cross section A - A'. Thrust R between 1.5 and 3.5 km depth, the hypocenters (circles; size proportional to magnitude), and backthrust (S) from Amadi (1992). Hypocenters shown are best-located aftershocks. The intersection of the conjugate planes at location P trends N70E (Amadi, 1992). (Taken from Dragovich and others, 1997)

Summary

Our knowledge of plate tectonics, geologic history and local historical seismicity indicates that the Puget Lowland is seismically active. Evidence is consistent with a high probability for destructive earthquakes within the study region. Mitigation of earthquake hazards requires that the geologic structures, kinematics, and dynamics of the area be better understood. The rest of this thesis uses seismicity of the northern Puget Lowland to locate and characterize active structures for the purpose of better understanding associated earthquake hazards. Locations of earthquakes, their focal mechanisms, and their planar distributions are examined in the next sections.

CHAPTER 2 SEISMIC STUDY

Highly accurate location of earthquakes has been possible since the installation of a seismic station telemetry network by the Washington Regional Seismic Network (WRSN) and the University of Washington (UW) in 1969 (Crosson, 1972). Coverage of southern Vancouver Island and the adjacent mainland has improved since 1975 when the Western Canadian Telemetered Network (WCTN) and the University of British Columbia (UBC) installed their first four digital seismograph stations on the west coast with expansion to twenty two stations by 1984 (Mulder, 1995).

Depth Distribution Analysis

Seismicity recorded by the expanded seismic network has fostered a better understanding of regional deformation. Two distinctive concentrations of earthquakes occur (Figure 10). In Washington, earthquakes shallower than ~30 km are considered to be crustal, occurring within the North American plate (Figure 5, region II; Crosson and Owens, 1987; Weaver and Baker, 1988; Stanley and others, 1996). None of the recorded events is believed to be associated with deformation at the boundary between the North American plate and the subducting slab, also referred to as the "locked zone" (Figure 5, region I and Figure 6; Crosson and Owens, 1987; Weaver and Baker, 1988; Stanley and others, 1996).

The WRSN's earthquake records from 1969 to 1995, provided by Steve Malone of the WRSN, were used for depth distribution analysis of the crustal region falling

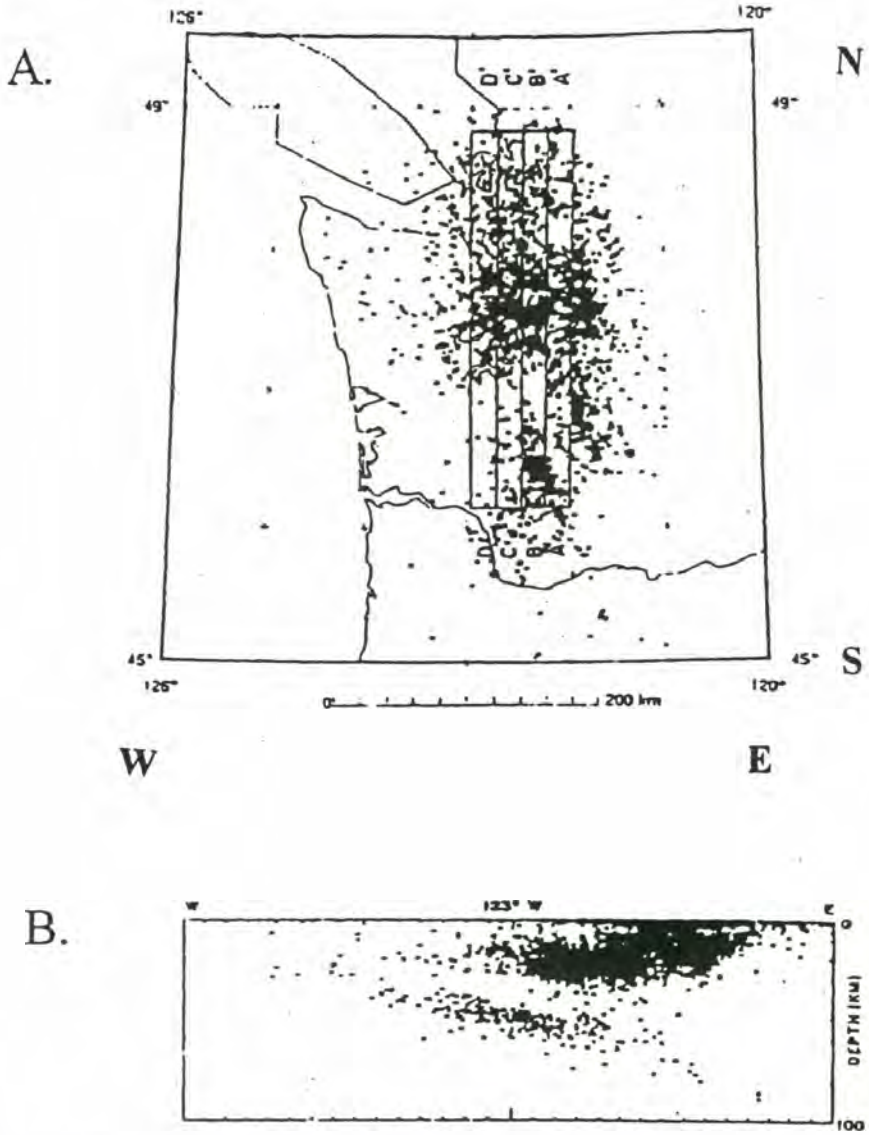

Figure 10. A.) Epicenters of earthquakes in the Washington Regional Seismic Network catalog from 1970 through 1986 lying west of 121° W, that were considered the best located events as defined by Crosson and others, 1987. N - S lines labeled A - D are locations of cross sections not included here. B.) E - W cross-section showing all hypocenters of all earthquakes plotted above. No vertical exaggeration, grid ticks are at 10 km intervals, with 123 W longitude at the center of the plot. Subcrustal earthquakes defining the Benioff zone are assumed to be within the subducted Juan de Fuca slab. (Taken from Crosson and others, 1987)

between 48°to 49° N latitude and 124° to 121° W longitude (Figure 11). All events chosen were 30 km depth or shallower and are considered to have occurred within the North American crust. The 1,230 events that fell within the boundaries of the region were used for analysis of the structures on which they occurred.

Regional Data and Results

From Figure 11 and 12 a transition from deeper earthquakes in the west to shallower earthquakes in the east is apparent. The number of earthquakes that occurred in each depth range within the bounds defined earlier were plotted (Figure 13). In addition to the transition mentioned above, a general bimodal distribution of all earthquakes is apparent with one concentration at very shallow (< 4 km) depth and another between 12 to 20 km depth (Figure 13). Similar plots were made for a more detailed study of how depth distribution changes from west to east (Figure 14). On this we can see that the majority of events occur between 123.5° and 121.5° west longitude (Figure 14). Virtually all recorded events west of 122.5° W were deeper than 10 km, while east of 122° W most recorded events were shallower than 10 km (Figure 14). The transition, from "deep" crustal to "shallow" crustal earthquakes appears to lie between 122.5° and 122° W longitude (Figure 14). This distribution of the occurrence of earthquakes within the crust is a function of the crustal rheology.

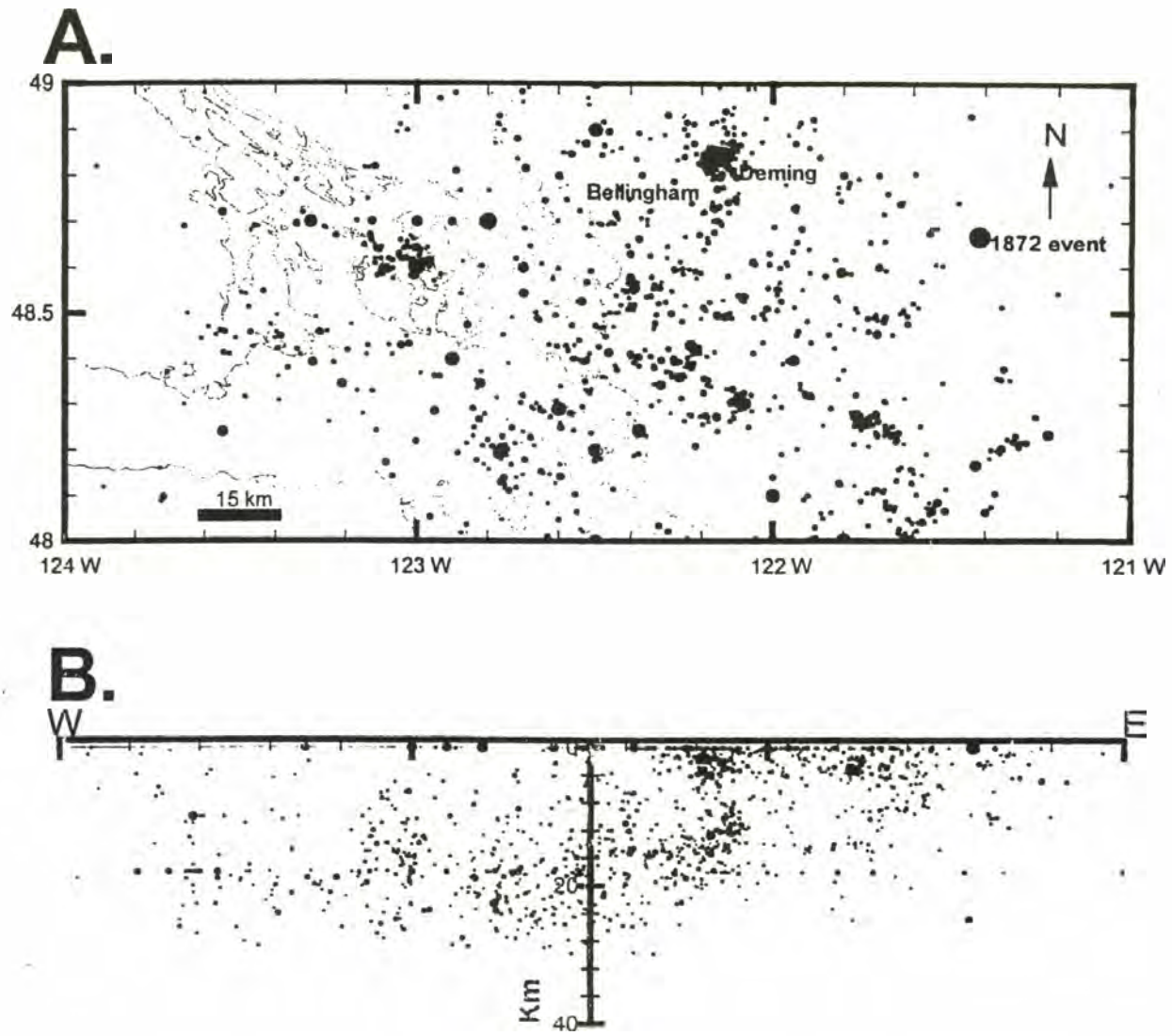

Figure 11. A.) Map showing epicentral locations of earthquakes occurring within the bounds of the depth distribution analysis. These events are all considered to be due to North American crustal deformation. B.) Hypocentral locations of earthquakes projected N - S along an E - W cross-section within the bounds of the depth distribution analysis. (No vertical exaggeration)

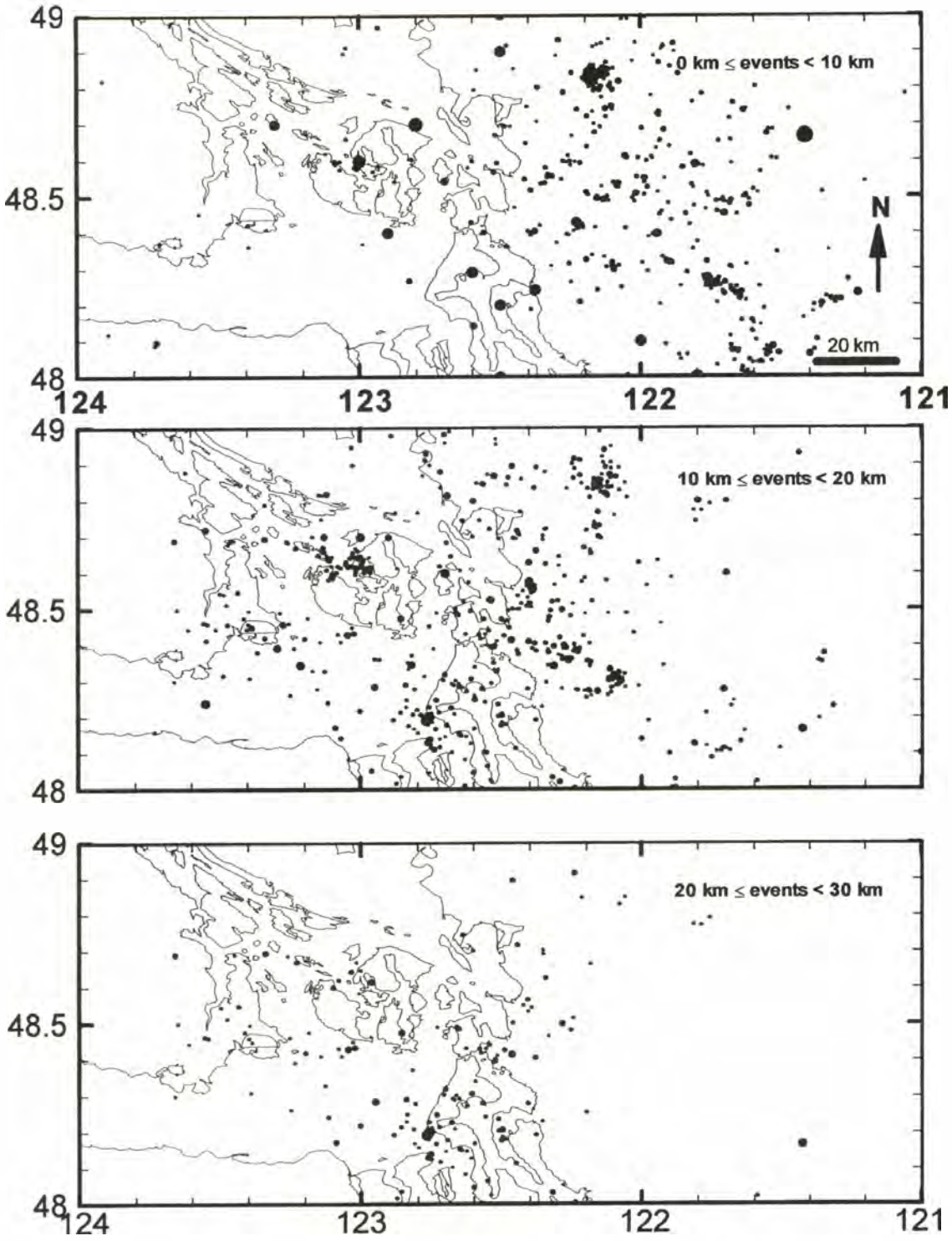

Figure 12. Epicentral locations of events were plotted as a function of the depth range into which they fell. Events shallower than 10 km primarly occurred in the eastern half of the study region. Between 10 and 20 km, events are scattered through the center of the study region. And events between 20 and 30 km are found primarily in the western half of the study region.

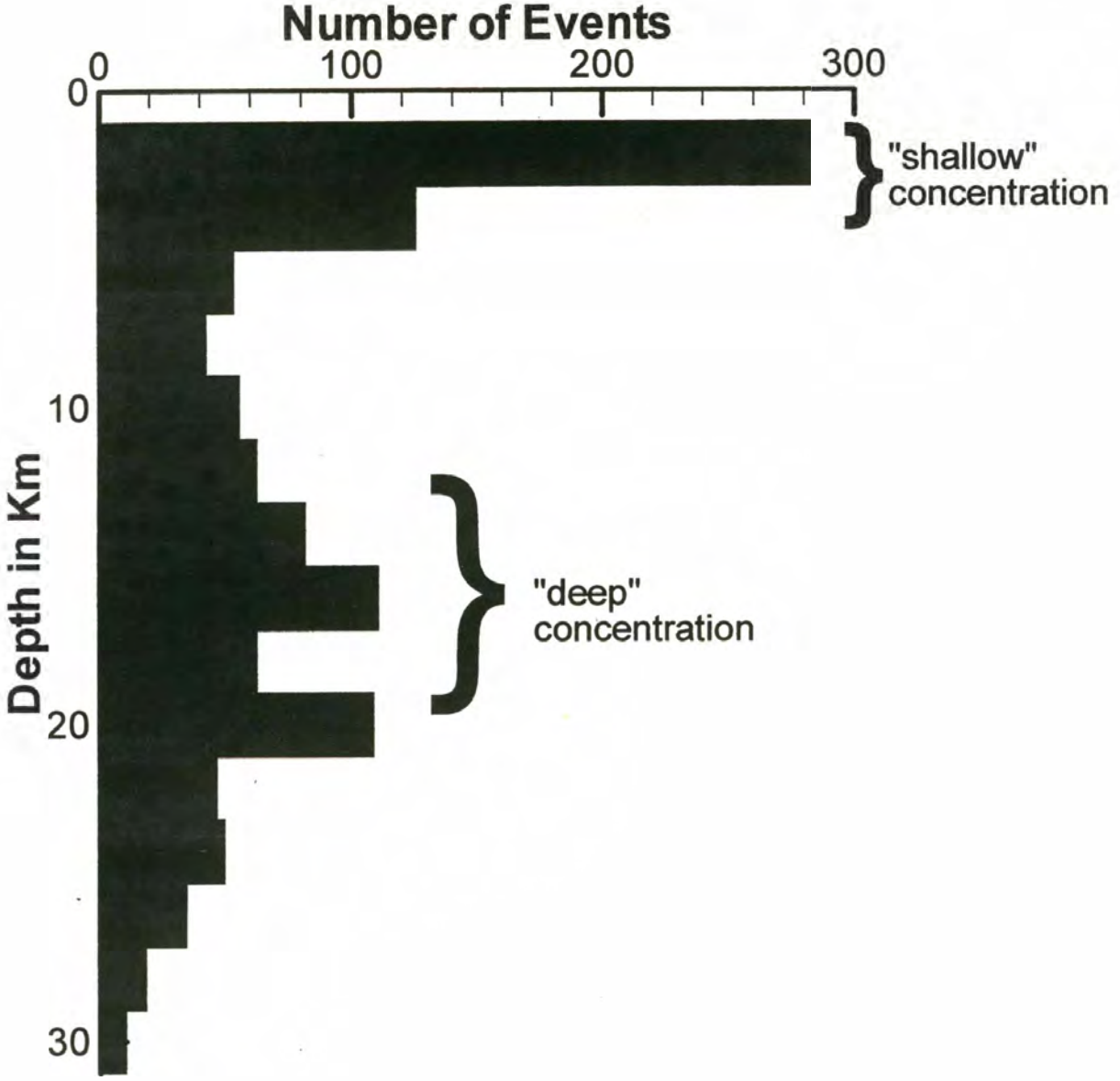

Figure 13. The number of events that occur within each depth interval in the depth distribrution analysis on Figure 11. A bimodal distribrution of events can be seen, with peaks in the 0 - 4 km depth and 12 - 20 km depth ranges.

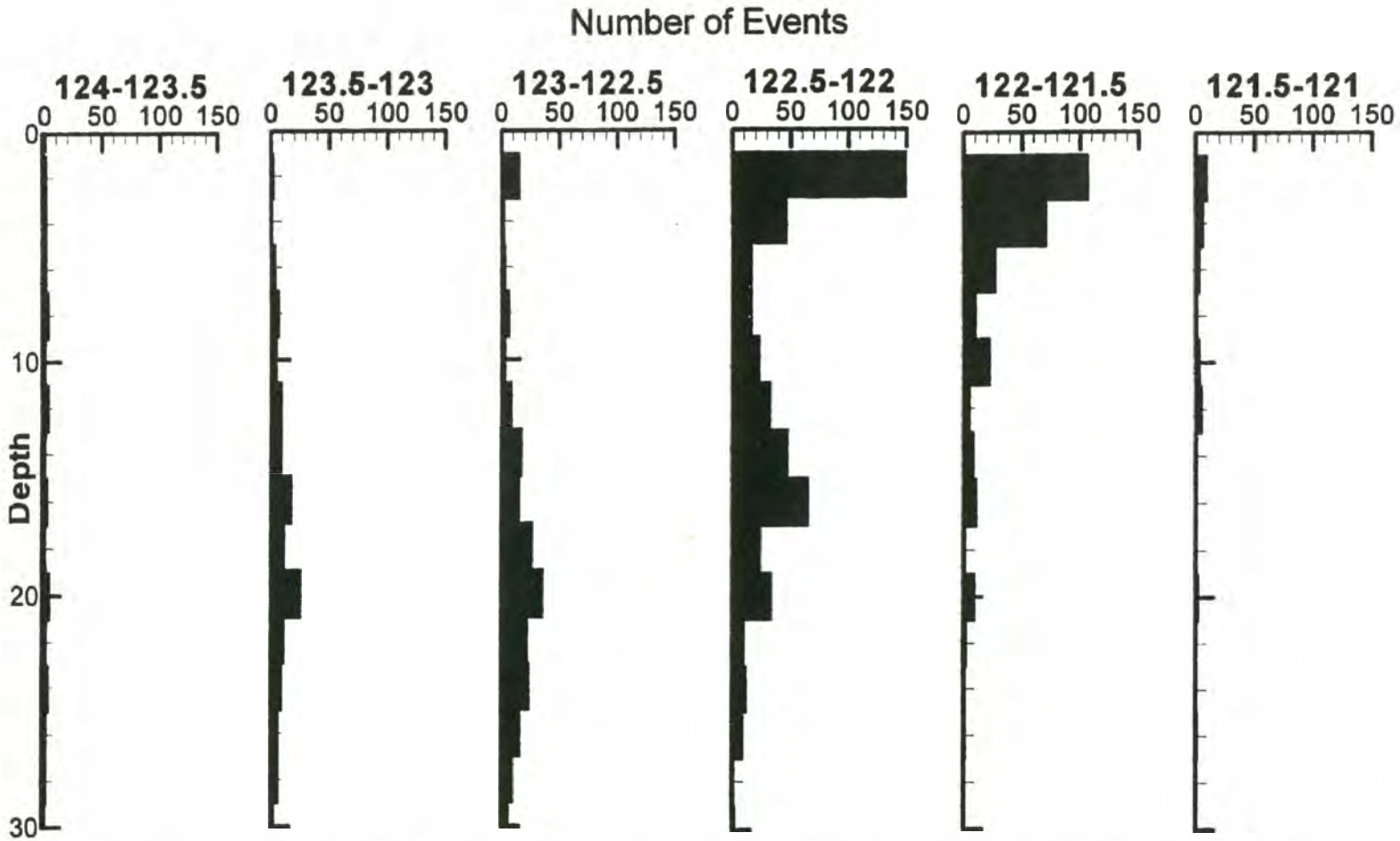

Figure 14. The number of events that occur within each of the 2 km depth intervals in the bounds of the 1/2° longitudinal sections in Figure 10. A majority of the events occur within 236.5° and 238.5°. There is a transition zone from 122.5° to122° of mostly deeper (>12 km depth) earthquakes to the west to mostly shallow (<12 km depth) earthquakes to the east. This can also be seen on Figure 10B.

Discussion

The distribution of events at depth appears to define a wedge-shaped body being deformed seismically. This could be interpreted as deformation within a cold crustal wedge (Lewis and others, 1992). Crustal temperatures are an important parameter of crustal rheology and thus influence the depth extent of faults and most other deformational structures (Sibson, 1983). Temperature distribution within the crust is due to the influence of the cold subducting slab and the magmatic arc (Figure 15). The brittle-ductile transition occurs around 350° C and the onset of substantial crustal melting begins around 450° C (Lewis and others, 1992). Earthquakes tend to initiate a short distance above the onset of weakening where the crust is strongest (Pratt and others, 1997). The earthquakes may be located along a detachment or deformation zone that marks the boundary between the relatively cold wedge and the underlying thermally weakened crust (Figure 16; Pratt and others, 1997). This interpretation is supported by the results shown on Figure 16 where the depth analysis of Figure 14 is superimposed on the geothermal modeling of Figure 15. Temperature control of rheology and present strain rate would imply seismic risk in the west due to deeper sources and seismic risk in the east from shallower sources.

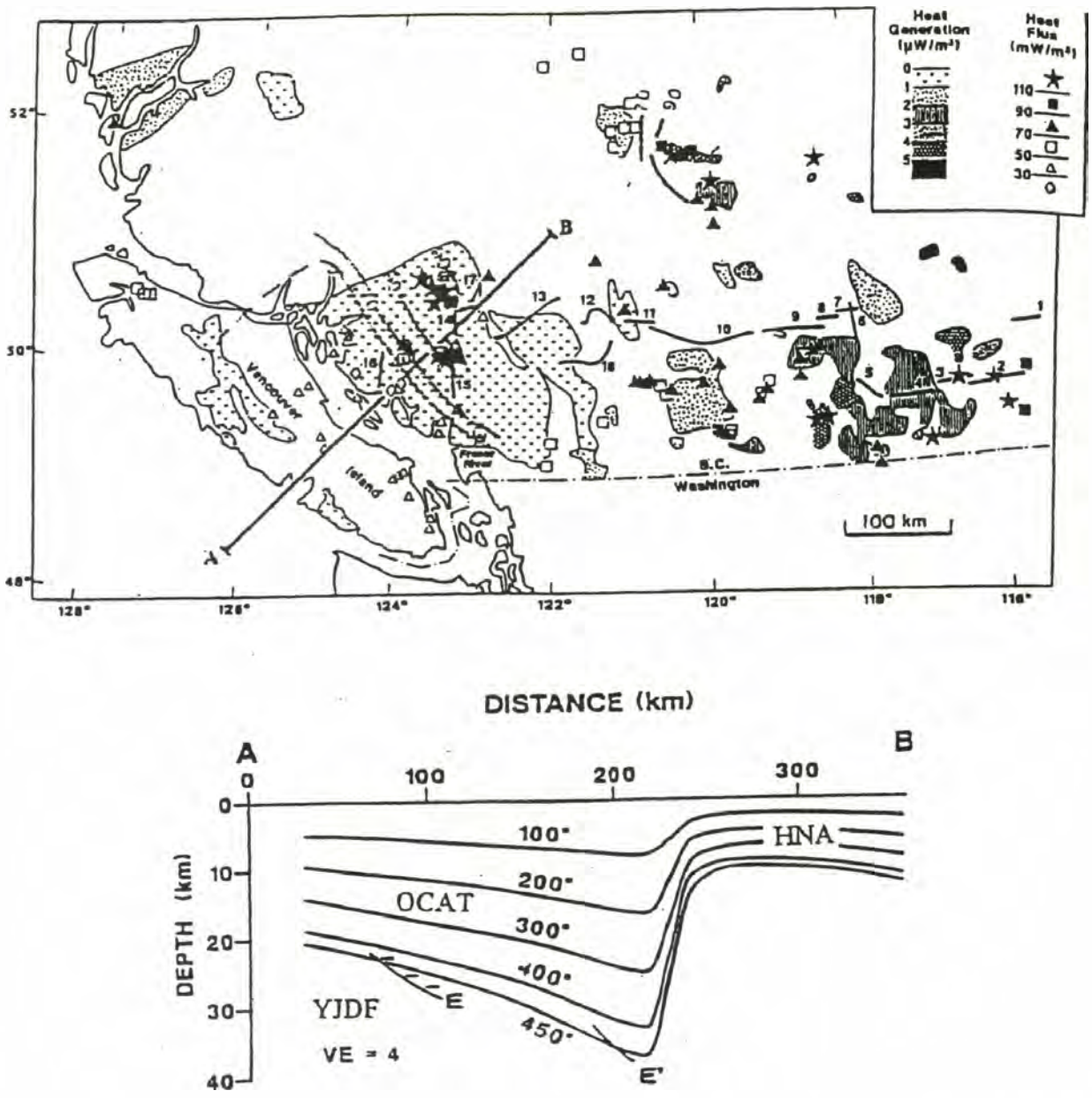

Figure 15. a.) Location map for cross-section A - B. b.) Heat flux and computed crustal temperatures along cross-section A - B. Vertical exaggeration is 4 to 1. Blackwell (1990) studied heat flux in Washington and Oregon and suggested that the heat flux in northern Washington is similar to that in British Columbia. The brittle ductile transition begins around 350° C and the onset of substantial melting begins around 450° C. The shape of the geotherms is the result of heat generation along the Cascade Volcanic Arc to the northeast in contrast to the cold slab to the southwest. HNA - Hot North American; OCAT - Old Cold Accreted Terrane; YJDF - Young Juan De Fuca. (Taken from Lewis and others, 1992)

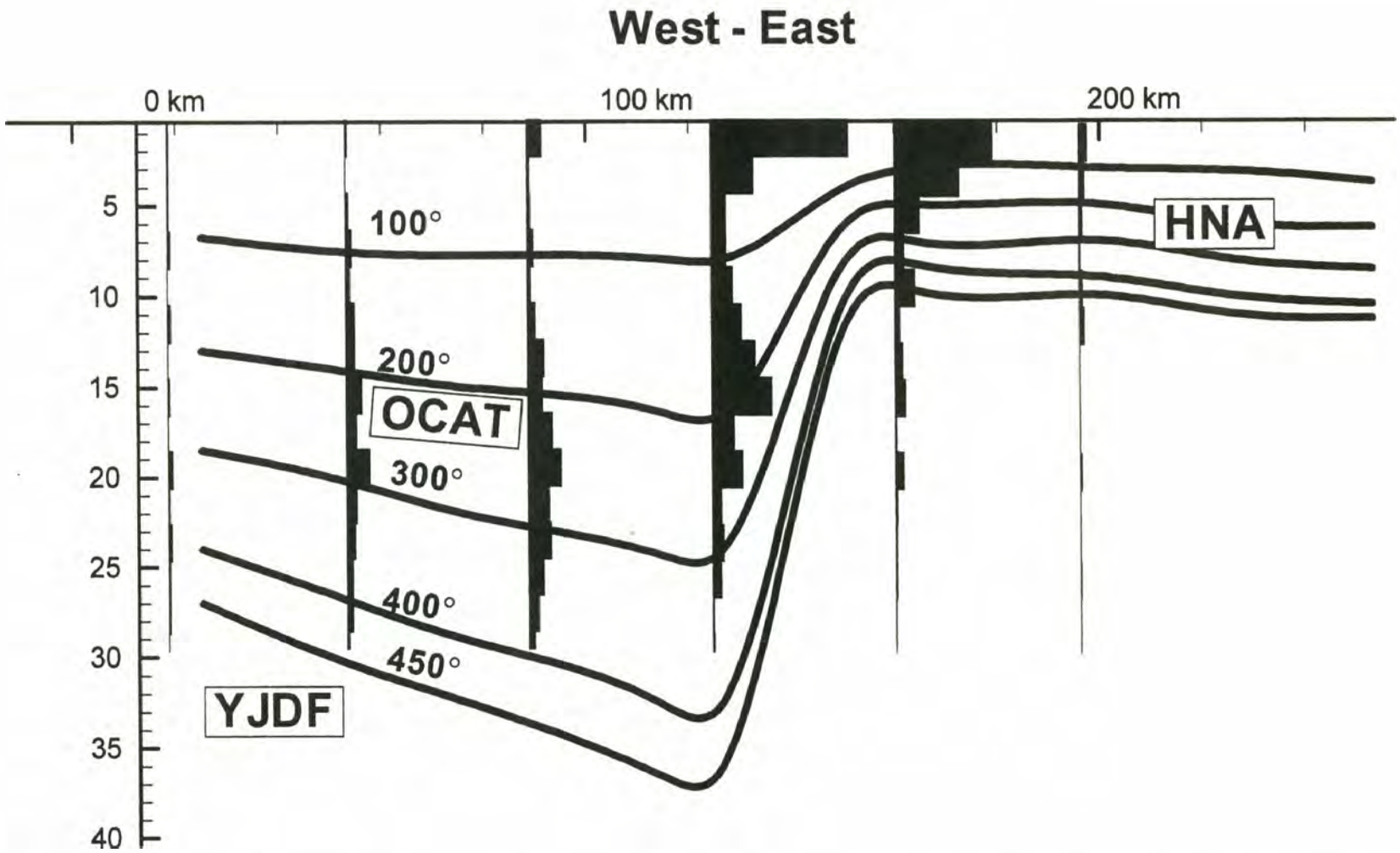

Figure 16. Geotherms taken from Figure 15 b are overlain on the depth distribrution graphs of Figure 12 to approximately the same scale. The distribrution of events as a function of depth from west to east closely parallels the expected geotherms for the region. This indicates that earthquake occurence in the study region is directly related to heat flow for the region. HNA - Hot North America; OCAT - Old Cold Accretted Terrane; YJDF - Young Juan de Fuca.

Focal Mechanism Analysis

Knowing the locations and orientations of possible fault planes is one step in understanding seismic risk. It would be better to know the sense of faulting as well. This is assessed in this section by using previously published focal mechanisms for the region of interest. These come from two independent sources, Qamar (1992) and Mulder (1995).

Focal mechanisms for more southerly earthquakes were determined by Qamar (1992) for all events having 10 or more picked first motions using the WRSN's database from earthquakes that occurred between 1970 and 1991. Of the 2303 such events, 22 were rejected by Qamar because their magnitude was less than 1.0, and 472 because they had ambiguous focal mechanisms. The WCTN's database was used by Mulder (1995) to analyze focal mechanisms for events to the north occurring between 1981 and 1991. For each event, the three acceptable criteria are: 1) magnitude greater than 1.0, 2) determined to lie within the North American plate, and 3) had data at four or more stations with depth errors less than 7 km (Mulder, 1995). This dataset had 111 events with focal mechanisms from southwest British Columbia and surrounding area (Mulder, 1995). Events from both datasets that fell within the bounds of the study region were used in this study (Figure 17).

Anderson's Theory of Faulting

Anderson (1942) provided a theoretical explanation for the three main types of faulting: normal, thrust, and strike slip (Figure 18). The theory states that if a

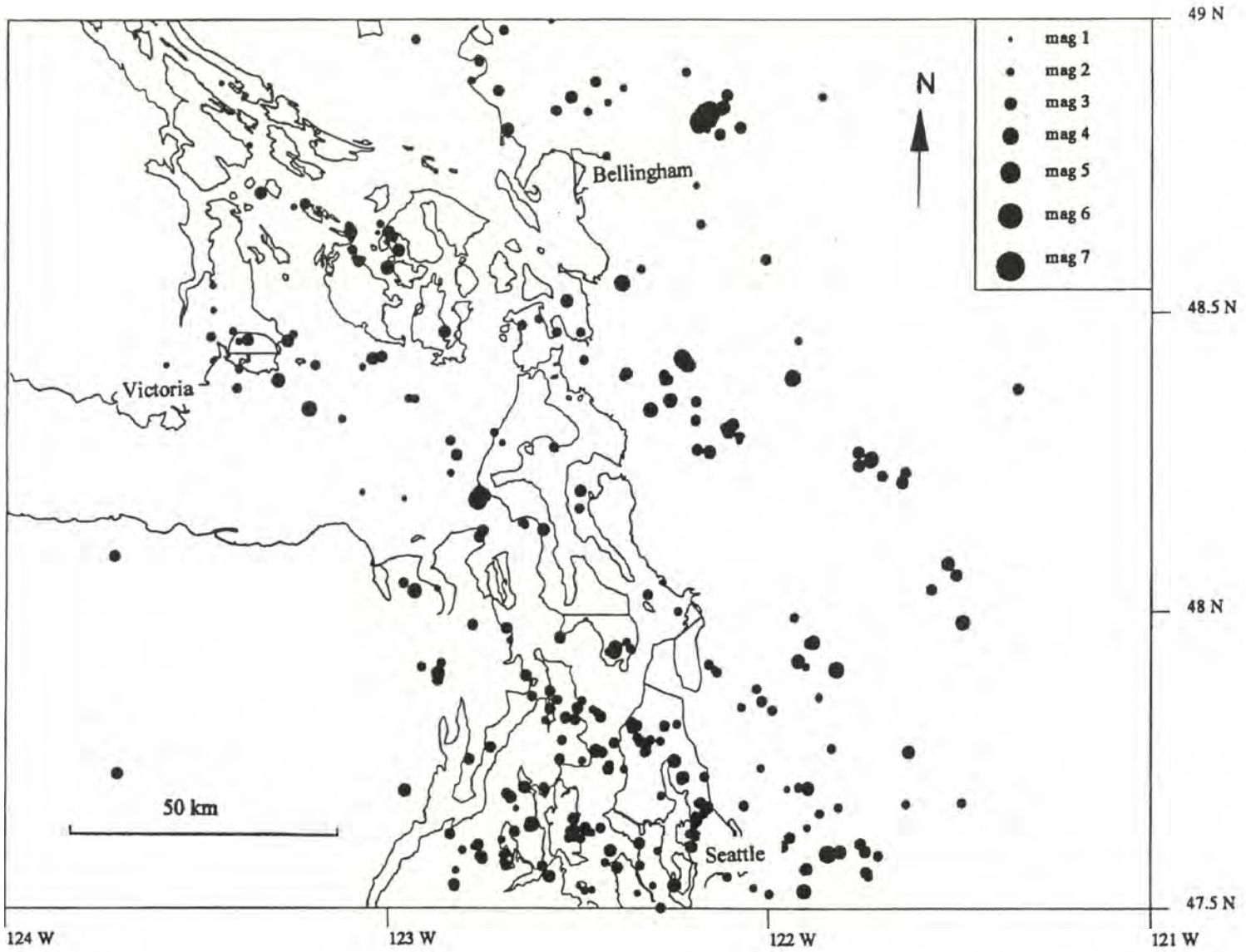

Figure 17. Epicentral locations of recorded earthquakes with focal mechanisms from both WRSN and WCTN. All events are 30 km or shallower. All events N of 48° were used for creating Table 1 and Figure 26.

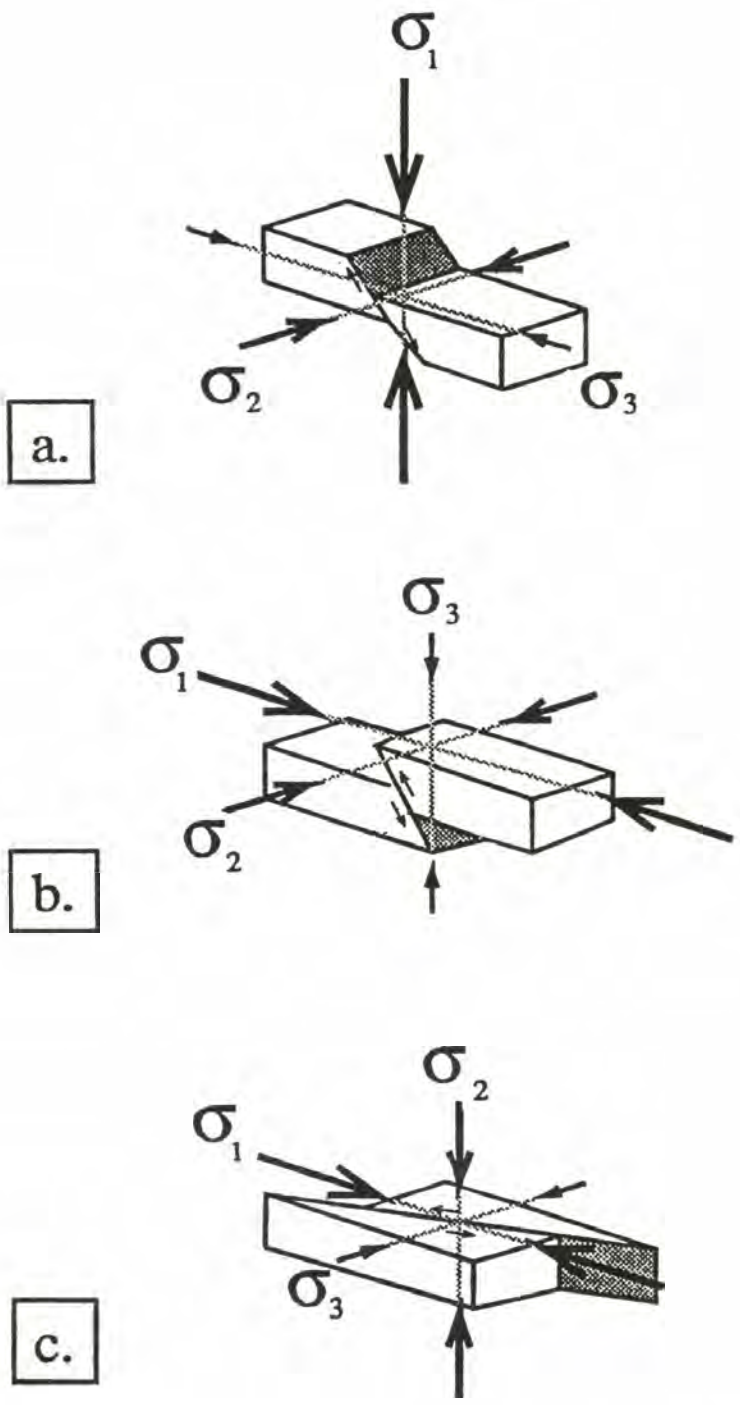

Figure 18. Anderson's theory of faulting, showing relationship between the principal stress axes orientation and the different ideal fault types. Length of principal stress arrows is proportional to the magnitude of the principal stresses. a.) Normal fault with maximum compressive stress vertical. b.) Reverse fault with minimum compressive stress vertical. c.) Strike-slip fault with intermediate compressive stress vertical. σ1, σ2, and σ3 are assumed to coincide with the Pressure, B and Tension axes in focal mechanisms respectively.

homogenous, unfractured rock is subjected to triaxial stresses ($\sigma 1$, $\sigma 2$, $\sigma 3$), it will fail by slip on one of two possible planes of maximum shear stress. These planes intersect along the intermediate stress axis and have poles that subtend angles less than 45 degrees to the greatest principal stress axis. Ideally, the type of fault that develops depends on which of the three principal stress axes is nearest to vertical (Davis, 1984; Twiss and Moores, 1992). Normal faults occur when $\sigma 1$ is vertical; reverse faults occur when $\sigma 3$ is vertical; and strike slip faults occur when $\sigma 2$ is vertical (Figure 18).

More realistically, rocks are not homogenous and unfractured. When subject to stress, they react in a manner similar to Anderson's theory, but slip tends to occur on preexisting zones of weakness due to the lower shear stresses needed to initiate movement. Thus, focal mechanisms are not always reliable indicators of the orientation of the principal axes. They are, however, more reliable for the orientation of the actual displacement during an earthquake.

Premise of Focal Mechanisms

Focal mechanisms are lower hemisphere spherical projections of seismic rays from an earthquake. Distribution of contrasting first motions can be used to deduce possible fault planes and stress conditions for the earthquake (Figures 19 and 20). Focal mechanisms have two perpendicular nodal planes. One of these is the fault plane. Which of the two planes is the fault plane cannot be determined solely from the first arrival data. Additional information is necessary. Focal mechanisms also have three principal axes; Pressure, B, and Tension. These are assumed to coincide with the three principal stress

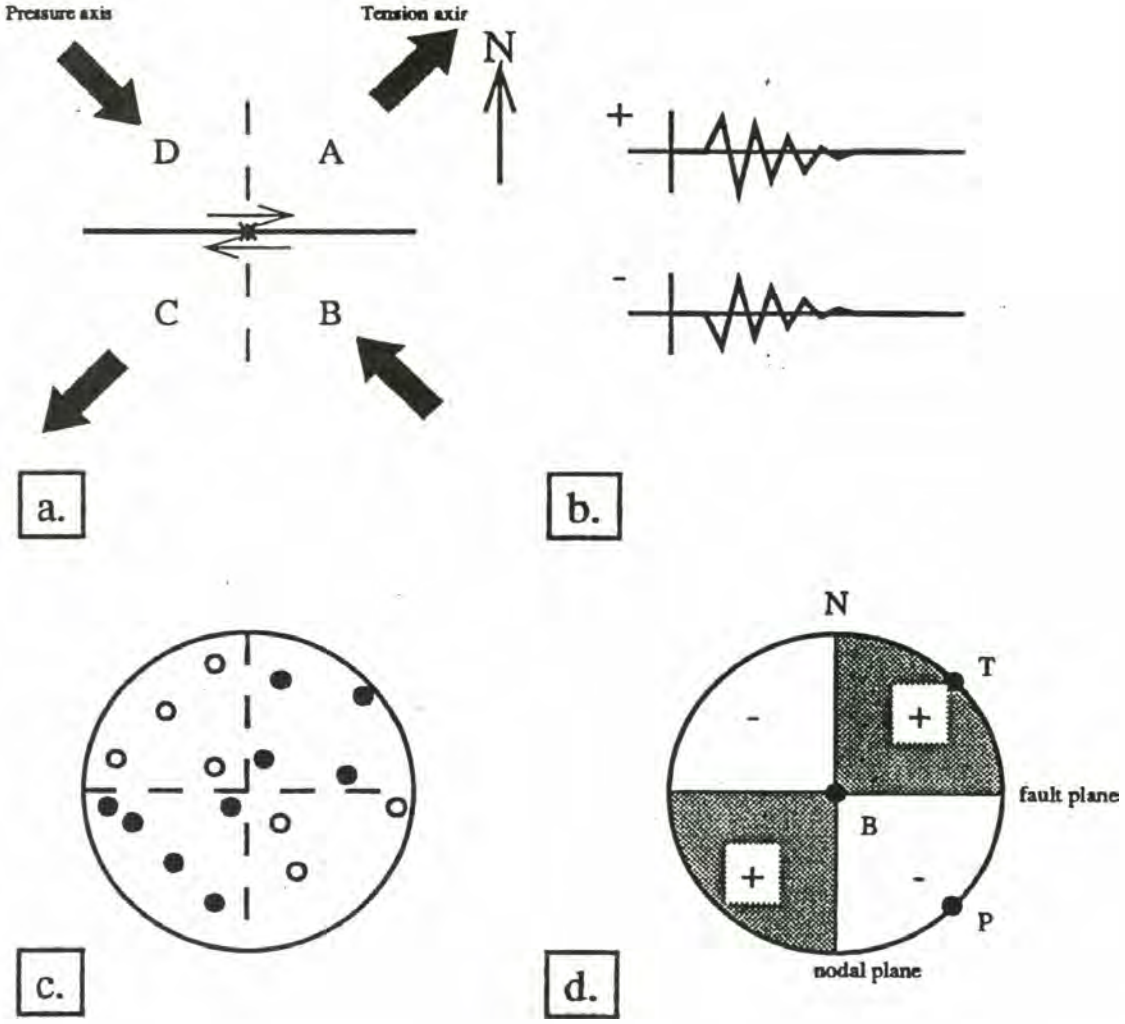

Figure 19. a.) Map view of a strike-slip fault. The first P-waves recorded at stations in sections A & C will be compressional (positive, up); the first P-waves recorded in sections B & D will be dilatational (negative, down). b.) Positive and negative first recorded P-waves. c.) Compressional and dilatational first motions for each seismograph that recorded the event plotted on a lower focal hemisphere. Azimuth of point plotted is that from event to seismic station, points plotted closer to the center are for recording stations farther away. d.) The corresponding focal mechanism.

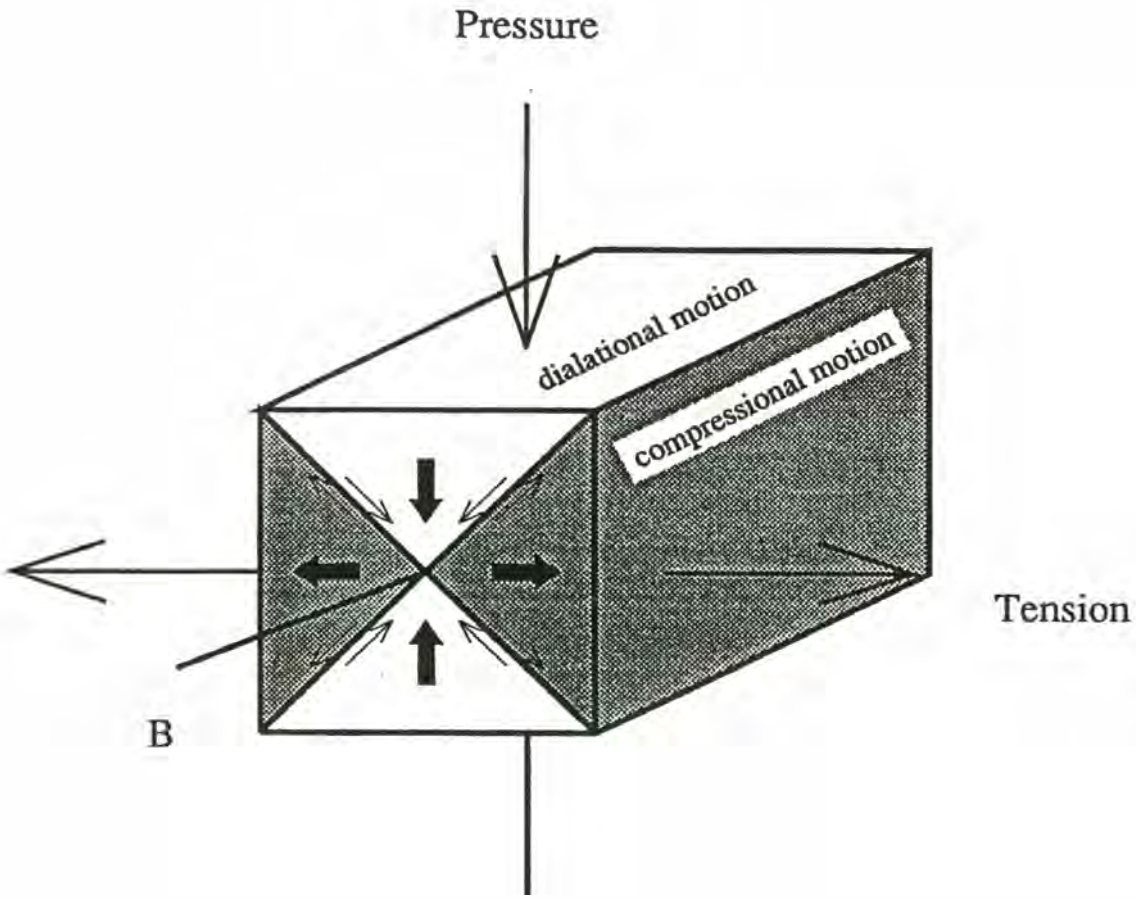

Figure 20. Two nodal planes separate the four quadrants into compressional and dialational. The pressure axis always bisects the dialational quadrant, while the tension axis always bisects the compressional quadrant. The B axis is always the intersection of the two planes.

axes (Figure 18 and 20):

Pressure $\Leftrightarrow$ $\sigma 1$ $\Leftrightarrow$ greatest principal stress

B $\Leftrightarrow$ $\sigma 2$ $\Leftrightarrow$ intermediate principal stress

Tension $\Leftrightarrow$ $\sigma 3$ $\Leftrightarrow$ least principal stress

Principal stresses that induced motion along the fault plane are determined from the nodal planes and the type of motion that occurred (Figure 20). The three principal stress axes are mutually perpendicular and the B axis is parallel to the intersection of the two nodal planes. The pressure axis lies 45° from the two nodal planes in the dilatational region (Figure 20). The tension axis lies 45° from the two nodal planes in the compressional region (Figure 20). From the focal mechanism, we can determine the type of motion that occurred (i.e. dip-slip, strike-slip, or oblique motion), and two possible nodal planes along which slip occurred (Figure 21).

Focal mechanisms are made by plotting observed earthquake first motions from seismograph stations located at various azmuths that encircle the earthquake focus at different distances (Figure 19). For any given focal mechanism, the earthquake focus is represented as the center of the lower focal hemisphere. Compressional and dilational first motions are plotted as a vector with a certain trend and plunge. The azimuth is the direction a P-wave would take to reach a seismic station. The plunge of the vector correlates with the angle downward from horizontal that the P-wave traveled in order to reach the seismic station. If enough stations that record the event are appropriately

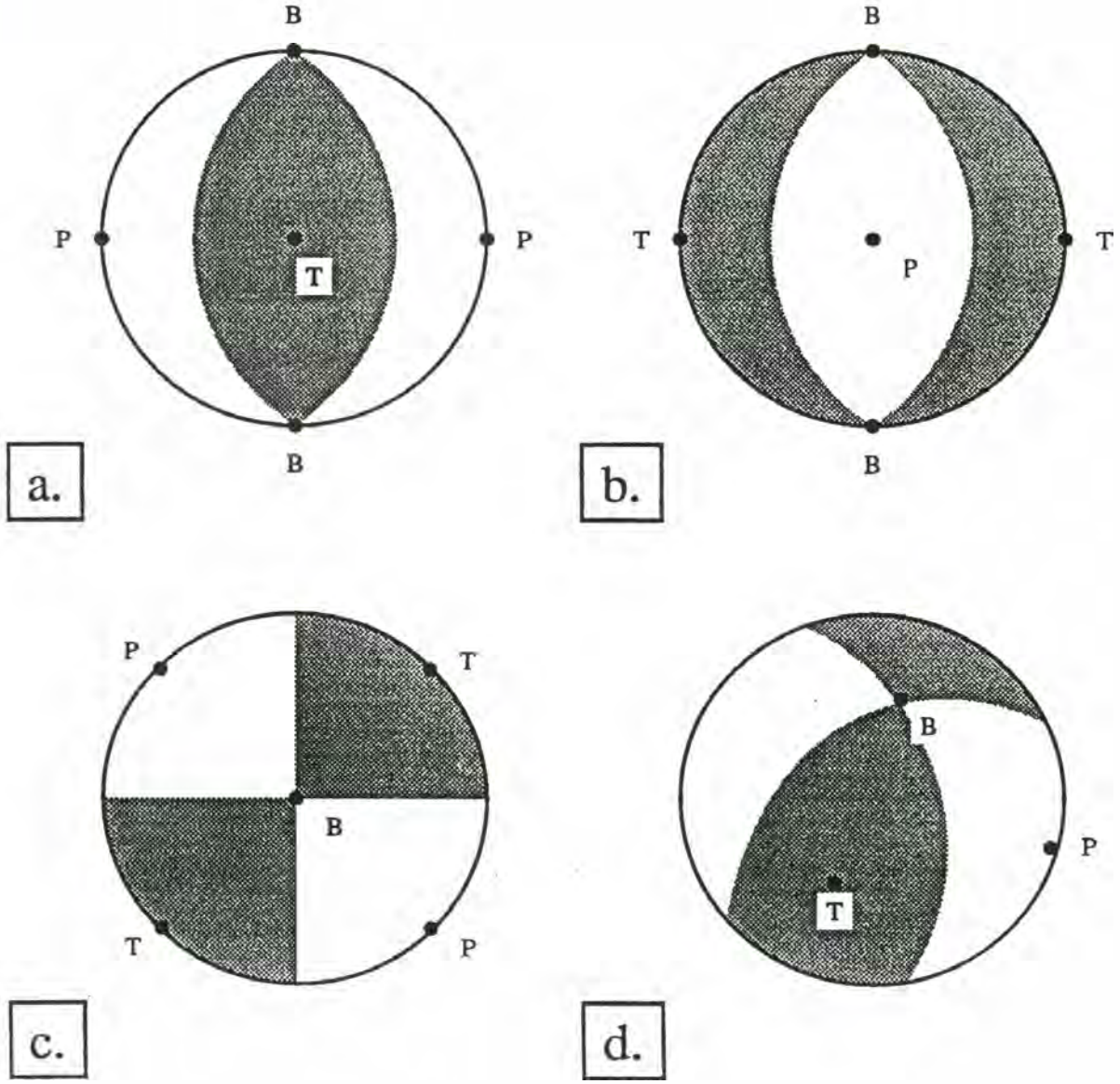

Figure 21. A few examples of common earthquake focal mechanisms. a.) North striking reverse faults. b.) North striking normal faults. c.) North striking left-lateral strike-slip fault or east striking right-lateral strike-slip fault. d.) Northwest striking left-lateral reverse fault or northeast striking right-lateral reverse fault.

distributed around the earthquake, two perpendicular planes that separate the dilatational from compressional arrivals can be found (Figure 19c). Ideally, the distribution of compressional and dilatational first motions plotted will represent both the slip motion that occurred on the fault plane and a plane perpendicular to the fault plane (Figure 21).

Seismic networks made possible the use of focal mechanisms to study the stresses that induce deformation. The overall orientation of the pressure axes for focal mechanisms of shallow earthquakes changes along the Cascadia coast (Figure 22). Pressure axes orientations do not parallel the direction of convergence of the subduction of the Juan de Fuca Plate. Instead, they parallel the strike of the subduction zone, changing from a NE-SW orientation in southwestern Washington to a NW-SE orientation in northwestern Washington (Qamar and Ludwin, 1992; Mulder, 1995). Deformation is likely the product of transpressive deformation due to the oblique convergence along the subduction front (Stanley and others, 1996). The pressure axes cluster almost horizontal NNW in the study region and N in the Puget Sound region (Figure 23; Mulder, 1995). The tension axes are distributed in a girdle whose pole coincides with the pressure axes. This relative consistency of pressure axes suggests that whatever controls the P axes controls the deformation.

Description of the Focal Mechanism Dataset

All events with epicenters that fell between 47.5° and 49° north latitude, 124° and 121° west longitude and were 30 km or shallower in depth were used for the focal mechanism study (Figure 17). All WRSN events were used, except for ambiguous ones. I

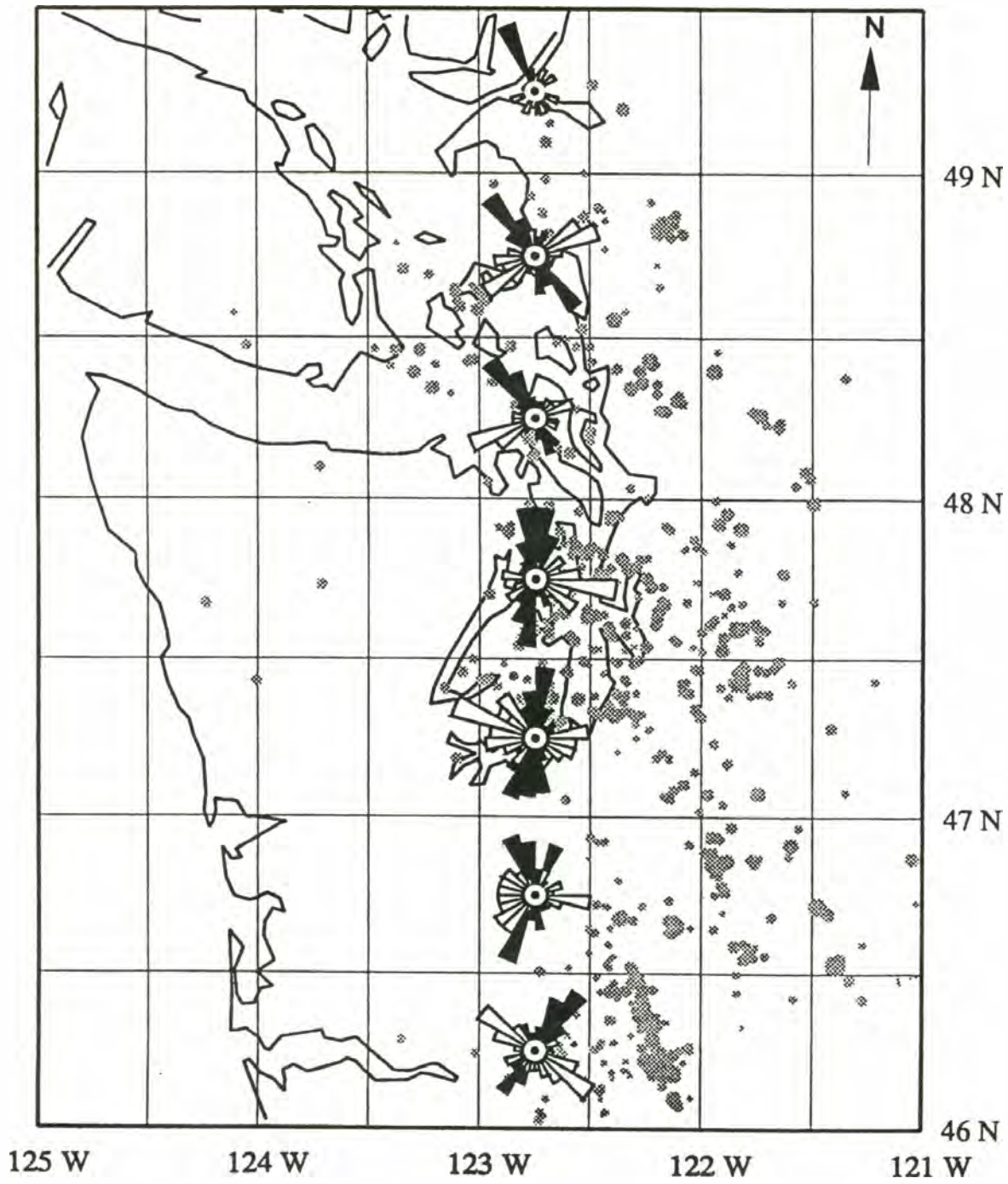

Figure 22. Rose diagrams showing the distribution of P and T azimuth. Black petals show P azimuth; white petals show T azimuth. Pressure directions show a rotation from northwest in the northern part of the region to northeast in the southern part of the region parallel to the trend of the subduction front. This indicates that faulting is the result of transpressive deformation from the parallel component of subduction, as opposed to compressive deformation from the perpendicular component of subduction. This was generated from focal mechanisms in the WRSN's database.

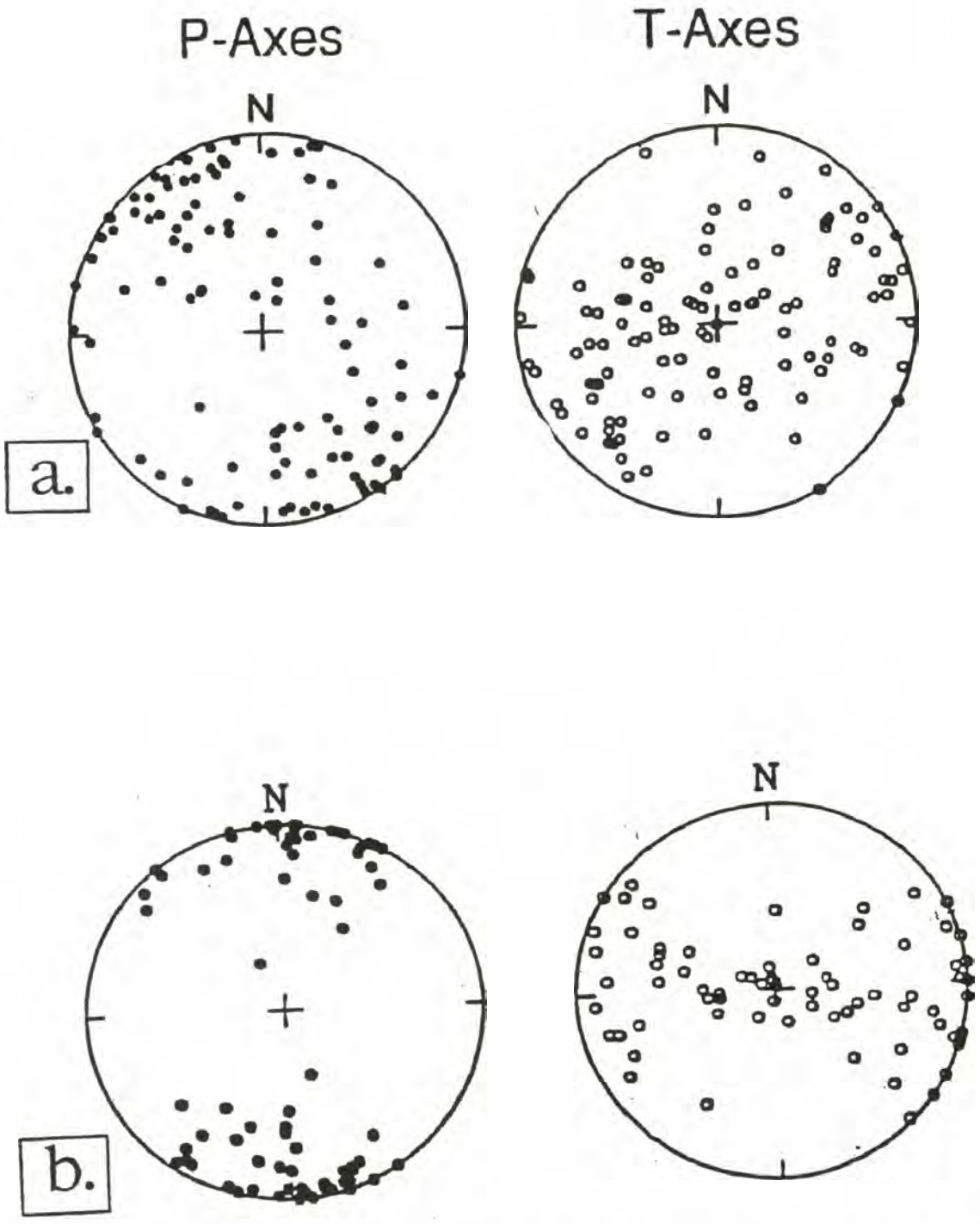

Figure 23. Plotted P and T axes on a lower focal hemisphere projection. a.) Events for southern British Columbia and northwestern Washington. b.) Events for west central Washington. Note the change in orientation of the axes. The tension axes have a girdled distribution indicating that the pressure orientation is the dominating factor in deformation. (Taken from Mulder, 1996)

added all events in the WCTN database that we did not already have focal mechanisms for. The result was 130 events from WRSN's database and 64 from WCTN's database.

Fault Classification Diagrams

The geometry of the stress axes and the fault and nodal planes that make up a focal mechanism is unique (Figure 20). This geometry allows any focal mechanism to be represented by the plunges of the three stress axes. Frolich (1993) created a ternary diagram that represented this relationship. For this study, Frolich's ternary diagram was modified to simplify presentation of this relationship. A fault classification diagram is a plot of the plunges of P, T, and B such that each of the three corners represent a different fault type and any position of the three axes can be plotted on it. The plunges of any two axes will determine the plunge of the third since all three axes are perpendicular. Because of this, an XY graph was developed for this study that uses the plunges of P and T along the X and Y axes. A constant plunge of B then defines a curved contour (Figure 24). For each possible P and T plunge combination there is a corresponding B plunge that can be found by taking the cross product of the P and T axes (Frolich and Davis, 1993). The plunge of B (Bp), as a function of the plunges of the P and T axes (Pp and Tp)is:

$$Bp = \text{asin}\left(1 - \sin^2 Pp - \sin^2 Tp \right)^{0.5}$$

All possible focal mechanisms can be plotted as a function of the plunge of P and T. The resultant graph appears as a triangular region with P, T, and B axes in each of the diagrams three vertices (Figure 24). At each of the three vertices is a "pure" fault motion:

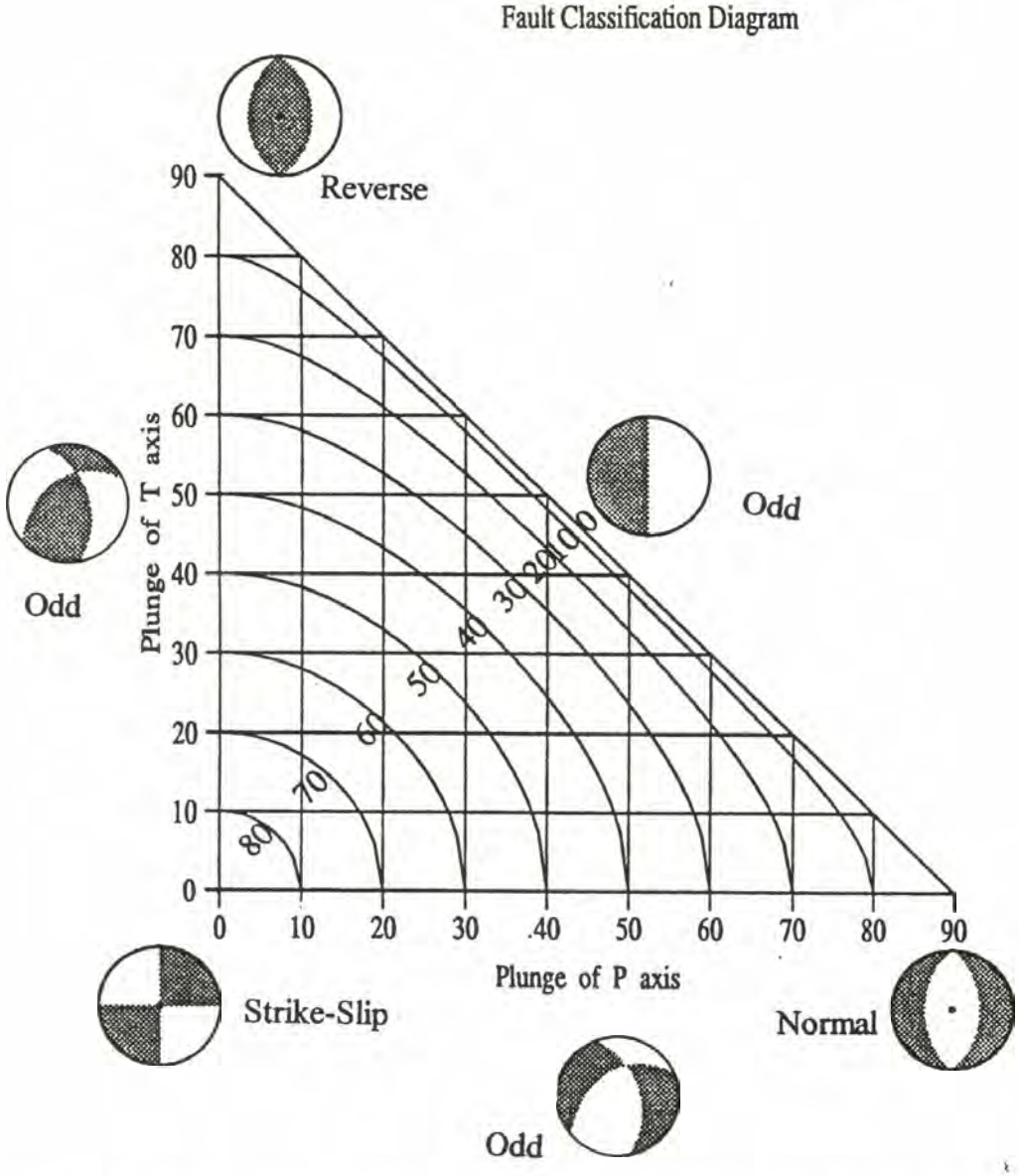

Figure 24. A Fault Classification Diagram, developed in this work, for the determination of fault types using focal mechanisms. The plunge of the P and T axes are plotted on this XY style graph. The plunge of the B axis can be found along the curved contours. In each of the three vertices is a principal axis with a plunge of 90. A reverse fault with the fault and nodal planes dipping 45 occurs when the plunge of the T axis is 90. All mechanisms with a T axis plunging greater than 45 are considered reverse. A normal fault with the fault and nodal planes dipping 45 occurs when the plunge of the P axis is 90. All mechanisms with the plunge of the P axis greater than 45 are considered normal. A strike-slip fault with the fault and nodal planes dipping 90 occurs when the plunge of the B axis is 90 or the plunges of P and T axes are 0. All mechanisms with the B axis plunging greater than 45 are considered strike-slip. Mechanisms with the P, T, and B axes plunging less than or equal to 45 are considered to be odd. Odd events are not predominantly reverse, normal or strike-slip.

normal, reverse and strike-slip, oblique slip faults fall in between. The type of motion that occurred along the fault can be defined by the plunge of P and T. To generalize, all events with their pressure axes plunging greater than 45° are considered normal, all events with their tension axes plunging greater than 45° are considered reverse, and all events with their B axes plunging greater than 45° are considered strike - slip (Figure 24). Events that don't fall into any of these categories are termed odd (Figure 24; Frolich and Davis, 1993).

Distribution of Faulting Style

A fault classification diagram for the region between 48° to 49° N and 124° to 121 ° W shows that all types of faulting have occurred (Figure 25). Table 1 gives the percentages of the types of earthquakes that have occurred at various depth ranges using the diagram explained above. Figure 26 shows the percentages of different types of events at different depths. From Figure 26 it is obvious that reverse faulting is most common near the 15 km depth range, with the second most common being reverse faulting at shallower levels. In contrast, strike slip faulting is more common than reverse faulting at an average 25 km depth. Normal events show a steady decline with increasing depth. Odd events are evenly distributed at all depths.

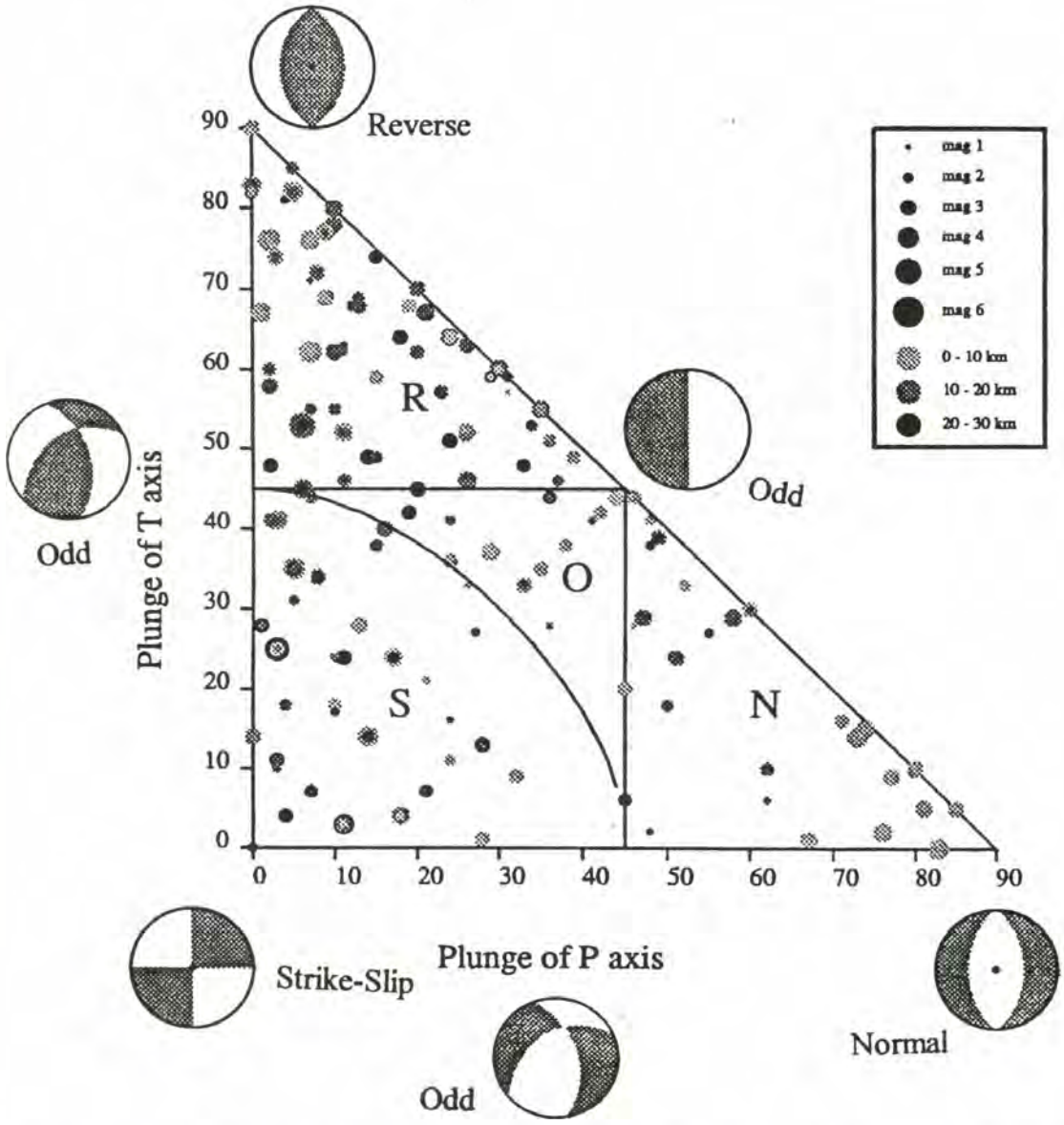

Figure 25. Fault classification diagram for all focal mechanisms from events in the study region between 48° - 49° N latitude and 124° - 121° W longitude. Events are scaled to magnitude and depth. R is in the region of reverse faulting focal mechanisms. S is in the region of strike-slip focal mechanisms. O is in the region of odd focal mechanisms. N is in the region of normal focal mechanisms.

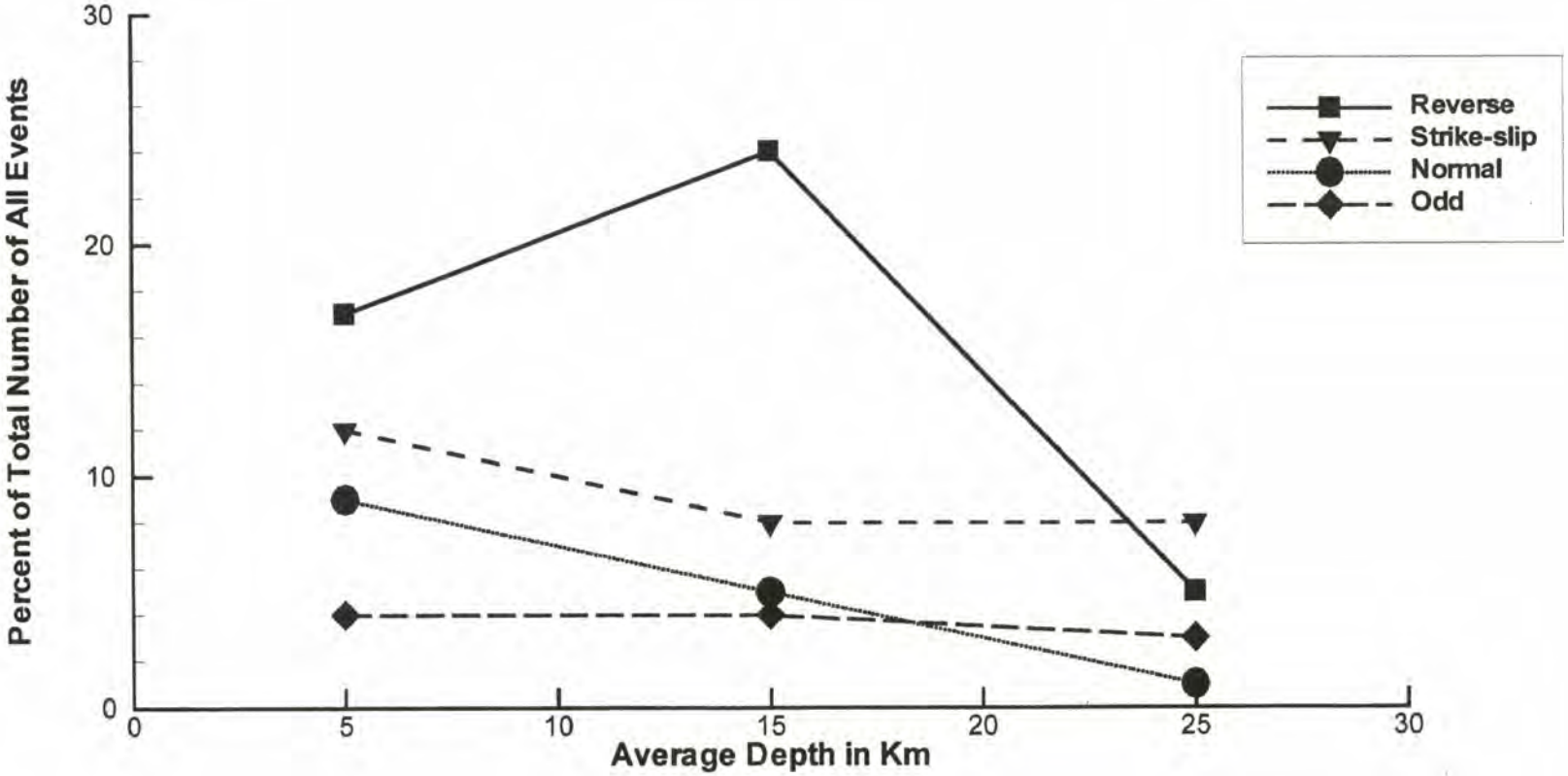

Figure 26. Graph of percentage of different fault types vs. the depth at which they occurred. Reverse events are dominant at an average of 15 km. Strike-slip events are more numerous than reverse events at depths greater than 20 km depth. The number of normal events declines steadily with depth. Odd events (not clearly any of the three other fault types) stay constant with depth.

Table 1. Percentages of the events in each specific depth and fault type.

Depth / Fault Type	0 - 10 km	10 - 20 km	20 - 30 km	Total %
reverse	17%	24%	5%	46%
strike-slip	12%	8%	8%	28%
normal	9%	5%	1%	15%
odd	4%	4%	3%	11%
Total %	42%	41%	17%	100%

The buttress for the traveling forearc, undergoing transpressive deformation, is generally considered to be along the southern edge of the study region. But, reverse and strike-slip events make up 74 percent of the focal mechanisms, which would be expected in a transpressive regime assuming the forearc is traveling parallel to the Cascade volcanic arc, towards the buttress in Canada. In this case, the majority of events expected are reverse with an overall north-south shortening of the forearc and strike slip faulting would be expected parallel to the Cascades. The results here suggest that the northern Puget Lowland is itself part of the traveling forearc, and not the relatively stable buttress.

Some generalizations can be made about the different levels in the crust by looking at the how fault types are distributed. The majority of the shallow crustal earthquakes (0 to 10 km) occur at a depth of less than 4 km. Crust at this level is likely to be brittle and heterogeneous. These conditions and preexisting zones of weakness can account for

events of all types. The domination of reverse events at 10 to 20 km indicates that a sub-horizontal pressure component is controlling deformation and it is consistent with a transpressive regime (Figure 24). Transpressive deformation is the result of traction between the subducting Juan de Fuca plate and the overriding North American plate. The transition to predominately strike-slip faulting at deeper levels is one of the more notable trends. Based on consistent NW-SE orientations of the P-axes, we can assume the forearc is deforming under fairly uniform stress conditions, although we can see from the girdle pattern on Figure 23 that the second and third principal stresses are probably close in value and somewhat interchangeable. Changes in the predominant type of faulting at-depth could be the result of swapping of σ_2 and σ_3 due to a higher lithostatic load or a change in the preferred orientations of preexisting zones of weakness

Discussion

Using the fault classification method described earlier, twelve maps were made that show focal mechanisms of each fault type (reverse, strike-slip, normal, and odd) plotted by depth (0 to 10 km,10 to 20 km and,20 to 30 km) (Figures 27 - 38). From each map, patterns in each of the different types of faulting are noted below. The maps extend south of the study region primarily to show the southern continuation of the southern Whidbey Island fault.

That earthquakes within Puget Sound are the result of transpressive deformation in the Cascadia forearc caused by oblique subduction is generally accepted. This is partially supported by focal mechanisms which shows reverse faulting is the predominant type of

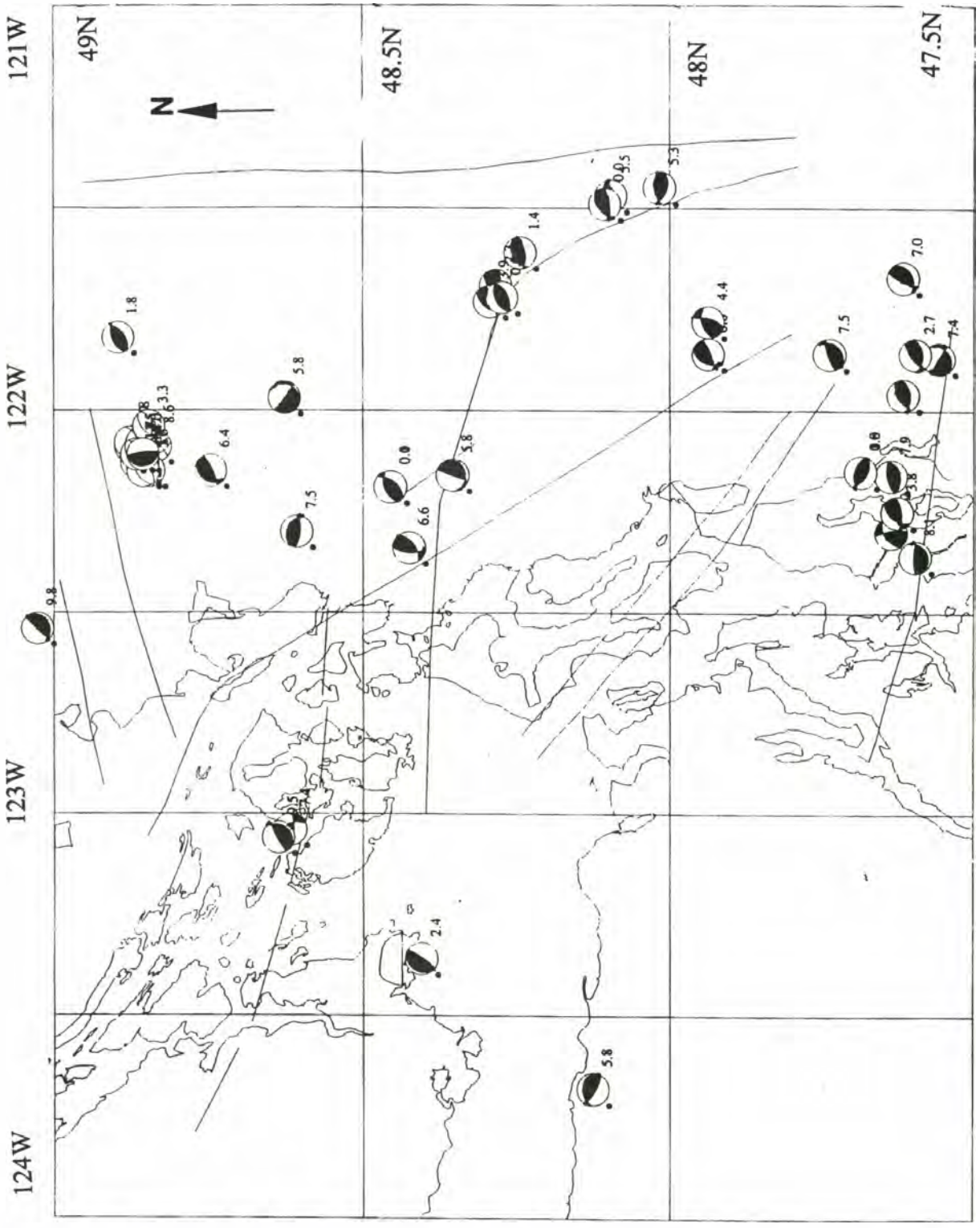

Figure 27. All focal mechanisms that were classified as reverse and fell between 0 and 10 km were plotted next to the epicenter. Next to each focal mechanism is the depth at which the event occurred. The major faults and lineaments from Figure 9 are plotted as well.

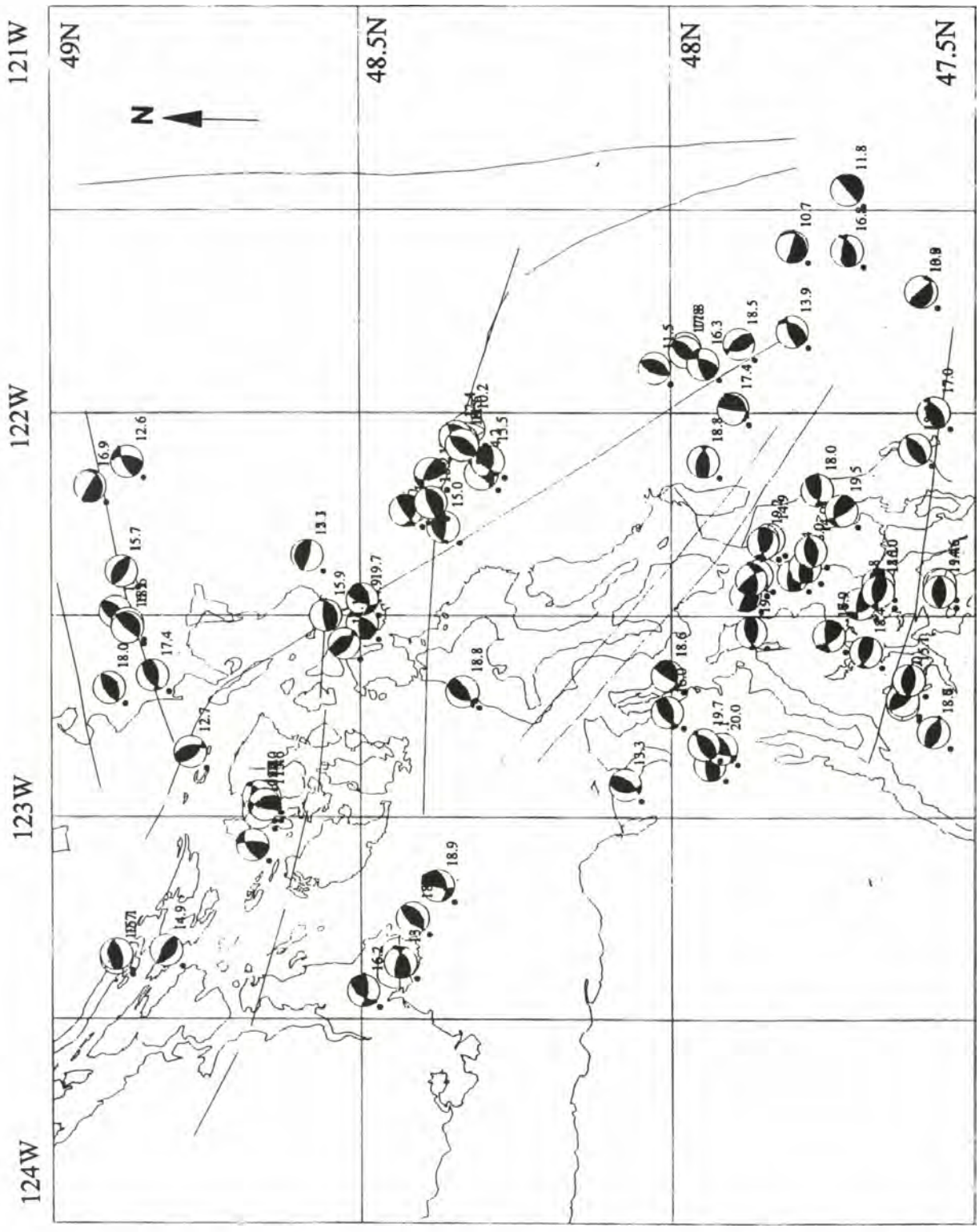

Figure 28. All focal mechanisms that were classified as reverse and fell between 10 and 20 km were plotted next to the epicenter. Next to each focal mechanism is the depth at which the event occurred. The major faults and lineaments from Figure 9 are plotted as well.

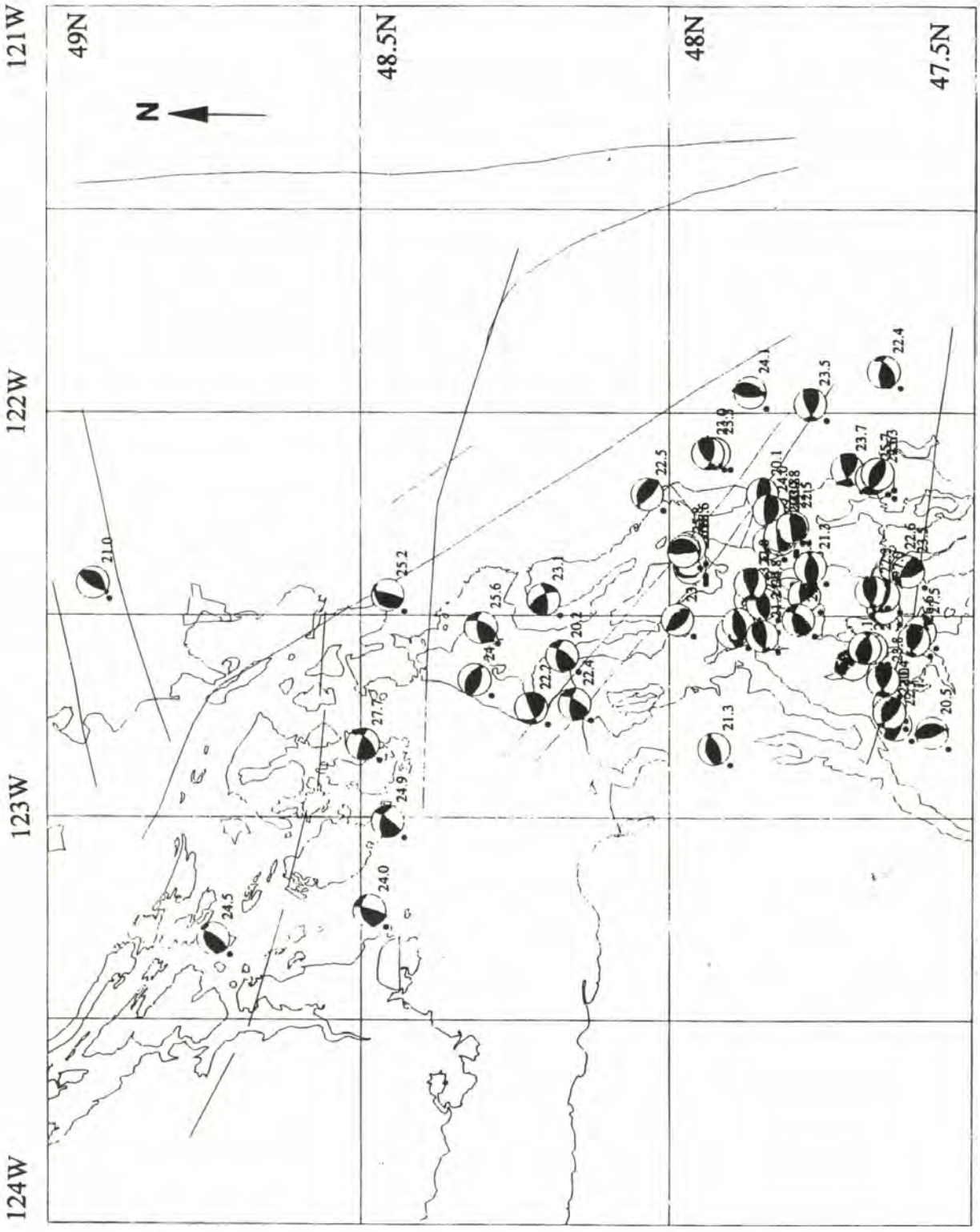

Figure 29. All focal mechanisms that were classified as reverse and fell between 20 and 30 km were plotted next to the epicenter. Next to each focal mechanism is the depth at which the event occurred. The major faults and lineaments from Figure 9 are plotted as well.

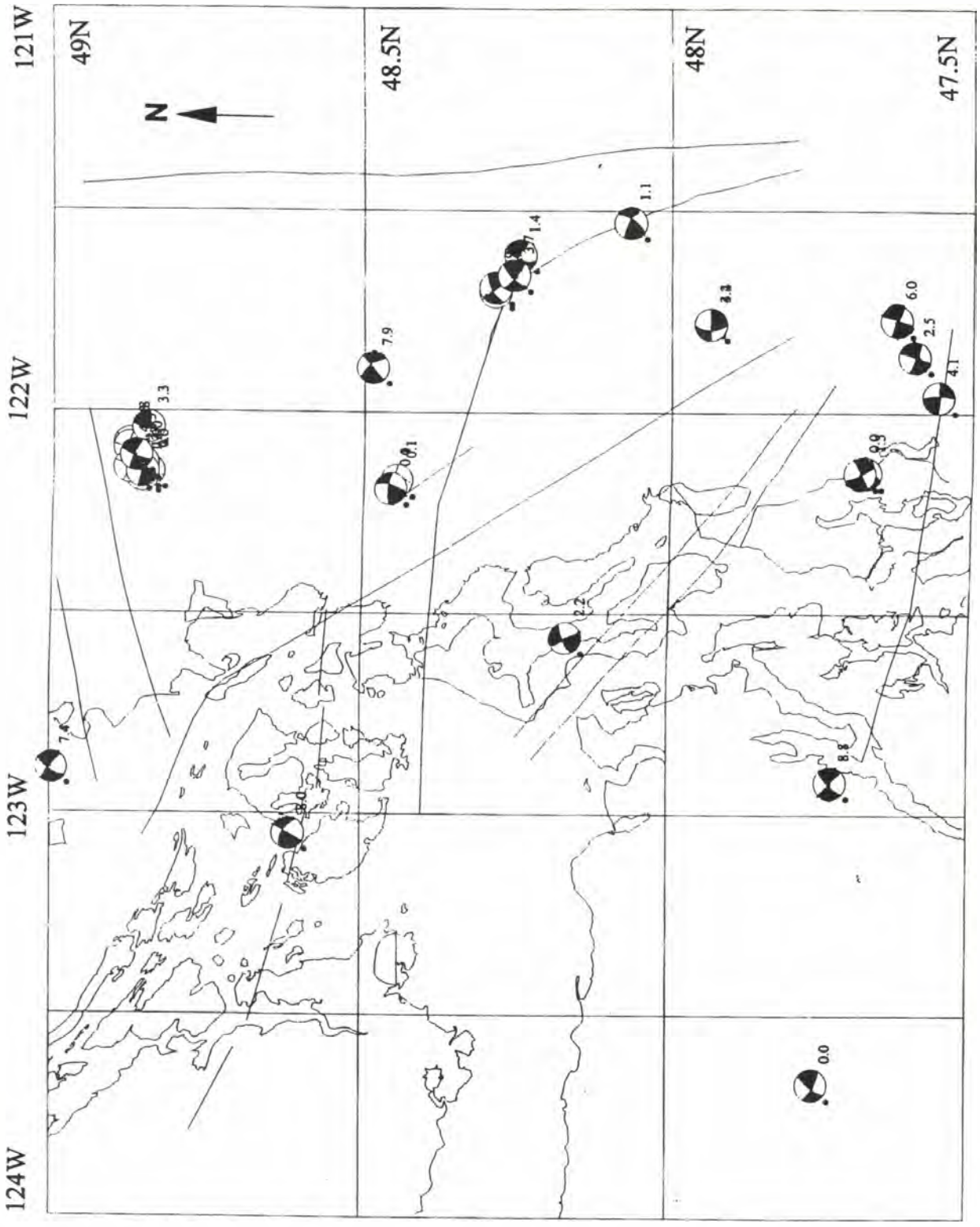

Figure 30. All focal mechanisms that were classified as strike-slip and fell between 0 and 10 km were plotted next to the epicenter. Next to each focal mechanism is the depth at which the event occurred. The major faults and lineaments from Figure 9 are plotted as well.

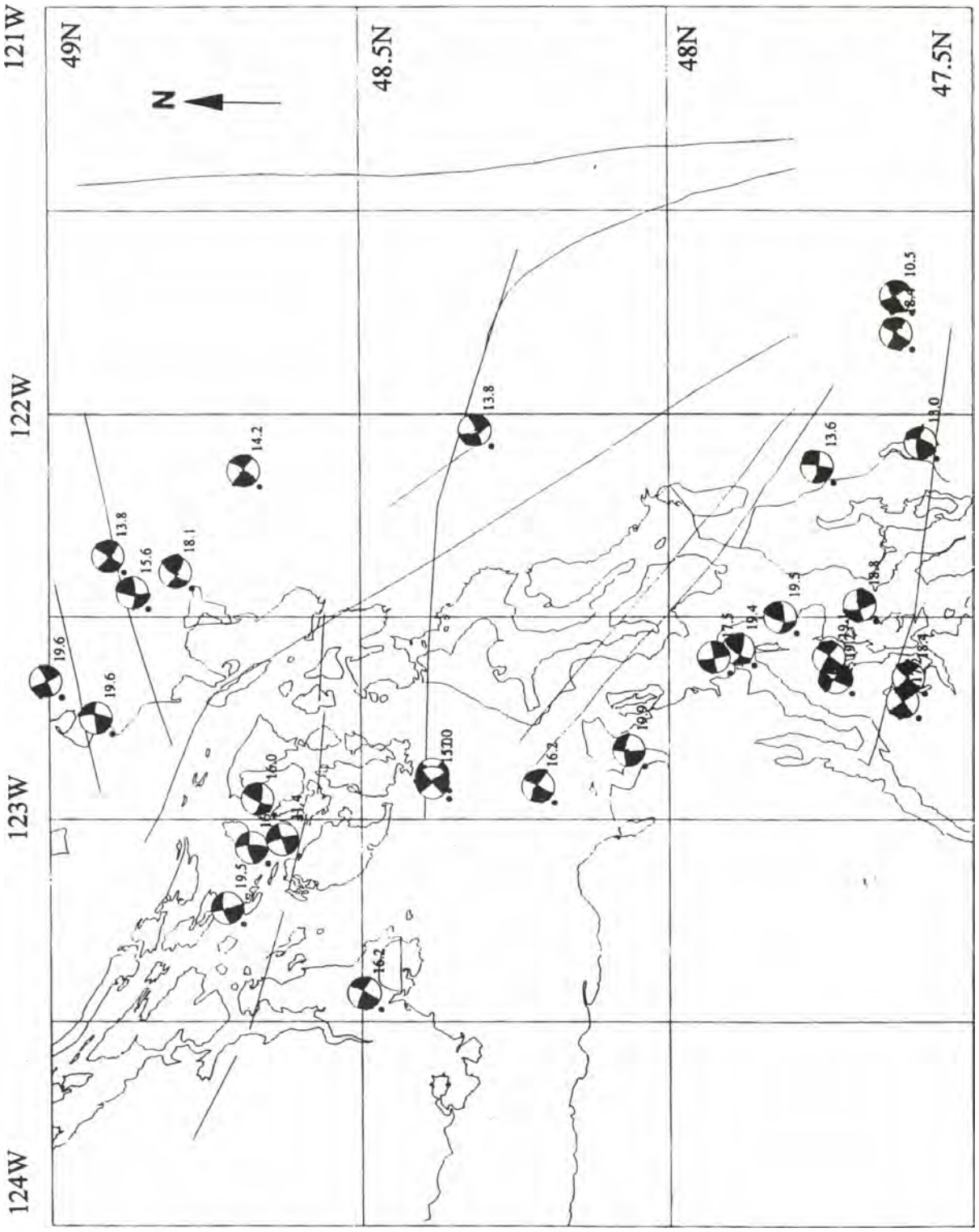

Figure 31. All focal mechanisms that were classified as strike-slip and fell between 10 and 20 km were plotted next to the epicenter. Next to each focal mechanism is the depth at which the event occurred. The major faults and lineaments from Figure 9 are plotted as well.

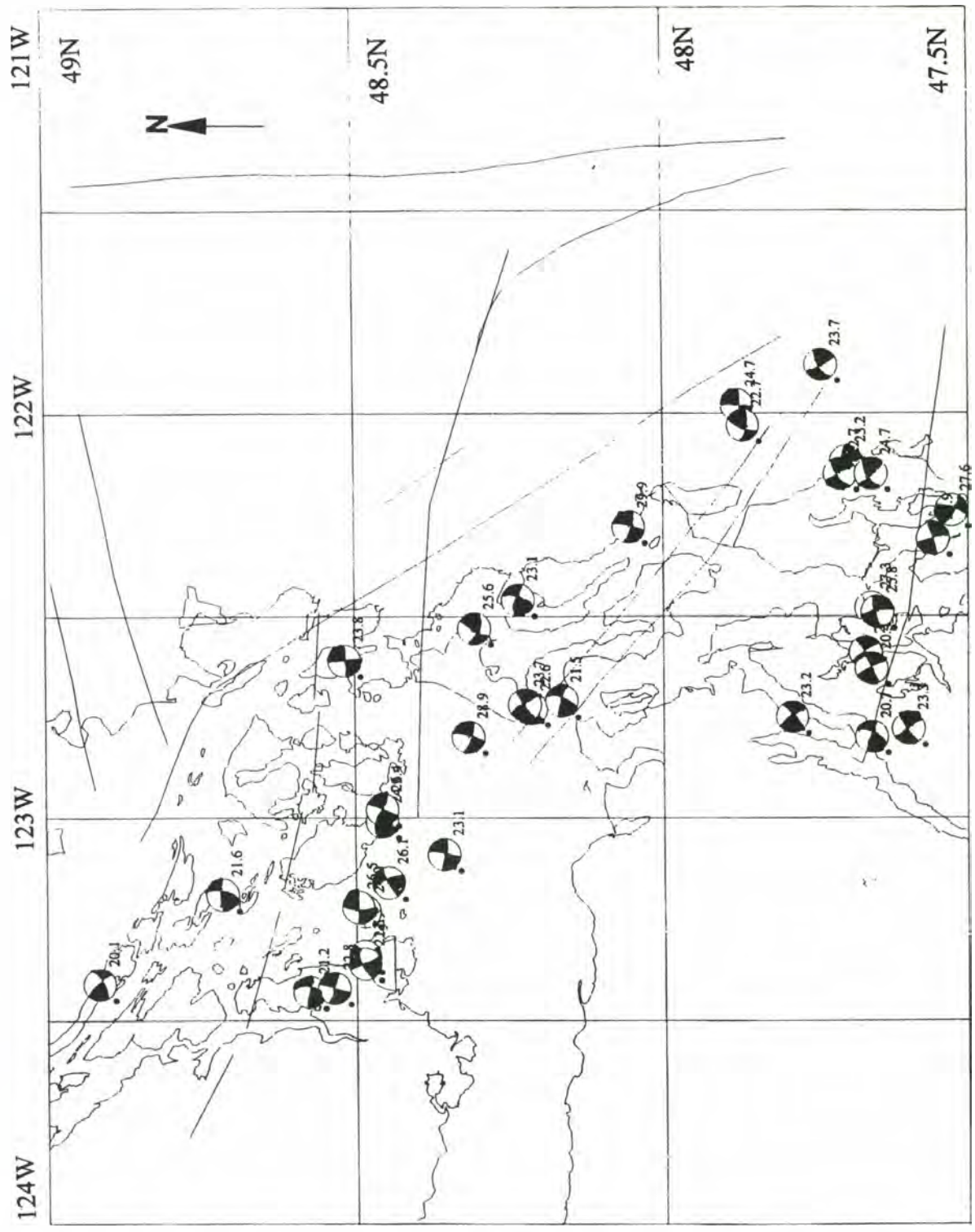

Figure 32. All focal mechanisms that were classified as strike-slip and fell between 20 and 30 km were plotted next to the epicenter. Next to each focal mechanism is the depth at which the event occurred. The major faults and lineaments from Figure 9 are plotted as well.

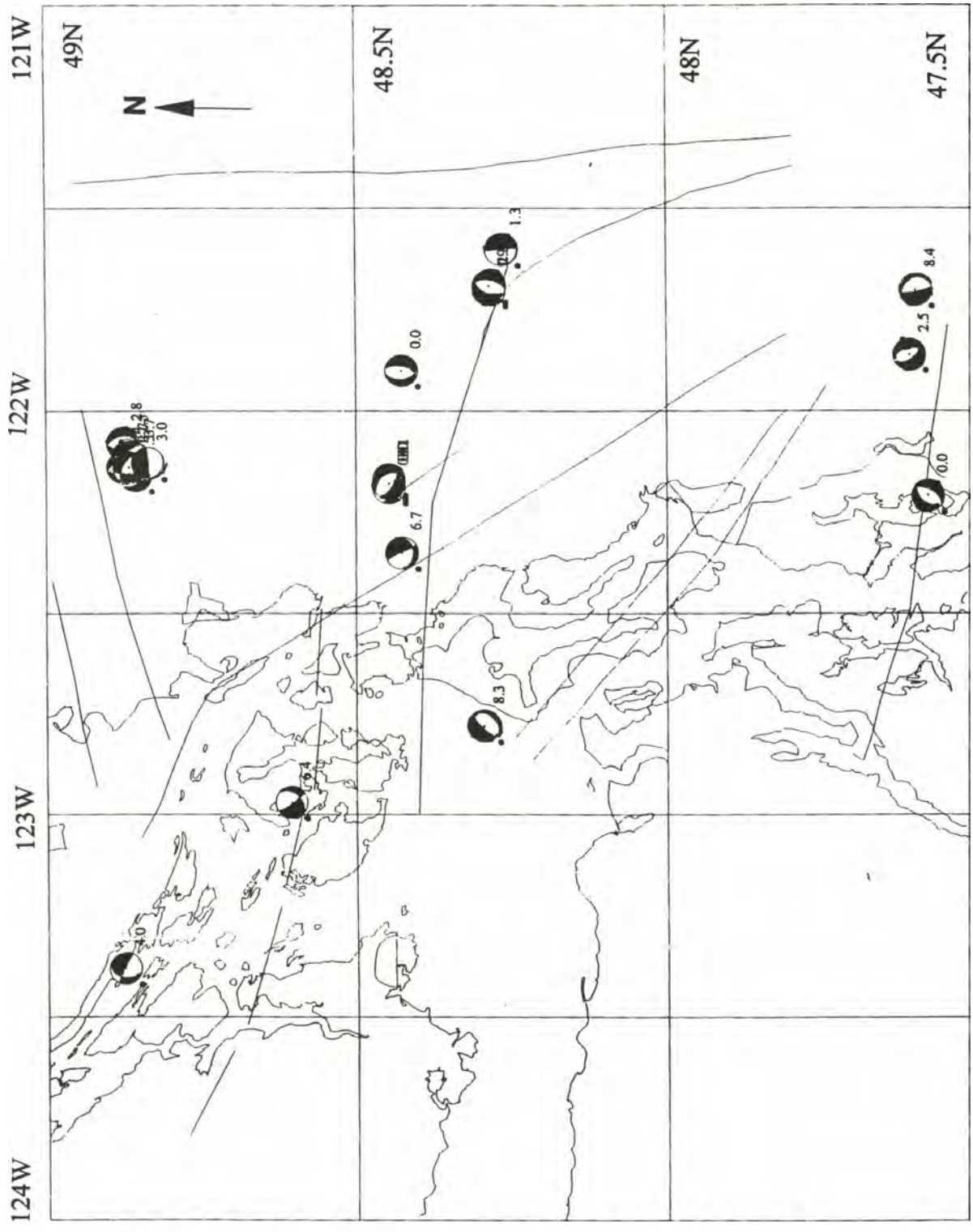

Figure 33. All focal mechanisms that were classified as normal and fell between 0 and 10 km were plotted next to the epicenter. Next to each focal mechanism is the depth at which the event occurred. The major faults and lineaments from Figure 9 are plotted as well.

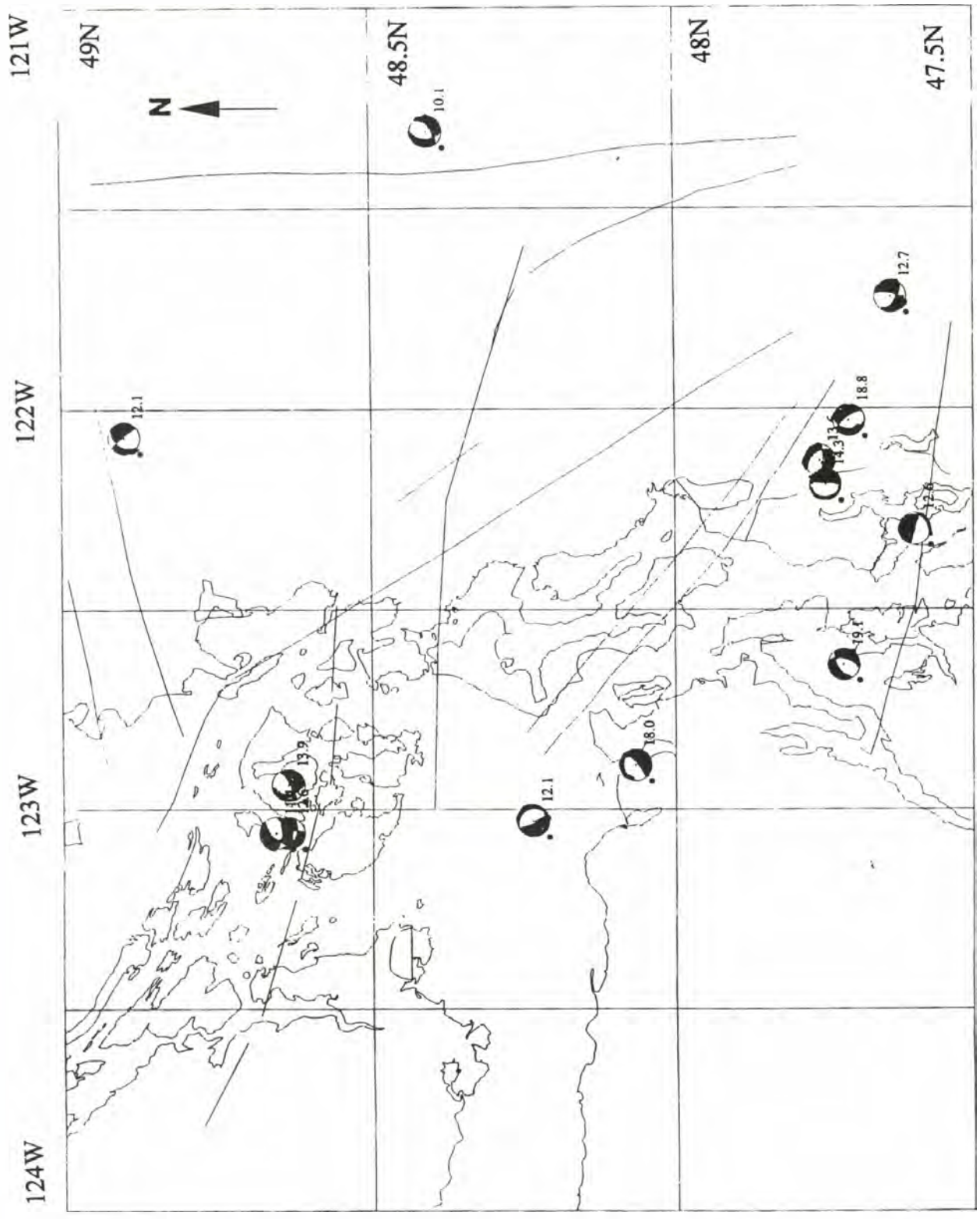

Figure 34. All focal mechanisms that were classified as normal and fell between 10 and 20 km were plotted next to the epicenter. Next to each focal mechanism is the depth at which the event occurred. The major faults and lineaments from Figure 9 are plotted as well.

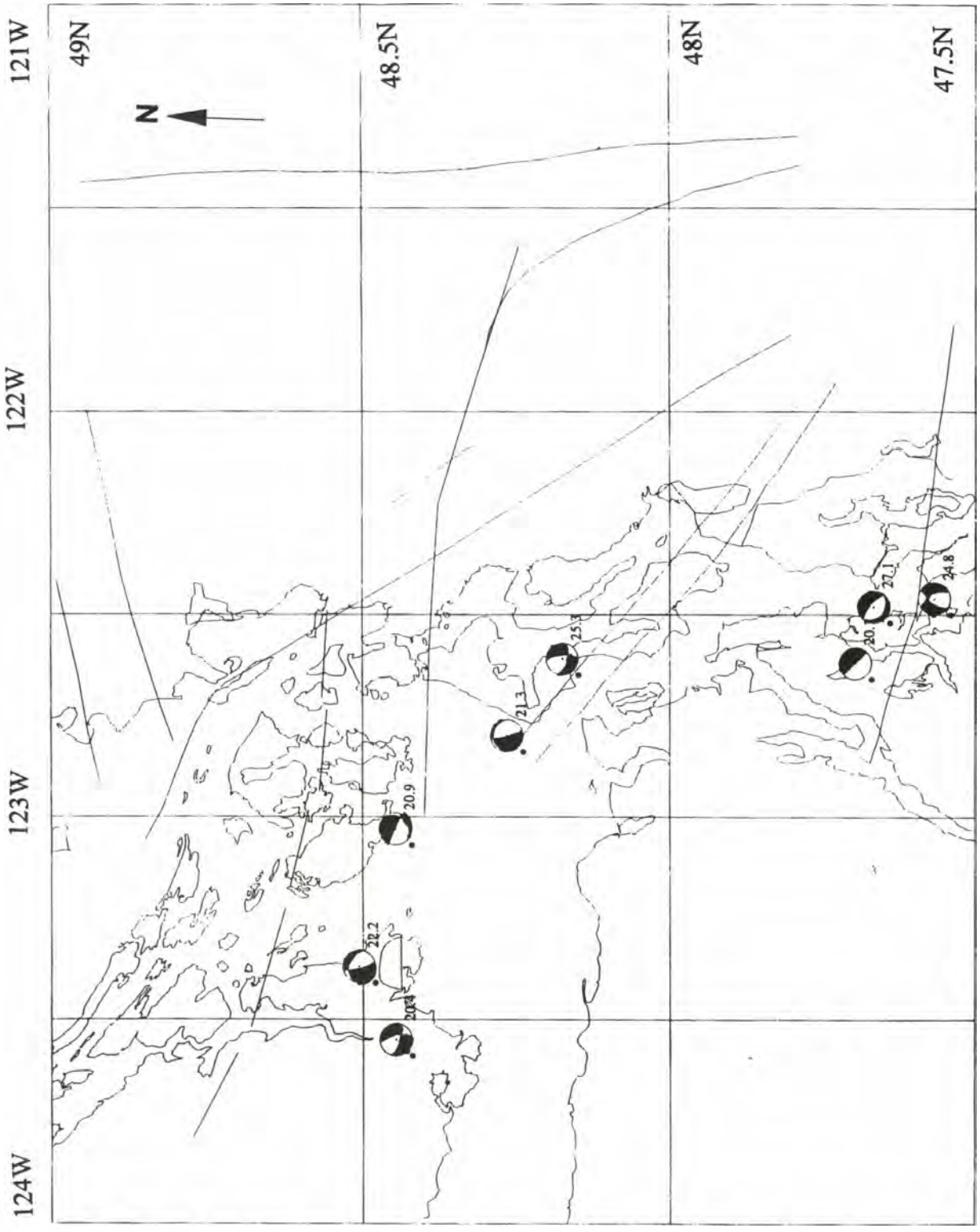

Figure 35. All focal mechanisms that were classified as normal and fell between 20 and 30 km were plotted next to the epicenter. Next to each focal mechanism is the depth at which the event occurred. The major faults and lineaments from Figure 9 are plotted as well.

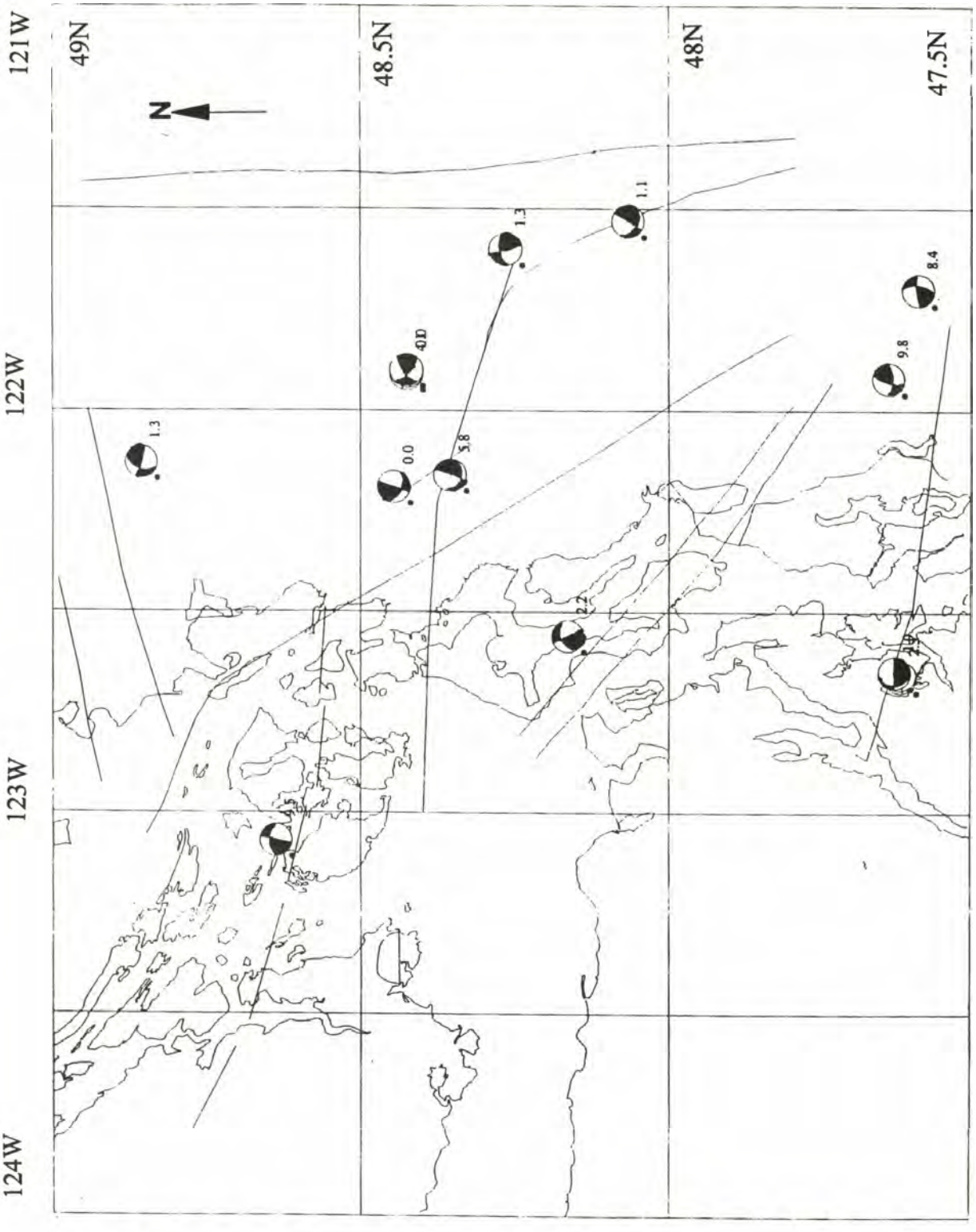

Figure 36. All focal mechanisms that were classified as odd and fell between 0 and 10 km were plotted next to the epicenter. Next to each focal mechanism is the depth at which the event occurred. The major faults and lineaments from Figure 9 are plotted as well.

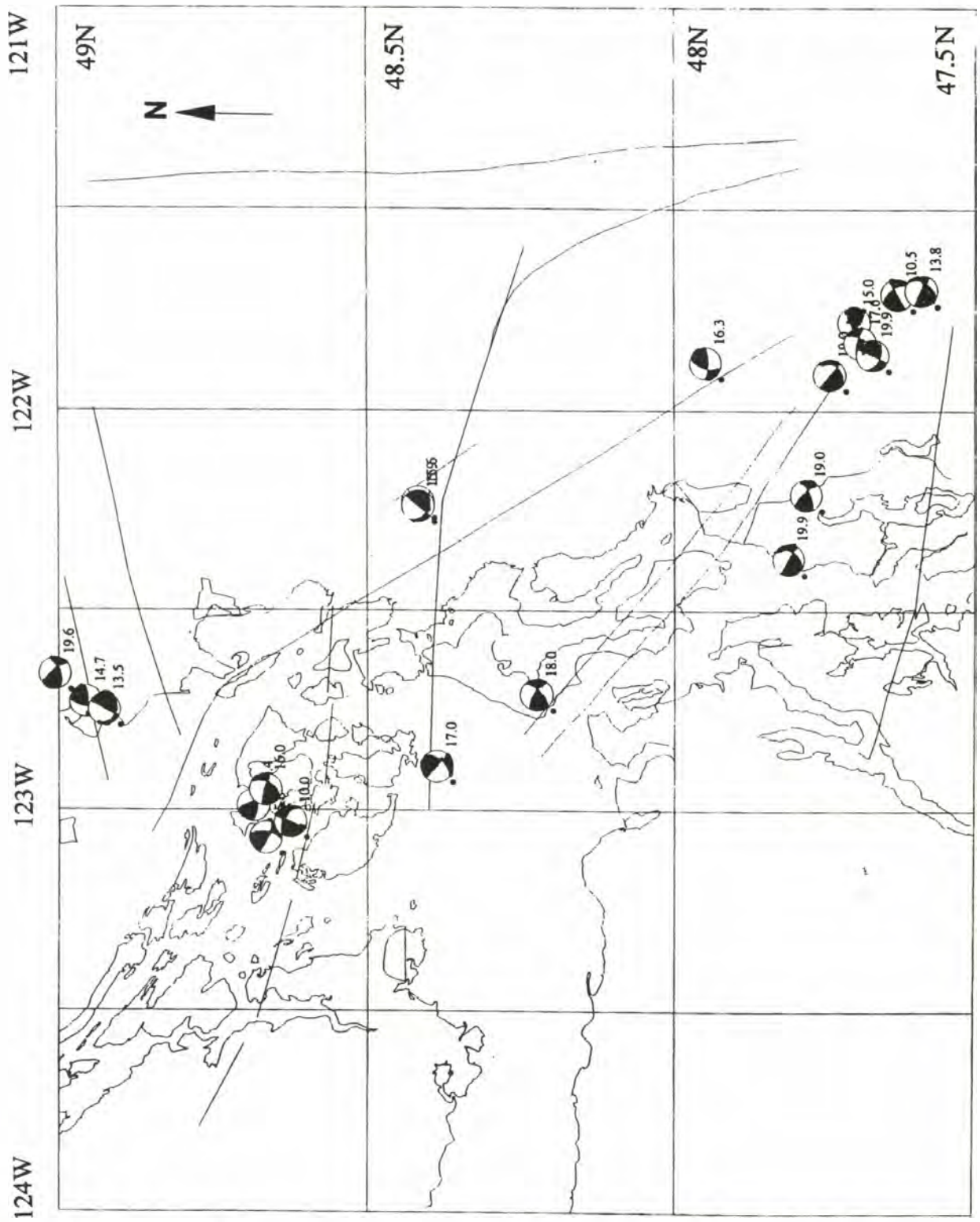

Figure 37. All focal mechanisms that were classified as odd and fell between 10 and 20 km were plotted next to the epicenter. Next to each focal mechanism is the depth at which the event occurred. The major faults and lineaments from Figure 9 are plotted as well.

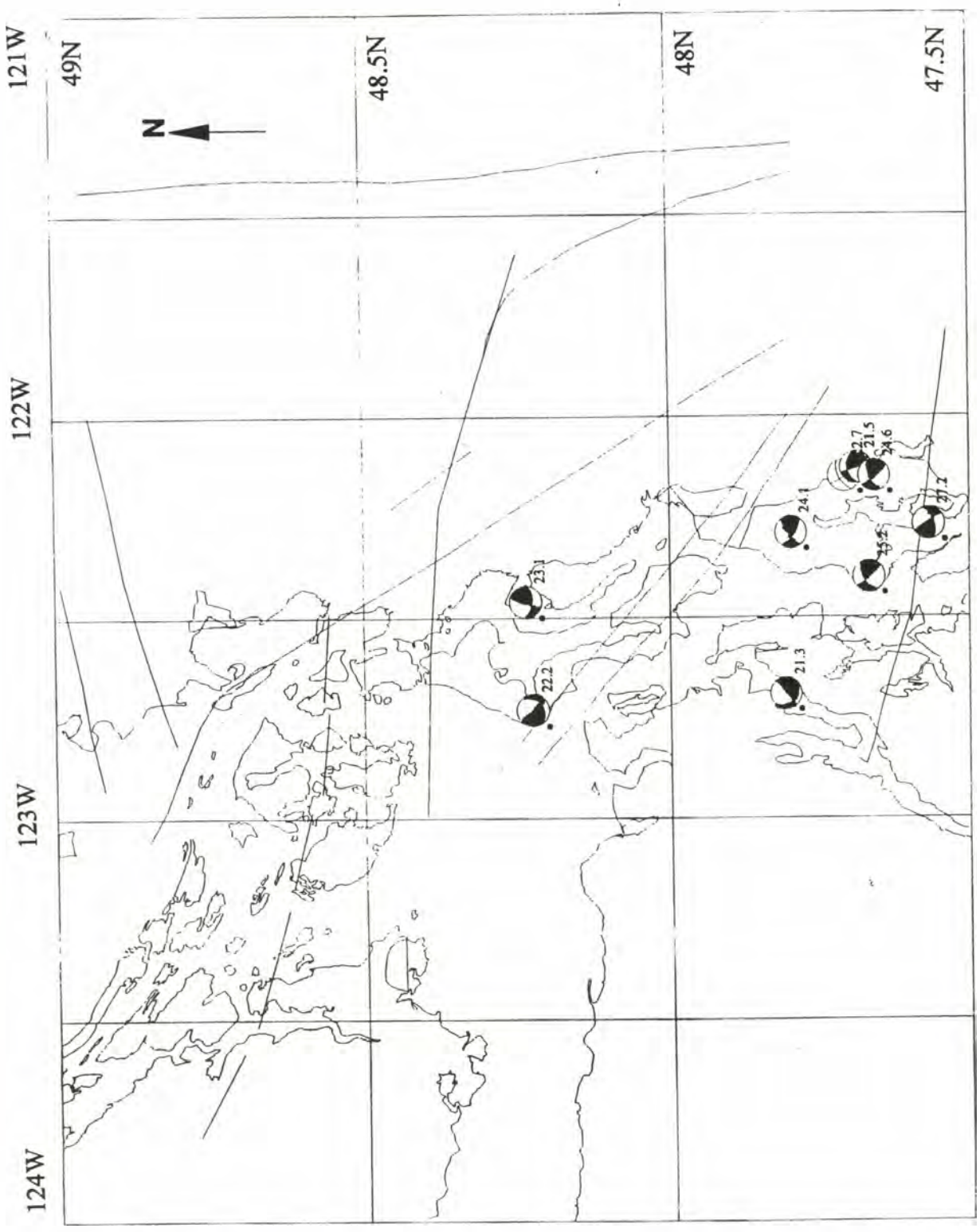

Figure 38. All focal mechanisms that were classified as odd and fell between 20 and 30 km were plotted next to the epicenter. Next to each focal mechanism is the depth at which the event occurred. The major faults and lineaments from Figure 9 are plotted as well.

event. South of 48° N and at depths greater than 10 km, reverse faults show a general east/west strike; north of 48° the majority of reverse faults show a general northeast/southwest strike (Figures 22, 27 - 29). Change in the orientation of reverse faulting is consistent with a change in the regional pressure direction, likely the result of the change in trend of the subduction front (Figure 1).

Of the shallow strike-slip events, half occur in the Deming area (Figure 30). The rest of the events north of 48° show a northwest/southeast right lateral strike slip or a northeast/southwest left lateral strike slip motion (Figures 30 - 32). This also is consistent with transpressive deformation as a result of the trench-parallel component of subduction. Many of the deeper (20 to 30 km depth) strike-slip events occur within the region of the Southern Whidbey Island fault zone, which is a segment of the boundary between two major crustal blocks (Johnson and others, 1996; Figure 32).

Normal events comprise only 15 percent of focal mechanisms in the region (Table 1; Figures 33 - 35). A cluster of shallow events occurs in the Deming region (Figure 33). The small percentage of normal events is also consistent with a transpressional regime (Figures 36 - 38).

Notable Fault Trends

1. A distinct trend of right lateral, transpressional strike-slip faulting, around 23 to 26 km depth, was found along the southern Whidbey Island fault (Figure 32). This zone stretches from 47.6° N along a northwest trend to 48.5° N and merges into southern Vancouver Island. On Figure 32, the right lateral strike - slip trace is visible. On

Figure 29, we can see that a component of transpressional motion accompanies the translational motion. While the events don't lie directly along the trend of the near-surface expression of the fault, they could have occurred on the same fault. Based on the location of these events and the northern trace of the southern Whidbey Island fault, they could have been on that fault if it dipped approximately 60° - 70° to the north. Farther southeast, the fault may be steeper because epicentral locations lie closer to the fault trace

2. On closer examination of the region of the trace of the Devils Mountain fault:
    a. The easternmost section of the Devils Mountain fault trace is believed to trend northwest. Figure 30 shows focal mechanisms that are consistent with this.
    b. To the west along the Devils Mountain fault trace the trend appears to change to east - west. Based on focal mechanisms, motion is mainly reverse faulting at around 12 to 18 km depth (Figure 28).
3. In the northern part of the study region is a northeast - southwest trending zone of reverse faulting at approximately 17 to 20 km depth (Figure 28). The zone of reverse faulting may continue to Orcas Island (Figure 2) where there are events with similar motions and orientations (Figure 28). This zone coincides with a lineament found using earthquake epicenters and magnetics data (Figure 9; Mulder, 1995).

The Deming events and events southwest of the southern Whidbey Island fault were not discussed in the analysis of the focal mechanism maps. The Deming area has many types of mechanisms all within a small cluster. Many could have originated on the Macaulay Creek fault since more than half of the recorded events in this area occurred

within a year before and after the 1990 magnitude 5.2 event (Figure 8 ; Dragovich and others, 1997). Events southwest of the southern Whidbey Island fault could have occurred on the Seattle fault and the Kingston Arch in an area that has been studied extensively.

Localized Analysis of Planar Seismicity

Trying to make sense of the clusters and elongate distributions of epicenters we see in Figure 11 is one of the keys in defining active structures and earthquake potential. Knowing if the local concentrations of events fall along a planar surface that might be a major fault, or if they are more widely distributed, apparently unrelated events that align along unrelated surfaces would be valuable. If they do the fall along planar surfaces, the orientation and inclination of those surfaces would be useful in describing the active structures. Knowing potentially active structures is useful in determining which of the two nodal planes in a focal mechanism is the fault plane. A determination of a likely sense of motion along potentially active structures can then be found using focal mechanisms of events that occurred in the vicinity of an active structure.

To see if earthquakes occurred along planar surfaces, events within small sampling volumes were analyzed using a Chi-square method (Bevington, 1969; Figure 39). The statistical analysis employed a program written by Dr. David C. Engebretson. The assumption is that events occurring along a fault surface would fall along a plane . Using Chi-square best-fit approach, we can then attach probabilistic meaning to "significant" or "unlikely" fault planes (Figure 39).

Chi-square is used to test the appropriateness of different probabilistic models. Chi-square is essentially the sum of the squares of the "misfit" to any given "model" and it measures the "closeness" of earthquake foci to a corresponding expected "model". For our purposes Chi-square for a data set having N foci is:

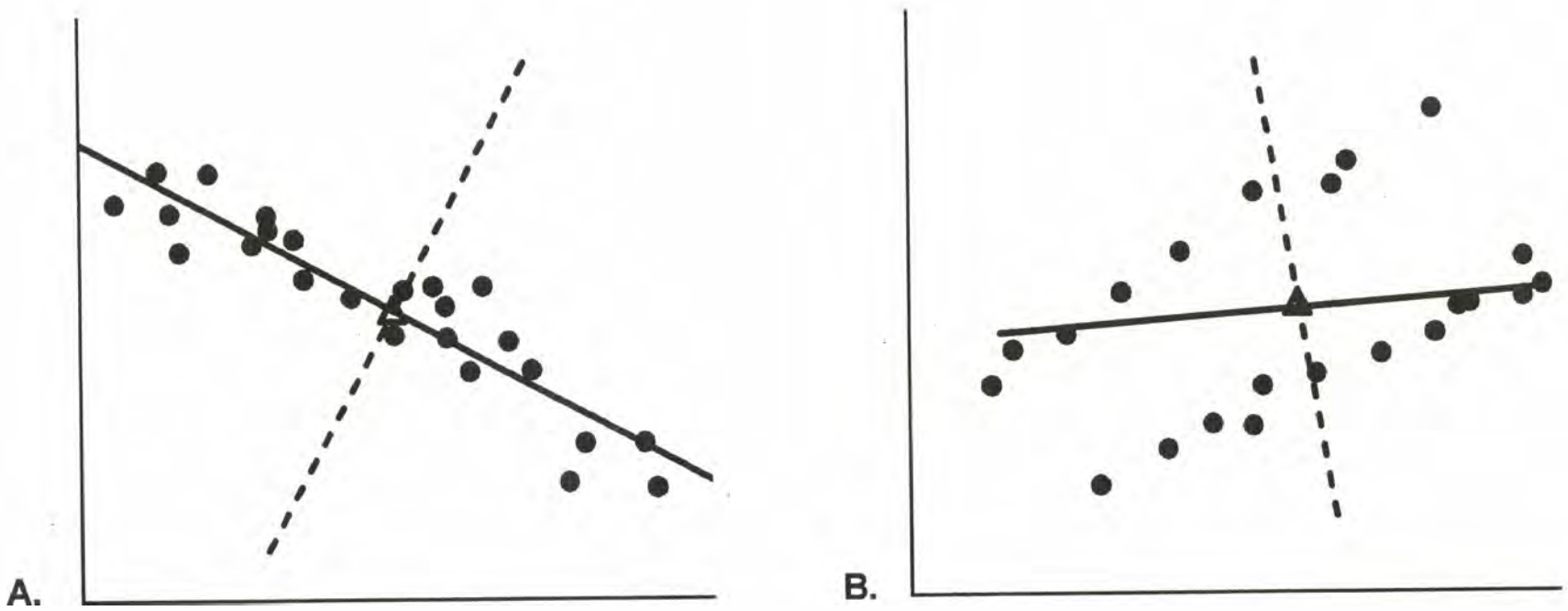

Figure 39. Two dimensional example of Chi-square approach. Points represent earthquake foci unweighted by magnitude. Triangle is their center of mass. Solid line is best fit. Dashed line is arbitrary alternative which would have a larger Chi-square value.because most points are farther from it. One shortcomming is that parallel planes - B, disorganized foci, and conjugate planes would all produce large chi square results and possible erroneous fits. Thus, some real planes may be lost in this analysis. However, it is unlikely that good fits - A, are false positives if enough data were used.

$$\chi^2 = \sum_{i=1}^{N} \left(\frac{\delta_i}{\sigma_i} \right)^2$$

where δi is the distance in km from the ith focus to the modeled plane. σi is the standard deviation in km for the quality in location of the event. δi is found through the dot product of the 3 dimensional position vector of the focus with the normal to a given (model) plane. σi is the root-mean-square error estimate given in the WRSN archives for each earthquake. The best-fit process involved a search in parameter space for all possible planes at 1 degree strike and 1 degree dip increments. All events are assumed to have equal "weight". That is, no weighting according to magnitude was applied. All model planes were forced to include the centroid of the foci dataset (center of gravity for a collection of unit masses representing the earthquake foci). Thus the fit involved two parameters (strike and dip). The lowest Chi-square value is associated with the best-fit plane.

Chi-square gives little indication if a best fit plane from one model is a better fit than another plane for a different modeled region. This is because it does not account for the size of the dataset used to calculate Chi-square values. Therefore, datasets with many events will tend to have larger Chi-square values than those with smaller datasets given a similar fit. Reduced Chi-square is used to remove the dependence of data set size. The reduced Chi-square values can be used to compare the "goodness of fit" relative to other best fit planes elsewhere in the study region. For our purposes reduced Chi-square is:

$$\chi_\nu^2 = (\chi^2 / \nu)$$

Where ν is the number of events minus the number of parameters plus one (in this case totaling three) calculated from the data to describe the distribution. An approximation for the standard deviation of the events in km from the best fit plane can then be derived by taking the square root of reduced Chi-square.

Uncertainties in the best fit planes were found using the F distribution which uses the ratio of χ_ν^2 for neighboring planes to χ_ν^2 for the best-fit plane. F distribution is:

$$f = \chi_\nu^2{}_{\text{(neighboring)}} / \chi_\nu^2{}_{\text{(best)}}$$

f values were calculated for planes at two degree increments from the best fit strike and dip. Variance in strike and dip of the best fit plane was determined to be where f reached two. This provided strike and dip uncertainties with a minimum of 75 percent confidence.

Subsets of seismic events were selected for analysis by passing a window of 0.15° latitude by 0.226° longitude over the study area at 0.05° increments. Chi-square and reduced Chi-square values were calculated for each subset. The results were written out to files and plotted according to set criteria (Figures 40 - 41). Figures 40 and 41 show best-fit planes that meet the specified criteria. Figure 40 shows planes that were determined under more stringent constraints than those in Figure 41, but both show the statistically significant clusters within the dataset. Due to depth distributions, each window was roughly cubic in shape, the exception is between 122.5° and 122° west longitude where a full range of depths was used (Figure 14).

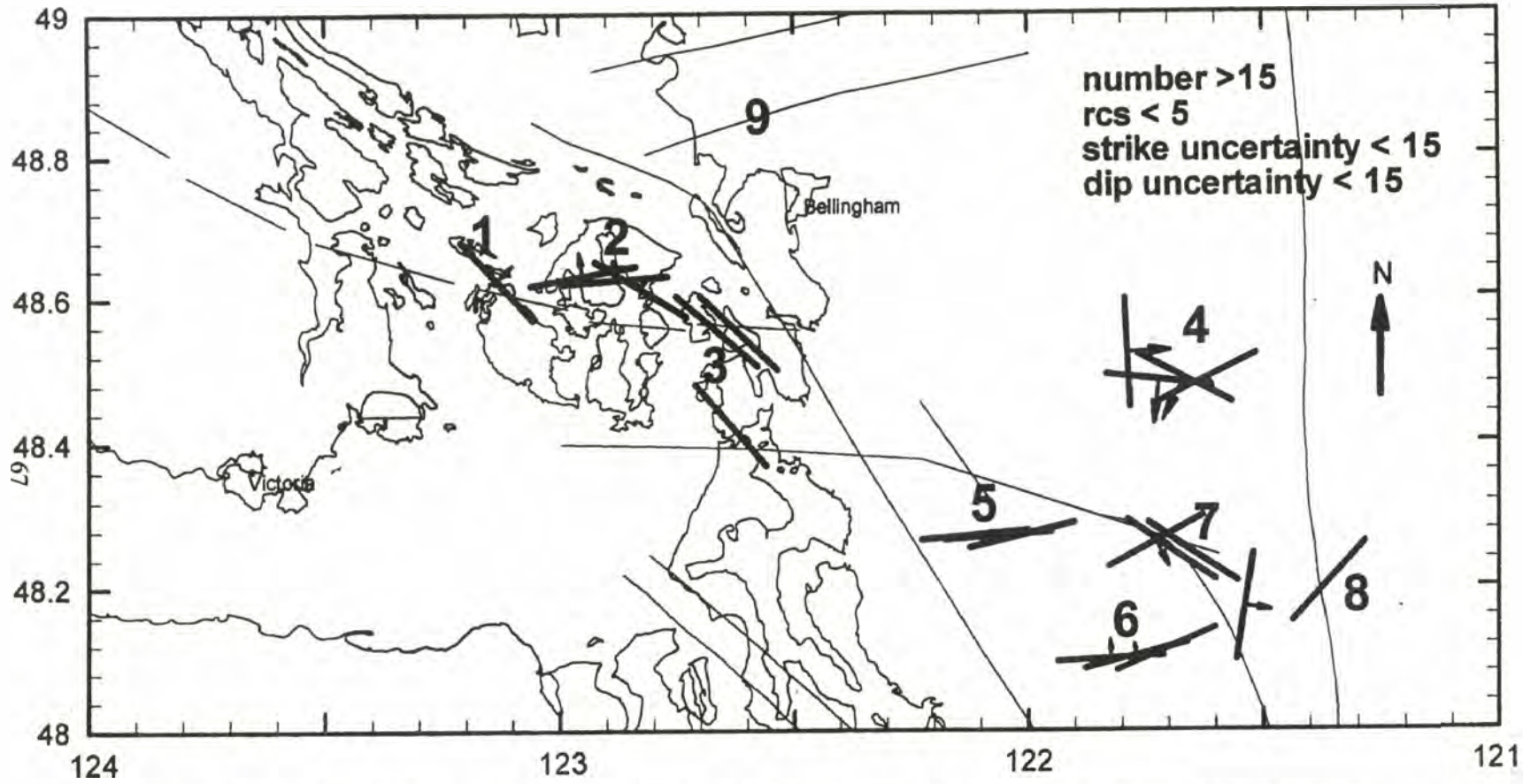

Figure 40. A plot of the best fit azimuths and dips that met the specified criteria. Number is the number of events that went into the window calculation; rcs is the reduced Chi-square value; strike and dip uncertainty in degrees for the best-fit plane. The strike lies along the thicker, longer line and the dip is drawn perpendicular and its legnth is inversely porportional to the angle of the dip Planes with dips that are vertical within the uncertainty do not have a dip vector drawn for them. 1 - 9 are planar clusters to be discussed. Faults from Figure 9 are plotted in gray.

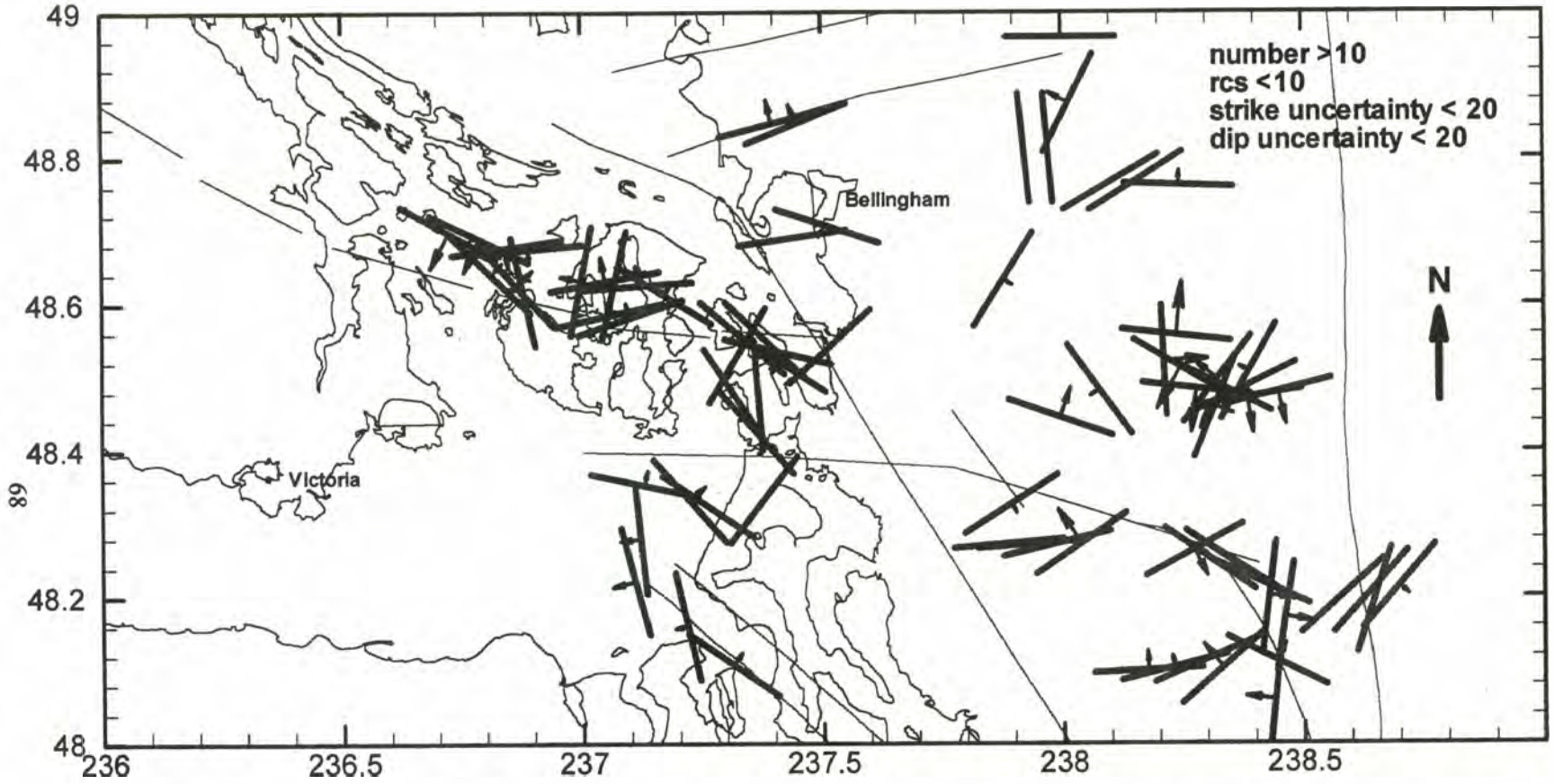

Figure 41. A plot of the best fit azimuths and dips that met the specified criteria. Number is the number of events that went into the window calculation; rcs is the reduced Chi-square value; strike and dip uncertainty in degrees for the best-fit plane. The strike lies along the thicker, longer line and the dip is drawn perpendicular and its legnth is inversely porportional to the angle of the dip Planes with dips that are vertical within the uncertaintydo not have a dip vector drawn for them. Faults from Figure 9 are plotted in gray.

Discussion

Clusters that met reduced Chi-square criteria were deemed significant (Figures 40 and 41). These significant trends are probably the result of earthquakes occurring along planar surfaces. These planar surfaces likely are preexisting zones of weakness, and faulting is the result of regional stresses. While these clusters can be deemed significant, there may be subsets with planar distributions of events that did not meet the selected criteria. A clear lack of results between 122.5° and 122° is most likely due to the bimodal depth distribution that merges events at two different depths giving poor Chi-square values. In retrospect, each mode should have been analyzed seperately. Clusters labeled 1 through 9 on Figure 40 are the most significant trends found using the Chi-square analysis.

Now that we have found trends that could likely be deemed fault planes, we can use our focal mechanisms (Figures 27 to 38) and find out the probable fault planes and thus, the sense of motion:

Cluster 1. A north-northwest strike of left lateral strike-slip and oblique-slip motion can be seen on a very steep to east dipping fault surface between 10 and 20 km (Figures 28 and 31).

Cluster 2. Correlates with a lineament found using earthquakes and magnetics data (Mulder, 1995). The focal mechanisms show possibly reverse or strike-slip events occurring along this zone, sense of motion cannot be determined (Figures 28 and 31).

Cluster 3. The center of the cluster is around 15 km. Based on this it might possibly be related to a reverse event on Figure 28.

Cluster's 4 & 6. There are no focal mechanisms in the vicinity of these planar clusters. Sense of motion cannot be determined.

Cluster 5. East-west striking steeply dipping reverse faulting around 15 km can be seen (Figure 28). This also falls just south of the trace of the Devil's Mountain fault.

Cluster 7. Clear shallow (< 4 km) southwest-northeast striking, southeast dipping reverse faulting can be seen (Figure 27). The strike-slip focal mechanisms follow both planar orientations, but are steep dipping with a clear sense of strike slip motion parallel to the Devil's Mountain fault (Figure 30). Based on this, I would say that there is northwest-southeast striking, right lateral strike-slip faulting at shallow (< 4 km) depths along this fault trace.

Cluster 8. Shallow reverse faulting can be seen along this cluster's orientation in Figure 27.

Cluster 9. This planar cluster shows up on Figure 42. It is noteworthy because it aligns with the Vedder Mountain trace seen clearly as a reverse fault in the focal mechanisms and correlates with a lineament found using earthquakes and magnetics (Mulder, 1995; Figure 28).

CHAPTER 3 SUMMARY AND CONCLUSIONS

Based on a depth distribution analysis, we see a clear transition from earthquakes that are deeper in the western part of the study region and shallower to the east (Figures 11, 12 and 14). The distribution of earthquakes and geotherms indicate that the brittle material being deformed is wedge-shaped (Figure 16). Crustal temperature distribution seems to control the depth extent of earthquakes (Figure 16). Because the crust is strongest at the base of the cool crust, this is the likely location where earthquakes will be initiated. Aseismic deformation likely propagates upward to become seismic deformation in the lower boundary of the cold crustal wedge where the brittle-ductile transition occurs (Figure 15 and 16). The result is that seismic risk in the eastern part of the study region comes from shallow earthquakes and in the western part from deeper earthquakes.

Using a new technique modified from Frolich (1993) for this study, a focal mechanism analysis shows deformation typical for a region exposed to both compressional and translational stresses due to the oblique approach of the Juan de Fuca plate (Figures 1 and 6). Compressional deformation was dominant overall, with translational events the next most abundant (Figure 25 and 26). This suggests that the study region is undergoing deformation as a result of the same regional stresses that induce deformation to the south.

A change from predominately reverse faulting at depths shallower than 20 km to predominantly strike - slip faulting at depths greater than 20 km could be the result of σ_2 and σ_3 changing places due to a higher lithostatic load or represent a change in the

preferred orientations of preexisting zones of weaknesses at depth. The majority of these events occur near a major structural boundary along the trace of the southern Whidbey Island fault, which juxtaposes different terranes against one another.

Results of the Chi-square statistical analysis and focal mechanism plots were used to locate potentially hazardous, active fault zones. Both orientation and sense of motion were possible to determine using these methods. Three fault zones that stood out the most were:

1. The southern Whidbey Island fault zone shows a clear sense of northwest trending right-lateral strike-slip motion around 23 to 26 km depth (Figure 32). This zone can be followed for more than 100 km and therefore may be able to provide a large slip surface. Slip surface area is directly related to earthquake magnitude potential and, therefore, the southern Whidbey Island fault should be considered capable of producing large destructive earthquakes.
2. The eastern section of the Devil's Mountain fault shows two planar orientations on Figure 41 cluster 7. These correspond with strike-slip and reverse focal mechanisms on Figures 27 and 30 and are likely two faults that may intersect. Although the trace here isn't clearly extensive, the events are shallow. A shallow event can result in more damage for a localized area than for a deeper one of the same size. Westward the Devil's Mountain fault may continue at greater depths with reverse motion.
3. The Vedder Mountain trace, clearly seen as a northeast striking reverse fault on Figure 28, can also be seen on Figure 41, and directly correlates with documented

lineaments on Figure 8. Focal mechanism suggest that this lineament may extend westward as far as Orcas Island, which would make this a major fault zone and therefore capable of producing damaging earthquakes.

Because a great deal of research has not been dedicated to better understanding active shallow structures within the northern Puget Lowland, this work serves as an introduction to some of the potentially active shallow structures. In addition to structures that were mentioned in this thesis that may provide zones of large magnitude or shallow destructive earthquakes, I believe other approaches to studying active structures may provide evidence for additional areas of concern. Large magnitude earthquakes do occur in and around the study region from both shallow and deeper focused earthquakes that can have destructive results. This is known from historical seismic records. Because a real threat from earthquakes does exist, precautions should be taken to prepare for such an event in an effort to reduce possible injury and property damage when it does occur.

References

Adams, J., 1992, Paleoseismology: A search for ancient earthquakes in Puget Sound, Science, v. 258, 1592 - 1593.

Amadi, E. E., 1992, The 1990 Nooksack Forks, Washington, earthquake sequence: sequence geometry and temporal characteristics, MS Thesis, Boise State University, 103.

Anderson, M.G., Richards, K. S., eds., 1987, Slope stability: geotechnical engineering and geomorphology: New York, Wiley, 648.

Atwater, B. F., 1987, Evidence for great Holocene earthquakes along the outer coast of Washington State, Science, v. 236, 942 - 944.

Atwater, B. F., Moore, A. L., 1992, A tsunami about 1000 years ago in Puget Sound, Washington, Science, v. 258, 1614 - 1617.

Atwater, B. F., 1996, Coastal evidence for great earthquakes in western Washington, in Assessing Earthquake Hazards And Reducing Risk In The Pacific Northwest, edited by A. M. Rogers and others, U. S. Geological Survey Professional Paper, 1560, I-54.

Beck, M. E., 1980, Paleomagnetic record of plate - margin tectonic processes along the western edge of North America, Journal of Geophysical Research, v. 85, n. B12, 7115 - 7131.

Beck, M. E., Rojas, C., Cembrano, J., 1993, On the nature of buttressing in margin-parallel strike-slip fault systems, Geology, v21, 755-758.

Bevington, P. R., 1969, Data reduction and error analysis for the physical sciences, McGraw-Hill, Inc., USA, 336.

Blackwell, D. D., Steele, J. L., Kelley, S., Korosec, M. A., 1990, Heat flow in the state of Washington and thermal conditions in the Cascade range, Journal of Geophysical Research, v. 95, n. B12, 19495-19516.

Blakely, R. J., Wells, R. E., Yelin, T. S., Madin, I. P., Beeson, M. H., 1995, Tectonic setting of the Portland-Vancouver area, Oregon and Washington: Constraints from low-altitude aeromagnetic data, Geological Society of America Bulletin, v. 107, n. 9, 1051 - 1062.

Brandon, M. T., Cowan, D. S., Feehan, J. G., 1993, Kinematic analysis of the San Juan thrust system, Washington: Discussion and reply, Geological Society of America Bulletin, v. 105, 839 - 844.

Brandon, M. T., Cowan, D. S., Vance, J. A., 1988, The late Cretaceous San Juan Thrust system, San Juan Islands, Washington, Geological Society of America Special Paper 221, 88.

Brown, E. H., 1987, Structural geology and accretionary history of the northwest Cascades system, Washington and British Columbia, Geological Society of America Bulletin, v. 99, 201 - 214.

Bucknam, R. C., Hemphill-Haley, E., Leopold,E. B., 1992, Abrupt uplift within the past 1700 years at southern Puget Sound, Washington, Science, v. 258, 1611 - 1614.

Cheney, E., 1987, Major Cenozoic faults in the Puget lowland of Washington, Washington Division of Geology and Earth Resources Bulletin 77, 149 - 168.

Cheney, E., 1977, Alternative interpretations of the seismic and geologic hazards to the Skagit nuclear power site

Chleborad, A. F., Schuster, R. L., 1990, Ground failure associated with the Puget Sound region Earthquakes of April 13, 1949, and April 29, 1965, United States Geological Survey Open File Report 90-687, 168.

Clague, J. J., Naesgaard, E., Sy, A., 1992, Liquefaction features on the Frasier delta: evidence for prehistoric earthquakes?, Canadian Journal of Earth Science, v. 29, 1734 - 1745.

Cowan, D. S., 1994, Alternative hypothesis for the Mid-Cretaceous paleogeography of the western cordillera, GSA Today, v. 4, n. 7, 181 - 186.

Crosson, R. S., 1972, Small earthquakes, structure, and tectonics of the Puget Sound region, Bulletin of the Seismological Society of America, v. 62, n. 5, 1133 - 1171.

Crosson, R. S., Owens, T. J., 1987, Slab geometry of the Cascadia Subduction Zone beneath Washington from earthquake hypocenters and teleseismic converted waves, Geophysical Research Letters, v. 14, n. 8, 824 - 827.

Davis, G. H., 1984, Structural geology of rocks and regions, John Wiley and Sons, Inc., 491.

Dragert, H., Hyndman, R. D., 1995, Continuous GPS monitoring of elastic strain in the northern Cascadia subduction zone, Geophysical Research Letters, v. 22, n. 7, 755 - 758.

Dragovich, J. D., Zollweg, J. E., Qamar, A. I., Norman, D.K., 1997, The Macaulay Creek Thrust, the 1990 5.2-magnitude Deming earthquake, and Quaternary Geologic anomalies in the Deming area, western Whatcom county, Washington-cause and effects?, Washington Geology, v. 25, n. 2, 15 - 27.

Easterbrook, D. J., 1963, Late Pleistocene glacial events and relative sea level changes in the northern Puget Lowland, Washington, Geological Society of America Bulletin, v. 74, 1465 - 1484.

Easterbrook, D. J., 1969, Pleistocene chronology of of the Puget Lowland and San Juan Islands, Washington, Geological Society of America Bulletin, v. 80, 2273 - 2286.

Easterbrook, D. J., Rahm, D. A., 1970, Landforms of Washington; the geologic environment, Union Printing Co., Washington

Easterbrook, D. J., 1976, Quaternary stratigraphy of north America, Mahaney, W. C., ed., Stroudsburg, Pa, Dowden Hutchinson and Ross, 512.

Easterbrook, D. J., 1992, Advance and retreat of Cordilleran ice sheets in Washington, U.S.A., Geographe physique et Quaternaire, v. 46, n. 1, 51-68.

Easterbrook, D. J., 1994, Chronology of the pre-late Wisconsin Pleistocene sediments in the Puget Lowland, Washington, Washington Division of Geology and Earth Resources, Bulletin 80, 191 - 206.

Engebretson, D. C., Cox, A. V., Thompson, G. A., 1984,Correlation of plate motion with continental tectonics: Laramide to Basin - Range, Tectonics, v. 3, n. 2.

Engebretson, D. C., Cox, A., Gordon, R. G., 1985, Relative motions between oceanic and continental plates in the pacific basin, Geological Society of America Special Paper 206, 59.

Engebretson, D.C., Easterbrook, D. J., Kovanen, D. J., 1995, Relationships of very large, deep-seated, bedrock landslides and concentrated shallow earthquakes, Abstracts with Programs - Geological Society of America, 27, 6, 377.

Engebretson, D.C., Easterbrook, D. J., Kovanen, D. J., 1996, Relationships of very large, deep-seated, bedrock landslides and concentrated shallow earthquakes, Abstracts with Programs - Geological Society of America, 28.

Engels, J. C.. Tabor, R. W., Miller, F. K., Obradovich, J. D., 1976, Summary of K-Ar, Rb-Sr, U-Pb, Pba, and fission-track ages of rocks from Washington state prior to 1975 (exclusive of Columbia Plateau basalts): U.S. Geological Survey Miscellaneous Field Studies Map MF-710, 2 sheets, scale 1:1,000,000.

England, T. D. J., Currie, L.D., Massey, N. W. D., Roden-Tice, M.K., Miller, D.S., 1997, Apatite fission track dating of the Cowichan fold and thrust system, southern Vancouver Island, British Columbia, Canadian Journal of Earth Sciences, v. 34, 635 - 645.

Fowler, C. M. R., 1993, The solid Earth: an introduction to global geophysics, Cambridge University Press, 472.

Frolich, C., Davis, S. D., 1993, Teleseismic B values; or much ado about 1.0, Journal of Geophysical Research, v. 98, n. B1, 631 - 645.

Gower, H. D., Yount, J. C., Crosson, R. S., 1985, Seismotectonic map of the Puget Sound region, Washington, U.S. Geological Survey map I-1613, scale 1:250,000.

Heaton, T. H., Kamamori, 1984, Seismic potential associated with subduction in the northern United States, Bulletin of the Seismological Society of America, v. 74, 933 - 942.

Jacoby, G. C., Williams, P. L., Buckley, B. M., 1992, Tree ring correlation between prehistoric landslides and abrupt tectonic events in Seattle, Washington, Science, v. 258, n. 5088, 1621 - 1623.

Johnson, S.Y., 1983, Stratigraphy, age and paleogeography of the Eocene Chuckanut Formation, northwestern Washington, Canadian Journal of Earth Sciences, v. 21, 92 - 106.

Johnson, S. Y., Potter, C. J., Armentrout, J. M., Miller, J. J., Finn, C., Weaver, C. S., 1996, The southern Whidbey Island fault: An active structure in the Puget lowland, Washington, GSA Bulletin, v. 108, n. 3, 334 - 354.

Jones, D. L., Cox, A., Coney, P., Beck, M., 1983, The growth of western north America, Scientific American, 70 - 84.

Karlin, R. E., Abella, S. E. B., 1992, Paleoearthquakes in the Puget Sound region recorded in sediments from Lake Washington, U.S.A., Science, v. 258, 1617 - 1620.

Keefer, David K., 1984, Landslides caused by earthquakes, Geological Society of America Bulletin, v. 95, 406-421.

Kovanen, D., 1996, Extensive Late-Pleistocene Alpine Glaciation in the Nooksack River Valley North Cascades, Washington, MS Thesis Western Washington University.

Lewis, T.J., Bentkowski, W.H., Hyndman, R.D., 1992, Crustal temperatures near the southern Canadian Cordillera transect, Canadian Journal of Earth Sciences, v. 29, 1197 - 1214.

Madole, R. F., Schuster, R. L., Sarna-Wojcicki, A. M., 1995, Ribbon cliff landslide, Washington, and the earthquake of 14 December 1872, Bulletin of the Seismological Society of America, v. 85, 986 - 1002.

Matthews, W. H., 1979, Landslides of central Vancouver Island and the 1946 earthquake, Bulletin of the Seismological Society of America, v. 69, n. 2, 445 - 450.

McCaffrey, R., 1994, Dependence of earthquake size distributions on convergence rates at subduction zones, Geophysical Research Letters, v. 21, n. 21, 2327 - 2330.

McLellan, R. D., 1927, The geology of the San Juan Islands, University of Washington Publications in Geology, v. 2, 185.

Mustoe, G. E., Gannaway, W. L., 1997, Paleogeography and paleontology of the early Tertiary Chuckanut Formation, northwest Washington, Washington Geology, v. 25, n. 3, 3 - 18.

Mulder, T. L., 1995, Small earthquakes in southwestern British Columbia (1975 - 1991), Masters Thesis University of Victoria, 117.

Naumann, C. M., Savigny, K. W., 1992, Large rock avalanches and seismicity in southwestern British Columbia, Canada, in Bell, D. H., ed., Landslides; Proceedings of the sixth international symposium, 6, 1187-1192.

Noson, L. L., Qamar, A., Thorsen, G.W., 1988, Washington state earthquake hazards, Washington Division of Geology and Earth Resources Information Circular 85.

Pratt, T. L., Johnson, S. J., Potter, C., Stephenson, W., Finn, C., 1997, Seismic reflection images beneath Puget Sound, western Washington State: The Puget Lowland thrust sheet hypothesis, Journal of geophysical Research, v. 102, n. B12, 27,469 - 27,489.

Qamar, A., Ludwin, R. S., 1992, Stress directions in Washington and Oregon inferred from earthquake focal mechanisms, Seismological Research Letters, v. 63, n. 1

Riddihough, R. P., 1977, A model for recent plate interactions off Canada's west coast, Canadian Journal of Earth Sciences, v. 14, 384-396.

Riddihough, R., 1984, Recent movements of the Juan de Fuca plate system, Journal of Geophysical Research, v. 89, n. B8, 6880 - 6994.

Rogers, A. M., Walsh, T. J., Kockelman, W. J., Priest, G. R., 1996, Earthquake hazards in the Pacific northwest - An overview, in Assessing Earthquake Hazards And Reducing Risk In The Pacific Northwest, edited by A. M. Rogers and others, U. S. Geological Survey Professional Paper, 1560, I-54.

Schuster, R. L., Logan, R. L., Pringle, P. T., 1992, Prehistoric rock avalanches in the Olympic Mountains, Washington, Science, v. 258, 1620 - 1623.

Stanley, W. D., Johnson, S. Y., Qamar, A. I., Weaver, C. S., Williams, J. M., 1996, Tectonics and seismicity of the southern Washington Cascade range, Bulletin of the Seismological Society of America, v. 86, n. 1A, 1-18.

Swanson, D. A., Haugerud, R. A., 1994, Geologic field trips of the Pacific Northwest, volume 2.

Twiss, R. J., Moores, E. M., 1992, Structural Geology, W. H. Freeman and Company, 532.

Wang, K., Dragert, H., Melosh, H. J., 1994, Finite element study of uplift and strain across Vancouver Island, Canadian Journal of Earth Sciences, v. 31, 1510 - 1522.

Weaver, C. S., Baker, G. E., 1988, Geometry of the Juan De Fuca plate beneath Washington and northern Oregon from seismicity, Bulletin of the Seismological Society of America, v. 78, n. 1, 264 - 275.

Wells, R. E., Engebretson, D. C., Snavely, P. D., Coe, R. S., 1984, Cenozoic plate motions and the volcano-tectonic evolution of western Oregon and Washington, Tectonics, v. 3, n. 2, 275 - 294.

Wells, R. E., Weaver, C. S., Blakely, R. J., 1998, For-arc migration in Cascadia and its neotectonic significance, Geology, v. 26, n. 8, 673-768

Williams, P. L., 1989, Evaluation of possible seismic triggering of giant landslides in Seattle, Washington, EOS, October 24, 1332.

Yamaguchi, D. K., Atwater, B. E., Bunker, D.E., Benson, B. E., Reid, M. S., 1997, Tree ring dating the 1700 Cascadia earthquake, Nature, v. 389, 922-923.